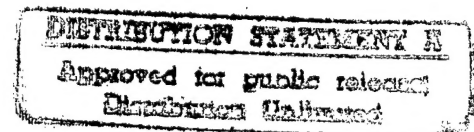Annual Report

Fundamental Aspects of Metal-to-Ceramic Brazing

Submitted to
Dr. George Yoder
Office of Naval Research
Arlington, Virginia 22217

Submitted by:Dr. Glen R. Edwards and Dr. Stephen Liu
Center for Welding, Joining and Coatings Research
Colorado School of Mines
Golden, Colorado 80401

October 1995

19970717 064

CSM

**CENTER FOR WELDING AND
JOINING RESEARCH**

Colorado School of Mines
Golden, Colorado 80401

DEPARTMENT OF THE NAVY
OFFICE OF NAVAL RESEARCH
SEATTLE REGIONAL OFFICE
1107 NE 45TH STREET. SUITE 350
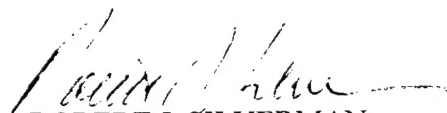SEATTLE WA 98105-4631

IN REPLY REFER TO:

4330
ONR 247
11 Jul 97

From: Director, Office of Naval Research, Seattle Regional Office, 1107 NE 45th St., Suite 350, Seattle, WA 98105

To: Defense Technical Center, Attn: P. Mawby, 8725 John J. Kingman Rd., Suite 0944, Ft. Belvoir, VA 22060-6218

Subj: RETURNED GRANTEE/CONTRACTOR TECHNICAL REPORTS

1. This confirms our conversations of 27 Feb 97 and 11 Jul 97. Enclosed are a number of technical reports which were returned to our agency for lack of clear distribution availability statement. This confirms that all reports are unclassified and are "APPROVED FOR PUBLIC RELEASE" with no restrictions.

2. Please contact me if you require additional information. My e-mail is *silverr@onr.navy.mil* and my phone is (206) 625-3196.

ROBERT J. SILVERMAN

Annual Report

Fundamental Aspects of Metal-to-Ceramic Brazing

Submitted to
Dr. George Yoder
Office of Naval Research
Arlington, Virginia 22217

Submitted by:
Dr. Glen R. Edwards and Dr. Stephen Liu
Center for Welding, Joining and Coatings Research
Colorado School of Mines
Golden, Colorado 80401

October 1995

TABLE OF CONTENTS

Acknowledgments

Project Summary

Research has continued to develop fundamental understanding of wetting and spreading of reactive metals on alumina and to model the metal-to-ceramic bonding process. A study was completed on the modeling of spreading kinetics of reactive brazing alloys on ceramic substrates. Based on nucleation and growth of islands of reaction product at the ceramic-metal interface, in particular, the Avrami type surface nucleation and growth kinetics, Dr. Alan Meyer developed a non-empirical theoretical spreading model for reactive metals. Dr. Paulo Camargo focused on the effect of minor contamination in the metal-to-ceramic bonding system. Residual oxygen in the system plays a fundamental role in the wetting and bonding process. Too low an oxygen content will result in non-spreading of the liquid filler metal. Too high an oxygen content will result in excess growth of the interfacial product layer which jeopardizes the mechanical integrity of the joint. These two research programs are complementary since they both expanded the understanding and modeling of the bonding mechanism. The concept of joining ceramic to metal using ductile, multilayer reactive metal coatings is also being developed. Mr. Don Bucholz, a Ph.D. student, is carrying out a program to explore the technological barriers of using multilayer coatings of ductile and reactive metals in brazing. Both diffusion bonding (solid state) and diffusion brazing (transient liquid phase bonding) are being examined. Satisfactory bonds have been obtained using the diffusion bonding process and detailed chemical and structural analysis of the bond region are in progress.

A short description of each of the three programs are given in the following.

1. Modeling of the Spreading Kinetics of Reactive Brazing Alloys on Ceramic Substrates: Alan Meyer (Concluded)

The objective of this study was to fundamentally model the spreading kinetics of liquid metal alloys on ceramic substrates without utilizing empirical curve fitting. A non-empirical theoretical spreading model for reactive metals on ceramics was derived based on the progress of the nucleation and growth of islands of reaction product at the ceramic-metal interface. The spreading radius as a function of time was predicted utilizing a computer program to numerically solve for the fraction of surface covered by reaction product with time based on Avrami-type surface nucleation and growth kinetics. Reaction

rate constants (k) of between 1.10^{-2} and 5×10^{-2} s^{-1} were obtained for copper-titanium alloys on alumina. Within the uncertainty in the measurements, the k values were not a function of composition and temperature (between 1120° and 1200°C, and 3 to 20 weight percent titanium). The rate constants values for silver-titanium alloys were between 1×10^{-3} and 3×10^{-3} s^{-1} which are an order of magnitude lower that the k values obtained for copper-titanium and alloys on alumina.

2. Role of Oxygen in the Cu-O-Ti/Sapphire Interfacial-Region Formation: Paulo Camargo (Concluded)

Most reactive metal brazing studies using sapphire as the substrate assumed stoichiometric dissociation of Al_2O_3 and that the oxygen released as the source of oxygen, ignoring the oxygen concentrations of the precursor alloy and gas phase, which could have a dramatic influence on the thermodynamic activity of the active element in the melt. Sessile drop experiments using sapphire single crystals were conducted with three Cu-Ti-O alloys containing 4 atomic percent titanium and 1200, 860, and 2400 ppm of oxygen. The oxygen partial pressure in the reactor was controlled to between 10^{-7} and 10^{-30} atm, with ppm-level additions of hydrogen to the argon gas carrier. Equilibrium between the hydrogen-oxygen-water vapor in the gas phase controlled the oxygen potential. Detailed sapphire/metal and metal/gas/interfacial regions were analyzed using SEM, EDS and XPS (X-ray photoelectron spectroscopy). Measurements and thermodynamic modeling showed that Ti-O coadsorbed to the surfaces and that $TiO_{(g)}$ gas phase assisted in the reactive metal brazing process. The thickness of the Ti-O co-adsorption layer (interfacial reaction product) increased dramatically with increases in the bulk oxygen concentration. By lowering the oxygen content to 100 ppm, flow of the molten filler metal was inhibited. The complex oxide layer (Cu_3Ti_3O, Cu_2Ti_4O) reported by other researchers was also observed to form as a result of high oxygen content (2400 ppm), high temperature, and long reaction time.

3. Diffusion Bonding Ceramic to Metal Using Ductile, Multilayer reactive Metal Coatings: Donald Bucholz (Research in Progress)

The main objectives of this study are to investigate and model the behavior of ductile, multilayer reactive metal coatings as filler metal for bonding ceramics to metals. Activities

for the past year were directed towards characterization of the bond layer, understanding the interface formation, variation of the initial ductile and reactive metal deposition conditions and their relation to process parameters. Detailed chemical analysis of the bond layer cross section was also necessary for the development of a multilayer interdiffusion model. Multilayer Ni/Ti coatings of 1 and 25μ total thickness, with variations in the total number of layers, were produced for joining specimens. They undergo heat treatment where time at temperature, temperature and bonding pressure are the process variables. The composition and structure of the multilayer coatings and bonded cross section were analyzed using x-ray diffraction, SEM/EDS. TEM work is also planned for the bond region characterization. Using literature data for comparison, the measured composition profiles are being modeled to understand the interdiffusion in the Ni-Ti multilayers.

Authors' note: This report consists largely of three independent technical papers (Sections I through III). To ensure that each of these sections can function as a stand-alone publication, some repetition of experimental procedures, governing equations, and references was required.

I.   MODELING OF THE SPREADING KINETICS OF REACTIVE BRAZING ALLOYS ON CERAMIC SUBSTRATES: COPPER-TITANIUM AND SILVER-TITANIUM ALLOYS ON POLYCRYSTALLINE ALUMINA

The objective of this study was to model the spreading kinetics of liquid reactive metals on ceramic substrates without utilizing empirical curve fitting. Most of the current reactive spreading models assume that complete reaction product coverage is always obtained at the substrate-liquid interface while the model developed in this study assumes that the spreading rate is controlled by the rate of reaction product nucleation and growth. The spreading kinetics of a metal brazing alloy liquid droplet on a ceramic substrate were modeled based on interfacial energy considerations and Avrami-type nucleation and growth reaction kinetics. The results of the model were compared to spreading data generated for the copper-titanium/alumina and silver-titanium/alumina systems.

Advanced ceramics are finding new applications in many areas including the aerospace, automotive, nuclear and electronics industries. However, cost considerations or additional mechanical, electrical or thermal property requirements frequently favor ceramic-metal or dissimilar ceramic component combinations. Joining these different materials by brazing with metal interlayers is a commercially viable technique. A fundamental understanding of the kinetics and thermodynamics of the processes occurring at the ceramic-metal interface will be useful in tailoring the interface to maximize strength and to control other physical properties (e.g. electrical or thermal conductivity).

A.   EXPERIMENTAL PROCEDURE

Two types of experimental testing incorporating a sessile drop testing configuration, Figure 1, were undertaken. First, a procedure was developed to generate isothermal spreading data for copper-titanium and silver-titanium alloys on alumina. This data was necessary to test the validity of the derived spreading model. Second, a methodology was developed for measuring the fractional coverage with time of the alumina surface by reaction product. This information can be used to calculate the surface reaction rate constant, k, for input into the computer model.

1. Materials Used

Two systems were chosen for this investigation: copper-titanium/alumina and silver-titanium/alumina. All of the studies were be performed on alumina because thermodynamic and surface energy values were available in the literature; relatively high purity polycrystalline material was easy to obtain and relatively inexpensive. The metal systems chosen were both simple binary systems with a non-reactive base metal (copper or silver) and a reactive metal addition (titanium), instead of the ternary and quaternary systems used in commercial brazing, so that complications due to the interactions between the different components could be avoided. First, the copper-titanium system was chosen because many of the currently used brazing alloys contain these two materials and because the furnace used is limited to approximately 1500°C which precludes the use of pure titanium. Several copper-titanium intermetallics exist for this system, but above 1000°C only a single liquid exists for approximately 45 to 95 weight percent titanium, Figure 2. The silver-titanium system was chosen for comparison to the copper-titanium system. Only low titanium compositions can be studied for this system due to a large solid-liquid two phase field for this system, Figure 3.

The substrates used for all of the tests were 0.64-mm-thick Coors AD-996 polycrystalline alumina substrates. The Coors AD-996 electronic substrate has a surface roughness of 75 to 125 micrometers (CLA), an average grain size of approximately 1.2 micrometers, and an impurity concentration of 0.4 percent [1]. The substrates were cleaned with nitric acid and rinsed with ethanol before testing.

In the majority of the sessile drop tests, a piece of pure titanium (99.99% purity) was introduced to a piece of pure copper (99.99% purity) or pure silver (99.9% purity) blocks during testing to obtain the desired test composition. For small number of the spreading tests, a piece of pre-alloyed copper- 20 w/o titanium (greater than 99% purity) was used.

2. Measurement of Spreading Radius versus Time

The spreading radius versus time was determined for liquid copper-titanium and silver-titanium alloys on alumina using a sessile drop configuration. All of the metal samples had a nominal mass of 1.20 ± 0.02 g and the titanium concentration was always within ± 0.2 weight percent of the desired composition.

Initially, spreading area and spreading radius data for liquid copper-titanium alloys on alumina were generated by heating samples in a vacuum furnace under an argon overpressure. The samples were held for variable times and temperatures, and the final drop contact diameters were measured after the samples were cooled. However, the results were inconclusive due to a large variation between samples as seen in Figure 4.

Therefore, it was concluded that an in situ measurement technique was needed. A tube furnace with a viewing window was used to obtain in situ diameter measurements of the sessile drop Figure 5. This system recirculated argon through an oxygen scavenger to reduce the oxygen partial pressure to approximately 0.006 Pa (50 ppb). The tests were performed at an argon overpressure of approximately 10 kPa. The nitrogen partial pressure was not measured an a nitrogen scavenger was not used. The nitrogen partial pressure was determined by the purity of the argon. Thus the nitrogen partial pressure was estimated to be approximately 1 Pa (10 ppm). The spreading of the drops was videotaped and the spreading diameter was measured from the videotape by freezing frames on a Leco Image Analyzer. These measurements, accurate to ± 0.1 mm, were corrected to account for the non-spherical contact area. The average radius was calculated by multiplying the measured radius by a proportionality constant. This constant was the ratio of the final radius measured perpendicular to the viewing direction divided by the final radius measured in the viewing direction. The assumption of an elliptical

contact area was consistent with experimental observations. A preferred spreading direction, probably related to the processing of the square plates, was observed; the maximum spreading radius was always oriented perpendicular to one of the plate edges.

In the second stage of testing, sessile drop tests were performed using three different initial metal configurations, Figure 6. The first configuration was a pre-alloyed block of copper-20 w/o titanium placed directly on an alumina plate (Figure 6a). The second configuration consisted of stacked titanium, copper and alumina (Figure 6b). In the third configuration, titanium was stacked on the alumina substrate and the copper was placed between two plates above the titanium (Figure 6c). At the desired test temperature, the liquid copper fell onto the titanium and formed a copper-20 w/o titanium alloy. In one special case, the copper and the titanium were placed side by side and the furnace was tilted at the test temperature to induce copper-titanium contact. This test technique resulted in the same test configuration as Figure 6c.

First, tests were performed at 1000, 1100, 1200 and 1300°C using the stacked configuration (Figure 6b) . Then, two tests were performed at 1200°C for all three sample configurations to evaluate the effect of the starting configuration on the spreading kinetics. Each test lasted approximately 26 hours (90 ks). Long testing times were used to obtain the equilibrium spreading radii.

Based on the results of the second phase of testing, the configuration shown in Figure 6c was the only one of the three configurations which resulted in "true isothermal" data. In the third phase of testing, this same configuration was used to generate spreading radius versus time data as a function of composition and temperature for copper-titanium and silver-titanium alloys on alumina. In some cases, the same sample configuration was attained by placing the titanium next to the silver or copper, and then tilting the furnace to achieve contact between the liquid metal and the solid titanium. Similar to the configuration in Figure 6c, tilting the furnace at the testing temperature prohibits contact between a reactive metal and a solid substrate until after the isothermal holding temperature is reached. In this phase of testing, copper-titanium/alumina samples were tested in a composition range of one to twenty weight percent titanium and a temperature range of 1120 to 1200°C; while silver-titanium/alumina samples were tested in a

composition range of one to five weight percent titanium and a temperature range of 1000 to 1100°C. A total of seventeen copper-titanium tests and four silver-titanium spreading tests were performed. These tests lasted for between ten and twelve hours (36 to 43 ks).

3. Fractional Coverage Measurements

The fractional coverage as a function of time of the alumina surface by reaction product was determined using short duration sessile drop tests. The same furnace set-up used for the spreading radius measurements was used for these tests (Figure 5). The following procedure was be used. The sample was held for a given time at a constant temperature using the sample configuration which resulted in "true isothermal" data (Figure 6c). In all of the tests, a 2.0-g liquid metal drop was allowed to spread on an alumina substrate for between 20 and 600 seconds under an argon atmosphere. The furnace was then shut down and the sample was exposed to air which oxidized the titanium and stopped spreading. After cooling to room temperature, the metal drops were dissolved by successively placing the samples in concentrated nitric and hydrochloric acids. Then the fraction of the alumina substrate covered by reaction product was measured using a Leco image analyzer. The surface were magnified 200 to 1000 times under a light microscope and the image was transferred to an image analyzer where the fractional coverage was determined using the Leco 2001 software package. Different coverage regions were correlated with their respective coverage times based on analyses of the videotapes of the spreading. The relatively large drops (2.0 g) were used to maximize the interfacial area. This precluded the extraction of other spreading information was from the videotapes because gravity is a factor in the determination of the drop geometry for drops of this size. Three sessile drop tests of varying times were performed for each composition and temperature to minimize surface roughness and surface cleanliness effects.

In the copper-titanium/alumina system, large spreading radius changes occurred even for very short times (less than 100 seconds). Rings of varying fractional coverage were observed on these samples. Thus, from five to eleven coverage regions were quantified for the three samples at each test condition. Ten area fraction measurements

were made on each coverage region, and the average fractional coverage and the standard deviation of the mean were determined. Fractional coverage measurements were made for times ranging from 30 to 390 seconds.

Only three fractional coverage measurements were obtained for each silver-titanium/alumina test condition because the relatively small radius changes limited the fractional coverage measurements to the initially covered region for each sample. Outside of the initially covered region, it was difficult to match the fractional coverage rings with time. For this system, fifteen area fraction measurements were made in each coverage region and then averaged. The tests lasted for 40 to 600 seconds.

4. Test Matrices

The final testing configuration (Figure 6c) was used to generate isothermal spreading radius versus time data for both the copper-titanium/alumina and silver-titanium/alumina systems. For both systems, the changes in spreading kinetics as a function of temperature and composition were quantified. Multiple tests at two temperatures (1120 and 1200°C) and one composition (Cu-20 w/o Ti) were performed to check the reproducibility of the measurements. The long time spreading data was also be used to calculate the reaction product/liquid interfacial energy (γ_{SL}^{II}). The fractional coverage versus time data was used to calculate the surface reaction rate constant, k. The test matrix for the copper-titanium/alumina system is presented in Table 1 and the test matrix for the silver-titanium/alumina system is presented in Table 2. At temperature and compositions where r(t) and k were both measured, the results were used to compare the theoretical model and the experimental data. This resulted in a total of thirteen comparisons because two of the silver-titanium/alumina spreading radius versus time runs revealed no measurable radius change with time.

Table 1:   Copper-titanium/alumina test matrix.

w/o Ti	Temperature (°C)		
	1120	1160	1200
1	r		
3	r,k		
5	r,k	r,k	r,k
7	r,k		
8.5	r		
10	r,k	r,k	r,k
15	r		
20	r(2),k	r,k	r(2),k

r = r(t) and γ_{SL}^{II}
k = reaction rate constant

Table 2:   Silver-titanium/alumina test matrix.

w/o Ti	Temperature (°C)	
	1000	1100
1		r,k
3		r,k
5	r,k	r,k

r = r(t) and γ_{SL}^{II}
k = reaction rate constant

B. RESULTS

In this section, spreading kinetics and wetting thermodynamics data for a series of copper-titanium and silver-titanium alloys on alumina are presented. The results of this research are divided into three major sections. The first important result is the generation of experimental curves of spreading radius versus time for the copper-titanium/aluminum and silver-titanium/alumina systems. The other two sets of data generated are input parameters for the theoretical spreading model which were not available in the literature: the solid-liquid interfacial energy (γ_{SL}), and the surface reaction rate constant (k). The equilibrium value of γ_{SL} was determined from the final spreading radius and k was determined from plots of fractional coverage (X) versus time as a function of composition and temperature.

1. Spreading Data

The sessile drop technique is frequently used to study the spreadability and wettability of liquid metals on ceramic and metal substrates [2-16]. In many of these studies, the contact angle is measured as a function of time. The wettability is then evaluated based on the minimum final contact angle or the time required to reach the final contact angle [2-7,9,12-18]. Similarly, the spreadability is evaluated based on the change in the solid/liquid contact area (or contact radius) with time [5,8,12]. In these analyses, the relative spreadability is determined from the maximum contact area (or radius) and the time required to reach the maximum spreading area (or radius). If a liquid drop of known volume assumes a geometry which can be approximated as a spherical cap, then the contact angle can be calculated from the spreading radius and vice versa [19,20,21]. Thus, contact angle and contact radius (or area) measure approximately equivalent phenomena for a spherical cap geometry.

In sessile drop experiments involving a non-reactive liquid on a ceramic substrate (i.e. copper or silver on alumina or silicon carbide [6,22]), the equilibrium contact angle is attained in a few seconds. In this situation, the information obtained from this test consists of either the final contact angle or the final solid-liquid interfacial contact radius. Thus,

the rate of sample heating from room temperature to the testing temperature and the total isothermal holding time are not important (except for holding times that are sufficiently long to cause metal volatilization and drop volume loss).

However, when a reactive metal is placed on a ceramic substrate, both the isothermal holding time and the sample heating rate are important. In general, when a reactive metal liquid is placed on a ceramic substrate and held at a constant temperature, the contact angle decreases and the spreading radius increases with time until constant values are reached. Thus, these tests must be conducted for longer times compared to similar non-reactive metals if the equilibrium contact angle or spreading radius are desired. In reactive systems, spreading kinetics data are needed to understand spreading mechanisms. Spreading radius, spreading area, or contact angle versus time are commonly used [2-8,12,13,15,16]. However, if the rate of spreading is related to the rate of reaction product formation, significant non-isothermal spreading can occur during the heating cycle, and the generation of isothermal spreading kinetics data becomes almost impossible without very rapid heating rates.

a. Effect of Initial Sample Configuration

Most sessile drop techniques for metal alloys on ceramics use one of two starting sample configurations. Either the metal is pre-alloyed to a given composition [8,12,13] or two or more pure starting materials are either stacked [3,7,14] or compacted together as powders [9] so that when the metal melts, the desired composition is achieved. For both of these techniques, the liquid metal is in contact with the ceramic substrate before the isothermal testing temperature is reached. Depending upon the heating rate and the difference between the solidus temperature and the testing temperature, some of the isothermal spreading data may be lost.

Ideally, the non-isothermal spreading would be eliminated by placing the liquid metal upon the ceramic substrate at the desired test temperature. Fujii, et al [15] were able to couple liquid aluminum to boron nitride at the desired test temperature by using a back pressure to push an aluminum drop onto a boron nitride substrate. Their primary goal was to break the oxide film on the liquid aluminum surface before testing, but this

experimental technique also resulted in complete (starting at time equal to zero seconds) isothermal data of contact angle versus time. Similarly, Ip, et al [18] placed liquid aluminum upon calcia and alumina using a graphite plunger arrangement. Using this method, only the contact angle could be reported since control of the liquid metal volume was difficult.

If an oxide film on the liquid metal is not a factor in spreading, then the metal alloy could be placed in a crucible, heated to the testing temperature and then poured onto the ceramic substrate. However, these techniques have a major experimental complication. Most reactive metals (e.g. titanium) either react with or dissolve the crucible materials. Dissolution results in a depletion of reactive metal from the liquid alloy and a decrease in the drop volume. These changes make test reproducibility extremely difficult. For liquid aluminum alloys, the oxide film barrier hinders reaction between the ceramic substrate and the liquid metal, but it also prevents reaction between the liquid aluminum and its container material. Aluminum alloys of known volume and composition could thus be introduced to a ceramic substrate at the desired testing temperature, while reaction between most other reactive metals and their containers complicate volume and composition control.

In this study, a different experimental approach eliminated the non-isothermal spreading of copper-20 w/o titanium alloys on polycrystalline alumina. In the solid state, the reaction of titanium with alumina is relatively slow. If a piece of titanium is placed on a alumina substrate, heated to 1300°C and then cooled back to room temperature, the titanium slides off the aluminum plate when it is tilted, leaving very little discoloration of the alumina surface where the titanium had rested. Similarly, liquid copper does not react with most ceramics. Therefore, if liquid copper is introduced to a combination of an alumina substrate with solid titanium already placed on the substrate, no significant spreading will occur until the copper dissolves the titanium. By introducing the liquid copper onto the alumina/titanium combination at the desired testing temperature, isothermal spreading kinetics data can be generated if the time for copper-titanium dissolution is small.

The spreading radii for the stacked starting configuration (Figure 6b), plotted as a function of time and temperature, are shown in Figure 7. At all temperatures, the spreading radius increased with time until a temperature-specific constant value was reached. The initial and final radii were smaller at lower temperatures, and the difference between the initial and final radii was larger at lower temperatures. These results are consistent with the data reported in the literature [2,3,5,7-9,12,15,16]. The spreading radius has been reported to increase with time to a constant value at an exponentially decaying spreading rate, while the contact angle exponentially decreases with time to a constant value. It has further been shown that an increase in temperature causes the initial and final spreading radii to increase (or correspondingly, the initial and final contact angles to decrease) while the differences between the initial and final radii (or contact angles) decrease.

Figure 8 shows the spreading radius versus time for the same sample runs, but including the spreading which occurred during the heat-up cycle. The negative times on the plot represent the non-isothermal spreading observed from approximately 1100°C to the testing temperature. All of the samples except the 1000°C sample showed significant spreading during the heat-up cycle from the point where the first liquid contacted the substrate to the isothermal holding temperature. Either the change in the initial spreading radius was only a temperature effect, or significant isothermal spreading kinetics data were lost during the heat-up cycle.

The spreading radii versus time plots for a copper-20 w/o titanium liquid in contact with alumina at 1200°C (for all three different starting configurations) are shown in Figure 9. The spreading which occurred before the sample reached 1200°C is again shown as negative times in Figure 10 (along with the short time spreading data at 1200°C). The pre-alloyed sample formed a liquid and began spreading first, but the stacked sample actually spread more rapidly once a liquid formed. The sample where no liquid contacted the substrate until 1200°C had a much lower spreading radius at t = 0 (upon reaching 1200°C) than the other samples, but all of the samples spread to similar final radii. This observation supports the conclusion that significant isothermal spreading data is lost for the first two sample configurations (Figures 6a and 6b).

b. Copper-Titanium/Alumina Isothermal Data

Next, utilizing the improved initial sample configuration (Figure 6c), a series of spreading radius versus time curves were generated for copper-titanium alloys on alumina as a function of liquid metal composition and temperature (Figures 11 to 13). These curves represent "true" isothermal data and can be used to test the proposed spreading model. All of the curves had a similar shape. The spreading radius increased with time with an exponentially decreasing rate of change. All of the samples had relatively small initial radii (between 2.2 and 4.4 mm) and the radius always increased with time to an equilibrium value. For all of these tests, the equilibrium spreading radius was attained in less than ten ks. For a given composition, the final radii were similar at all three temperatures. Two spreading regimes were observed as a function of composition. At low titanium compositions (at or below 7 w/o titanium), the final spreading radii were only 3.4 to 5.1 mm. Conversely, for higher titanium concentrations, the final radii values ranged from 8.5 to 13.2 mm.

c. Silver-Titanium/Alumina Isothermal Data

Four spreading radius versus time curves were generated for the silver-titanium/alumina system using the sample configuration shown in Figure 6c. The results are shown in Figure 14. For this system, the radius versus time curves are nearly flat. The initial radius for a silver-5 w/o titanium alloy on alumina at 1000°C was 4.70 mm, while the initial radii at 1100°C only varied from 3.1 to 3.2 mm for titanium concentrations from one to five weight percent. The maximum overall radius change was very small (less than 0.5 mm) and for both of the 5 w/o titanium samples, no measurable radius change occurred. The silver-1 w/o and 3 w/o titanium samples exhibited behavior similar to copper-titanium alloys on alumina (increasing radius with time at an exponentially decreasing rate) but the overall change in radius was much less for these samples.

2. Determination of Solid-Liquid Interfacial Energies

The spreading radius for a given drop volume may be modeled by computer simulation. Similarly, for a spherical cap of known volume, a given spreading radius has a unique contact angle. The drop geometry leads to three simultaneous equations that can be solved for the contact angle, θ:

$$V = \frac{1}{2}\pi h\left(r^2 + \frac{h^2}{3}\right) \qquad (1)$$

$$R = \frac{1}{2}\left(\frac{r^2}{h} + h\right) \qquad (2)$$

$$\tan\theta = \frac{r}{R - h} \qquad (3)$$

where V = drop volume
       h = drop height
       r = spreading radius
       R = radius of curvature

The volume of a liquid metal alloy sample weighing 1.2 grams was estimated using the pure metal liquid densities given by Iida [23] and Equation 1. For small contact angles, using the spreading radius to calculate the contact angle has been shown to be more accurate than a direct measurement of the contact angle [19].

Next, if the liquid-vapor and solid-vapor energies are known, the solid-liquid interfacial energy can be calculated at equilibrium by solving the Young Equation for γ_{SL}. For this study, the solid-vapor interfacial energy for alumina/argon from Nikolopoulos [11] was used along with a "rule-of-mixtures" approximation for the liquid-vapor interfacial energy which was calculated using the pure liquid data of Iida [23].

The uncertainties in the volume calculation, the measured radius, and solid-vapor and liquid-vapor interfacial energies lead to uncertainties of 60 to 80 mJ/m^2 for the solid-liquid interfacial energy values and $\pm$ 4 degrees for the contact angles.

a. Copper-Titanium/Alumina System

The contact angle versus composition as a function of temperature for copper-titanium alloys on alumina is shown in Figure 15. These value are similar to the contact angles of 14 to 108 degrees reported by Naidich[17] for copper alloys containing 1 to 8 a/o titanium (less than 7 w/o titanium) at 1150°C.

The contact angle is a strong function of composition and a weak function of temperature. A transition from a non-wetting to a wetting contact angle (θ less than ninety degrees) was observed near five weight percent titanium. Four regions of contact angle behavior as a function of titanium concentration were obtained for the 1120°C tests. Pure copper had a non-wetting contact angle of approximately 142 degrees. Small titanium additions (one to five weight percent) resulted in a major improvement in wettability and non-wetting contact angles of 100 to 110 degrees were obtained. Between five and ten weight percent titanium, a transition from a non-wetting to relatively small wetting contact angle occurred. In this region, the contact angle decreased from 110 degrees down to less than fifteen degrees. Above ten weight titanium, the contact angle remained approximately constant (between one and fifteen degrees) up to titanium compositions of thirty weight percent.

The two contact angle plateaus and the wetting transition are similar to results obtained by Kristalis et al [24] for the NiPd-Ti/Al$_2$O$_3$ system. In the NiPd-Ti/Al$_2$O$_3$ system, three wetting plateaus corresponding to the formation of three different titanium oxide reaction products (Ti$_5$O$_9$, Ti$_3$O$_5$, and Ti$_2$O$_3$) were observed as the titanium concentration was varied from one to thirty atomic percent. The plateaus observed in this study for the copper-titanium/alumina system may correspond to two different titanium oxide reaction products. The reaction products were not identified in this study. However, several reaction products with distinctly different colors were observed under the light microscope during the fractional coverage measurements for the samples with compositions corresponding to the transition region of the contact angle curves. An example of the formation of two different reaction products on the same sample is shown in Figure 16. The two phases appeared rusty-orange and dark purple under the light

microscope. For the majority of the samples displaying dual reaction products, parallel bands of each reaction product, similar to those shown in Figure 16, were observed.

The resulting equilibrium solid-liquid interfacial energies (γ_{SL}^{II}) are plotted in Figure 17. The γ_{SL}^{II} curves had the same general shape as the contact angle curves. The interfacial ranged from approximately 2320 mJ/m^2 for pure copper at 1120°C to between 35 and 150 mJ/m^2 for titanium concentrations above ten weight percent. For all three temperatures, γ_{SL}^{II} decreased with increasing temperature although the decrease was relatively small for the higher titanium concentrations.

The equilibrium contact angle (θ) and γ_{SL}^{II} values were also calculated for copper-20 w/o titanium alloys in contact with alumina as a function of temperature and sample configuration. The results are listed in Table 3. Unlike what was found in previous studies [4-7,9,14-16], the contact angle does not decrease significantly with temperature. Instead, these values are approximately constant from 1100 to 1300°C.

Table 3: The equilibrium contact angle (θ) and the solid-liquid interfacial energy (γ_{SL}^{II}) for copper-20 w/o titanium on polycrystalline alumina.

T (°C)	Starting Configuration	q (°)	γ_{SL} (mJ/m^2)
1000	stacked	33.5	355
1100	stacked	16.2	117
1200	pre-alloyed	24.1	128
	pre-alloyed	12.9	42
	stacked	10.6	30
	stacked	6.6	15
	Cu(l) on Ti(s)	8.1	20
	Cu(l) on Ti(s)	12.9	41
1300	stacked	12.1	-17

Although conventional sessile drop tests cannot be used to analyze the isothermal spreading kinetics, these tests can be used to evaluate the equilibrium contact angle and the solid-liquid interfacial energy at long times. (Assuming oxidation of the drop does not hinder spreading, and depletion of the liquid metal by reaction and volatilization does not significantly decrease the drop volume). The similar contact angle and solid-liquid interfacial values obtained at 1200°C for the three starting configurations support this conclusion.

With the exception of the 1000°C and 1300°C tests, the γ_{SL} values are very small (less than 150 mJ/m^2) and positive. (The small negative value for 1300°C reflects the uncertainties in the calculation.) These results support the hypothesis that the formation of a TiO$_x$ reaction product at the interface is the major factor in the improved wetting and spreading of these alloys on alumina. Very low values of solid-liquid interfacial energy cannot be obtained between a metallic liquid and an ionocovalent solid because of the differences in bond character. However, oxides of titanium are known to take on a metallic character [25]. A liquid metal in contact with a metallic solid could have very similar bonding and a much lower interfacial energy.

The initial contact angles for copper-20 w/o titanium alloys on alumina (upon dissolution at 1200°C) were 105 and 97 degrees for the Cu(l) on Ti(s)/alumina sample configuration. These values suggest that only small improvements in the wettability of alumina are obtained by adding titanium to copper until a reaction occurs. Once reaction occurs, the contact angle is actually the contact angle of copper-titanium on a titanium oxide with alumina surrounding the drop and not the contact angle of copper-titanium on alumina. The contact angle of high purity copper on polycrystalline alumina at 1200°C and an oxygen partial pressure of approximately 10^{-5} Pa is 116 degrees [20] which is only 11 to 19 degrees higher than the initial contact angle for copper-20 w/o titanium on alumina at this temperature and oxygen partial pressure. The contact angle after the titanium-alumina reaction is complete is 90 to 100 degrees lower than either of these angles.

The γ_{SL}^1 values were estimated assuming initial contact angles of pure copper on alumina. For this study, a contact angle of 116 ± 4 degrees was used for pure copper on

polycrystalline alumina because the data was obtained using the same furnace set-up and atmosphere control as the current study [20].

The high initial contact angles obtained for copper-20 w/o titanium alloys on alumina support this assumption. The same γ_{SV} and γ_{LV} values used in the γ_{SL}^{II} calculation were used in this calculation. The resulting γ_{SL}^{I} value were approximately 2317 mJ/m^2 at 1120°C, 2347 mJ/m^2 at 1160°C and 2377 mJ/m^2 at 1200°C.

b. Silver-Titanium/Alumina Data

The equilibrium contact angle for the four silver-titanium/alumina samples is shown in Figure 18. All of the 1100°C samples had a non-wetting contact angle between 93 and 120 degrees while the 1000°C sample with a five weight percent titanium concentration had an 85 degree contact angle. No wetting transitions or plateaus were observed but this was expected since the titanium concentrations were below the critical titanium concentrations where a transition occurred in the copper-titanium/alumina system. Higher titanium concentrations could not be tested in this temperature range because higher concentrations result in a solid plus liquid two phase mixture (see Figure 3) The γ_{SL}^{II} values were calculated based on the contact angle are plotted in Figure 19. In this composition range, γ_{SL}^{II} of between 1460 and 1935 mJ/m^2 were obtained. These values are similar to the interfacial energy values obtained for copper-titanium alloys on alumina at 1120°C with corresponding titanium concentrations.

The γ_{SL}^{I} values were estimated assuming initial contact angles of pure silver on alumina were obtained. Limited data is available for the contact angle of pure silver as a function of temperature [26,21-27]. The data that is available shows a strong dependence on oxygen partial pressure, surface roughness, and test method. As a first approximation, the contact angle of 144 degrees at 1000°C reported by MacDonald and Eberhardt [22] and the experimentally determined contact angle of 119 degrees at 1100°C were used in the estimation of γ_{SL}^{I}.

The previous contact angles correspond to $_{SL}^{I}$ values of 2337 mJ/m^2 at 1000°C and 1935 mJ/m^2 at 1100°C.

3.   Determination of Reaction Rate Constant, k

A necessary parameter for the evaluation of the proposed spreading models is the reaction rate constant, k. It should be stressed that this is the rate constant for the formation of a monolayer of reaction product on the surface of the ceramic substrate which is not the same as the rate constant for parabolic thickening. In general, the monolayer formation rate constant should be greater than the parabolic rate constant since the surface layer must form before the reaction product can significantly thicken. The reaction rate constant values would only be similar if the surface nucleation rate is very slow and the bulk diffusion rates of the reacting species are very high. In this case, a few islands of reaction product will nucleate and grow into the substrate. The completion of the surface monolayer will then occur by the growing together of the large product "islands" and the growth rate would be approximately the same in all directions.

While the values for the parabolic thickening rate have been reported for several systems the rate of surface coverage has not been quantitatively studied. This is because the commercially successful alloys have very rapid coverage rates and thus one hundred percent coverage is achieved in only a few seconds. Therefore, these k values must be experimentally determined. In this study, an attempt was made to measure k as a function of temperature and composition for the same systems for which spreading data were generated.

First, utilizing the improved sessile drop technique, an experiment was performed for verification of product nucleation and growth at the ceramic-metal interface. Molten copper was dropped onto solid titanium stacked on alumina at approximately 1200°C. The liquid metal was allowed to spread for approximately 120 seconds. After cooling, the metal was dissolved using nitric and hydrochloric acids and the alumina surface was examined using optical microscopy.

The microstructure at several metal/ceramic contact radii is shown in Figure 20. The initially covered surface is completely covered with reaction product. Outside of the initial radius, islands of reaction product are observed. The fraction of the surface covered with reaction product decreases as the relative coverage time decreases (as the radial distance increases). Finally, no reaction product was observed outside of the liquid

metal/substrate contact area. The presence of reaction product islands beneath the drop supports reaction product nucleation and growth. The absence of reaction product ahead of the drop refutes a metal volatilization and condensation mechanism.

The fractional coverage as a function of time for an Avrami-type surface nucleation and growth mechanism (2-D) is:

$$X = 1 - \exp(-kt)^2 \tag{4}$$

This equation can be rearranged to solve for k:

$$k = \exp\left\{\frac{\ln\left[\ln\left(\frac{1}{1-X}\right) - 2\ln t\right]}{2}\right\} \tag{5}$$

If the fractional coverage is known for a given time, the reaction rate constant can be calculated. In this study, pairs of fractional coverage time data for copper-titanium and silver-titanium alloys on alumina were used to calculate k. At each composition and temperature, the mean value of k and the standard deviation of the mean were calculated.

Several factors were considered in the determination of k. First, the spreading rate is extremely sensitive to atmospheric conditions. Therefore, X(t) was measured using the same furnace and atmospheric conditions as the spreading radius measurements. Second, the same driving force as the spreading drop should be achieved. This precludes the use of an immersion method (dipping the substrate into molten metal) since the immersion free energy change differs from the spreading free energy change by an $(A \gamma_{LV})$ term. Therefore, the same sessile drop geometry used for the spreading measurements was used for the X(t) measurements.

a. Copper-Titanium/Alumina System

The fractional coverage of an alumina substrate by reaction product versus time for copper-titanium alloys is shown in Figures 21-31. The error bars represent the standard deviation of the mean for ten measurements performed for each sample condition. The three different symbols on each plot represent results from three different sample runs. There is considerable scatter in the data but the increase in fractional

coverage with time is still apparent. Several of the plots show a clear increase in fractional coverage with time. For example, 10 w/o titanium at 1160°C (Figure 27), 20 w/o titanium at 1160°C (Figure 28), and 10 w/o titanium at 1200°C (Figure 30) all exhibit a continuous increase in coverage with increasing time. Other test conditions displayed an increase in coverage with time for a given sample but with a poor correlation between samples. Samples exhibiting this type of behavior are 5 w/o titanium at 1120°C (Figure 22), 7 w/o titanium at 1120°C (Figure 23), 10 w/o titanium at 1120°C (Figure 24), 20 w/o titanium at 1120°C (Figure 25), 5 w/o titanium at 1160°C (Figure 26), 5 w/o titanium at 1200°C (Figure 29) and 20 w/o titanium at 1200°C (Figure 31). Only a 3 w/o titanium samples at 1120°C (Figure 21) showed a significant decrease in coverage with time and this was only a single data point.

Representative fractional coverage micrographs are shown in Figure 32. The reaction product initially forms small islands (Figure 32a). The islands grow together (Figure 32b) until eventually islands of non-reacted alumina are surrounded by reaction product (Figure 32c). Finally, the entire surface is covered by reaction product (Figure 32d). The large standard deviation in some of the fractional coverage measurements is partially due to the non-uniform growth of the islands. The reaction product islands or alumina islands shown in figures 32b and 32c can be very large and are randomly dispersed in a given coverage region.

Two other coverage anomalies are shown in Figure 33. First, for some samples, the fractional coverage is greater at the outer radius of a given coverage region (Figure 33a). It appears that the drop sometimes takes a relatively large step forward, and the nucleation and growth process starts at the outer edge of the drop and moves inward. In several cases, multiple rings of this type were observed beneath the drop. Also, surface irregularities appear to influence the uniformity of the surface coverage. On several samples, a nearly circular region was observed where the fractional coverage was lower inside the circle and greater at the edge of the circle (Figure 33b and c). The circle is hypothesized to be an artifact from the processing or inspection of the alumina plates. It is further hypothesized that edge of the circular region acts as a non-heterogeneous nucleation site while the circular region has fewer nucleation sites than the base alumina

substrate. This type of behavior supports the proposed nucleation and growth mechanism. If evaporation/condensation ahead of the drop controlled spreading, then a uniform coverage would be expected beneath the drop.

Based on the above X(t) data, the reaction rate constant was calculated from Equation 107. The average k-values and the standard deviation of the mean for the copper-titanium/alumina system are listed in Table 4. The k values ranged from 0.012 to 0.036 s^{-1}. The standard deviation of the mean was very large. In one case (5 w/o Ti at 1200°C) it was larger than k itself.

Table 4: The average surface reaction rate constant (k) for copper-titanium alloys on polycrystalline alumina. The uncertainties are the standard deviation of the mean.

T(°C)	Ti (w/o)	k (s^{-1})
1120	3	0.012 ± 0.007
1120	5	0.014 ± 0.006
1120	7	0.029 ± 0.016
1120	10	0.017 ± 0.016
1120	20	0.023 ± 0.017
1160	5	0.022 ± 0.016
1160	10	0.036 ± 0.004
1160	20	0.020 ± 0.013
1200	5	0.022 ± 0.027
1200	10	0.016 ± 0.005
1200	20	0.043 ± 0.015

b. Silver-Titanium/Alumina System

The fractional coverage versus time for silver-titanium alloys on alumina is shown in Figure 34. The error bars represent the standard deviation of the mean for fifteen measurements at each test condition. All four test conditions exhibited similar coverage behavior. The fractional coverage was very small (less than five percent) for the first 300 seconds. The coverage then increased with increasing time. The behavior was similar to the copper-titanium/alumina fractional coverage data except the coverage rate was much slower for the silver-titanium/alumina system. While greater than 99 percent coverage was frequently obtained in less than 100 seconds for copper-titanium alloys on alumina, complete reaction product coverage was not obtained for silver-titanium alloys on alumina after 600 seconds.

Representative fractional coverage micrographs are shown in Figure 35. The island formation is similar to the islands formed for copper-titanium alloys on alumina except that a more needle-like product growth is observed for the silver-titanium alloys on alumina.

For this system, the k values ranged from 0.0012 to 0.0027 s^{-1} which are an order of magnitude smaller then the copper-titanium/alumina k values. The average k values and the standard deviation of the mean are given in Table 5.

Table 5:   The average surface reaction rate constant (k) for silver-titanium alloys on polycrystalline alumina. The uncertainties are the standard deviation of the mean.

T(°C)	Ti (w/o)	k (s^{-1})
1000	5	0.0016 ± 0.0010
1100	1	0.0021 ± 0.0010
1100	3	0.0012 ± 0.0011
1100	5	0.0027 ± 0.0015

c. Variable Reaction Rate Exponent (n) Values

In all of the previous k calculations, the reaction rate exponent (n) in Equation 107 was assumed to be equal to 2. A more general solution of this equation for k is:

$$k = \exp\left\{\frac{\ln\left[\ln\left(\frac{1}{1-X}\right) - n\ln t\right]}{n}\right\} \qquad (6)$$

The validity of the n equal to 2 assumption can be tested by varying n and solving for k. If n=2 is the best fit for k, then it should have the lowest standard deviation of the mean. The effect of variations in n on k were studied for copper-20 w/o titanium alloy samples on alumina at 1120°C. This test condition was chosen because a large number of fractional coverage versus time data pairs were available (11 total). The reaction rate exponent was varied form 1.00 to 3.00 by increments of 0.25 along with an n-value of 4.00. For each n-value, the mean value of k and its standard deviation were determined. A summary of the values is given in Table 6. For n between 1.50 and 3.00, the standard deviation is approximately a constant value (0.017 to 0.018). The smallest standard deviation for k is obtained at n equal to 2.00 ($\pm$ 0.0017) but this is extremely close to the standard deviations obtained for n equal to 1.50, 1.75, 2.25, 2.75 and 3.00 ($\pm$ 0.018). For n-values outside of this region, the standard deviation increases slightly. Based on these results, n equal to 2 is a reasonable assumption but values of n from 1.50 to 3.00 could used.

Table 6:   Values for the surface reaction rate constant (k) obtained by varying n at 1120°C for a copper-20 w/o titanium alloy on alumina. The uncertainty of k is the standard deviation of the mean.

n	$k\ (s^{-1})$
1.00	0.025 ± 0.026
1.25	0.023 ± 0.020
1.50	0.023 ± 0.018
1.75	0.023 ± 0.018
2.00	0.023 ± 0.017
2.25	0.023 ± 0.018
2.50	0.023 ± 0.018
2.75	0.023 ± 0.018
3.00	0.024 ± 0.018
4.00	0.024 ± 0.019

C. DISCUSSION

In this section, the resulting radius versus time curves predicted by the model are presented. The theoretical curves generated using the computer model are compared to the experimentally generated isothermal data. The significance of the results and the shortcomings of the comparison are discussed.

In addition, the utilization of the in situ videotaping technique revealed major differences in the spreading behavior of a reactive liquid metal drop on a ceramic substrate depending on the initial sample configuration. An qualitative analysis of the melting and spreading behavior of the three different sample configurations is presented. The analysis gives further insight into the mechanisms governing spreading.

1. Theoretical Model Versus Experimental Data

The theoretical model was evaluated for both the copper-titanium/alumina and silver-titanium/alumina systems using the computer model previously developed. For each test condition, the computer model was evaluated three times. The average γ_{SV}, γ_{LV}, γ_{SL}^{I} and γ_{SL}^{II} were used in all three runs while three different k values were evaluated. The three different k values evaluated were the mean value of k, an upper bound value of k, and a lower bound value of k. The upper bound of k was the mean value of k plus the standard deviation of the mean and the lower bound was the mean value minus the standard deviation. For the case where the standard deviation was greater than the mean, the smallest k-value obtained for that test condition was used for a lower bound. The errors in V, γ_{SV}, γ_{LV}, γ_{SL}^{I} and γ_{SL}^{II} were not incorporated into the evaluation of the model, since they only change the initial and starting radii and they do not affect the general shape of the curves.

The computer model and the experimental spreading data were compared for eleven conditions in the copper-titanium/alumina system and for two conditions in the silver-titanium/alumina system.

a. Copper-Titanium/Alumina System

While the model was tested for both the copper-titanium/alumina and silver-titanium/alumina systems, the best comparisons were made for the copper-titanium alloys with high titanium concentrations on alumina because of the large changes in spreading diameter. The predicted spreading radius versus time curves (with upper and lower limits) for the copper-titanium/alumina system along with the corresponding experimental data are plotted in Figures 36 to 49. The error bars represent the uncertainty in the measurement of the spreading radius. For curves displaying large changes in radii, the error bars are not visible on the graphs because they are smaller than the data points. In general, the experimental data match the shape of the predicted curves but the experimental data do not always fall within the bounds of the theoretical model predictions. An excellent correlation is obtained at 1160°C for copper-5 w/o titanium on alumina (Figure 44). Relatively good fits are obtained at 1120°C for 3 w/o titanium and 20 w/o titanium (Figures 36 and 43); at 1160°C for 20 w/o titanium (Figure 46); and at 1200°C for 20 w/o titanium (Figure 48). At 1120°C for 10 w/o titanium and at 1200°C for 5 w/o titanium (Figures 42 and 47, respectively), the experimental data points are between the theoretical results for the average k and the lower bound k but these two sample conditions exhibited very large uncertainties in k. The experimental data points for the remaining four conditions (Figures 37, 38, 45 and 49) were usually below the theoretical result for the lower bound k. A condition where all of the data points are below the theoretical lower bound suggests that either the model is incorrect or that the surface reaction rate is lower than the calculated value.

b. Silver-Titanium/Alumina System

The predicted spreading radius versus time curves for the silver-titanium alloys on alumina are shown in Figures 50 and 51. The corresponding experimental spreading data are also shown on these curves. The error bars again represent the uncertainty in the measurement of the spreading radius. Experimental data for the silver-1 w/o titanium system at 1100°C compared rather poorly with the theoretical model while data for the silver-3 w/o titanium system displayed a close fit between the experimental data and the

theoretical curves. However, the small changes in the spreading radii with time hinder the ability to compare the experimental and theoretical results. Although experimental spreading radius data were available for four test conditions, only two were analyzed. The silver-5 w/o titanium tests at 1000 and 1100°C were not evaluated because the radius changes were less than the uncertainty in the radius measurements, and because squares of pure titanium were found inside the metal drops during dissolution of the drops for fractional coverage measurements. The presence of pure titanium suggests that the metal drops were within the liquid plus solid two-phase field, which invalidates the density, geometry and titanium concentration assumptions used in evaluating the spreading model.

c. Validity of Model

Based on the theoretical spreading curves and the spreading data presented for copper-titanium and silver titanium alloys on alumina, the proposed spreading model can not be conclusively verified, but the results support the mechanism proposed in the model. The theoretical curves exhibit general shapes similar to the experimental curves, and the experimental and theoretical spreading times are of the same order of magnitude. Interfacial reaction product island development and growth micrographs obtained during the determination of the fractional coverage as a function of time further support the proposed spreading model.

Several factors hinder the conclusive verification of the model. First, the model is only a first approximation, and to simplify the model, homogeneous reaction product nucleation and growth was assumed. However, the alumina surfaces were heterogeneous, containing both grain boundaries and surface defects. The preferred growth regions and preferred growth directions shown in Figures 16, 32, 33 and 35 illustrate the non-homogeneous nature of the reaction product formation. For non-homogeneous nucleation and growth, slower reaction rates would be expected at longer times (after the preferred nucleation sites are exhausted), and the fractional coverage with time would deviate from a simple two-dimensional Avrami-type equation.

Conclusive verification of the model was also hindered by experimental reproducibility problems. The theoretically predicted spreading rates are exponentially

related to the reaction rate constant (k) and large deviations in k were obtained. In addition, multiple spreading tests at the same test condition also displayed large experimental variability (Figures 43 and 49).

Another difficulty encountered in the evaluation of the model was the uncertainty in the interfacial energy value inputs used to evaluate the computer model. The reaction product- liquid interfacial energy value (γ_{SL}^{II}) was determined based on the final spreading radius, which results in a forced match between the final theoretical and experimental radii. However, the uncertainty of $\pm$ 60 to 80 mJ/m^2 in the other interfacial energy values could significantly shift the initial radius, and thus the overall curve. The model could be more closely scrutinized if more reliable interfacial energy data (and especially totally independent γ_{SL}^{II} values) were available, but current experimental and theoretical capabilities preclude the generation of more reliable interfacial energy data for reactive metal/ceramic systems.

d. Importance of Initial Sample Configuration

The initial spreading kinetics can be qualitatively analyzed based upon the time at which the first liquid forms, and upon the titanium concentration of the liquid during the thermal cycle. Both factors are strongly influenced by the starting sample configuration. In this section, the proposed melting and dissolution paths for the three initial sample configurations are discussed for the copper-titanium/alumina system. Frames from the in situ videotapes are utilized to support the proposed melting and dissolution mechanisms.

e. Pre-Alloyed Copper-Titanium Alloy

According to the binary copper-titanium phase diagram (Figure 2) [28], copper-20 w/o titanium should be completely molten at 885°C. However, in this study, melting was not observed at temperatures less than approximately 1000°C. This may have been due to the oxide layer formed on the outside of the metal sample. When a liquid forms, it is not outwardly visible until the thermal expansion of the liquid drop breaks the oxide layer. Once this occurs, the liquid has the same composition as the initial solid (weight fraction, $X_{Ti} = 0.20$) which corresponds to a mole fraction of approximately 0.26. For this

configuration, non-isothermal spreading was observed for between 2.2 and 3.4 ks, while the sample was heated from approximately 1000°C to 1200°C.

The sessile drop morphology for a typical spreading cycle is shown in Figure 52 for a pre-alloyed copper-titanium alloy on alumina at 1200°C. The camera was tilted slightly along the tube furnace axis to obtain a clearer contrast between the metal and the substrate. The alloy melted before 1200°C and formed a non-wetting contact angle (Figure 52b). Before 1200°C was attained, the drop had already achieved a wetting contact angle (Figure 52c-d) and considerable spreading had already occurred before 1200°C was attained (Figure 52e). Finally, the drop stopped spreading and eventually formed a pancake-like shape (Figure 52f).

f. Titanium Stacked on Copper

The melting of solid titanium in contact with solid copper is more complicated, but it can still be qualitatively explained by the binary phase diagram (Figure 2). In this system, the first liquid formed has a composition between two intermetallics, Ti_2Cu + TiCu. This liquid forms at the copper-titanium interface. Then as the copper and titanium mutually dissolve into the liquid, the copper concentration increases until only CuTi remains and the liquid resolidifies. In reality, the resolidification of the drop was not observed because of the slower dissolution kinetics of the solid copper by the liquid alloy relative to the dissolution of the solid titanium by the same liquid. The experimentally observed dissolution and melting path is shown schematically in Figure 53. First, a liquid formed between the copper and titanium at approximately 982°C. The actual temperature at which this was observed was higher than that predicted from the phase diagram because the layer must be nearly 0.2 millimeters thick before it can be easily resolved. Next, the liquid front moved into both the copper and the titanium. Surprisingly, the titanium dissolved more quickly than the copper and eventually there was only a copper-titanium liquid on top of a solid piece of copper. As more solid copper dissolved, the liquid volume increased and the liquid flowed off the solid copper. At this point, a titanium-rich liquid contacted the alumina substrate and began spreading (at approximately 1120°C). Finally, at 1140°C, the entire drop was liquid.

While the difference between the temperature at which liquid first contacted the alumina substrate and the isothermal holding temperature was somewhat less than that for the pre-alloyed samples, the extent of spreading was somewhat greater. This result was unexpected because the time required to reach the isothermal holding temperature after the first liquid was formed was similar for both the stacked and pre-alloyed sample configuration. (The stacked samples took 2.0 and 3.0 ks to equilibrate, while the pre-alloyed samples required 2.2 and 3.4 ks.) However, the stacked samples initially formed a titanium-rich liquid with a titanium mole fraction as high as 0.56. Assuming the activity is to be approximately equal to the mole fraction, one can conclude that the stacked sample configuration resulted in an initial titanium activity as high as 0.56. That activity decreased with time to 0.26 as the drop became completely molten. In contrast, the pre-alloyed samples constantly maintained a titanium activity of 0.26 in the liquid. The higher initial titanium activity of the stacked sample configuration could explain the more rapid spreading observed during the heat-up cycle.

Representative photographs from the spreading cycle for a copper-20 w/o titanium alloy at 1200°C for a titanium stacked on copper initial test configuration are shown in before the copper was completely dissolved and most of the spreading was finished before 1200°C was attained.

g. Liquid Copper on Solid Titanium

When the liquid copper was introduced to the solid titanium at 1200°C, the liquid was always at the desired temperature. (As an aside, the copper always melted at a temperature between 1085 and 1105°C and crept down between the plates and fell at 1200°C. This observation supports the conclusion that it was the formation of an oxide layer and not temperature measurement inaccuracies which led to the higher melting temperatures for the copper-titanium alloy.) The liquid was not at the desired composition until the solid titanium was completely dissolved, but complete dissolution only required 10 to 25 seconds. In addition, the spreading was expected to be slower during dissolution, because the liquid was copper-rich. This resulted in a lower titanium concentration and activity. Thus the isothermal data lost was even less than the 10-to-25-s

dissolution time because the titanium-lean liquid should manifest slower spreading kinetics.

The dissolution of titanium by liquid copper and the formation of a copper-20 w/o titanium alloy on alumina at 1200°C is shown in Figure 55. Utilizing this starting configuration, the copper dissolves the titanium at the desired test temperature in only a few seconds. An initially non-wetting contact angle is achieved. Several steps in the resulting isothermal spreading cycle are shown in Figure 56. At long times, the drop flattens but it is spherical throughout the majority of the spreading cycle.

Overall, the best isothermal kinetics data were obtained by introducing the liquid copper to the solid titanium at the desired test temperature. This resulted in the loss of less than twenty seconds of spreading data while the solid titanium dissolved into the liquid copper. Significant data (on the order of kiloseconds) was lost during the heat-up cycles for both the pre-alloyed and initially stacked metal sample configurations. The worst experimental condition occurred for the stacked metal samples where a high activity, titanium-rich liquid alloy was formed during heating.

D. CONCLUSIONS

A non-empirical theoretical spreading model for reactive metals on ceramics was derived based on the progress of the nucleation and growth of islands of reaction product at the ceramic-metal interface. The spreading radius as a function of time was predicted as a function of time utilizing a computer program to numerically solve for the fraction of surface covered by reaction product with time, based on Avrami-type surface nucleation and growth kinetics. The only inputs to the model were the drop volume, four interfacial energies (substrate/liquid, reaction product/liquid, substrate vapor and liquid/vapor), and the reaction rate constant.

The theoretical curves and the experimental data exhibited a relatively good correlation. A conclusive verification of the model was hindered by large uncertainties in the experimentally determined k values and spreading rate data, and the large uncertainties in the interfacial energy values published in the literature.

Reaction rate constants of between 1×10^{-2} and 5×10^{-2} s^{-1} were obtained for copper-titanium alloys on alumina. Within the uncertainty in the measurements, the k values were not a function of composition and temperature (between 1120° and 1200°C, and 3 to 20 w/o titanium). The k values for silver-titanium alloys were determined to be between 1×10^{-3} and 3×10^{-3} s^{-1}, values which are an order of magnitude lower than the k values obtained for copper-titanium alloys on alumina.

Micrographs of the formation and growth of reaction product islands at the ceramic-metal interface support the proposed spreading mechanism.

The use of the conventional sessile drop configurations was shown to result in the loss of significant spreading kinetics data during the heat-up cycle for reactive metal liquids on ceramic substrates. The non-isothermal spreading of copper-titanium alloys on alumina was avoided by introducing the liquid copper to the solid titanium/alumina at the test temperature. Because relatively rapid spreading began shortly after the metal contacted the substrate, any sample configuration which allowed liquid metal/ceramic contact below the test temperature could not be used to generate true "isothermal" data.

Without these data, the modeling of reactive metal spreading is complicated since time and temperature are both variables.

The determination of the equilibrium contact angle and the solid-liquid interfacial energy was not significantly affected by the starting sample configuration. Regardless of the starting sample configuration, similar contact angles (7 to 24 degrees) were obtained for copper-20 w/o titanium on polycrystalline alumina at 1200°C. The slightly lower energy values for the pre-alloyed copper-titanium samples may have been caused by sample oxidation during heating. However, this is not conclusive because of the relatively large experimental errors in these measurements.

By introducing the liquid copper to the solid titanium at the testing temperature, the contact angle for copper-20 w/o titanium on polycrystalline alumina was found to be 97 to 105 degrees before the titanium reacted with the alumina. This supports the hypothesis that additions of titanium to copper or silver melts do not significantly increase the wettability of copper on alumina, but that the liquid alloy wets a titanium oxide reaction product.
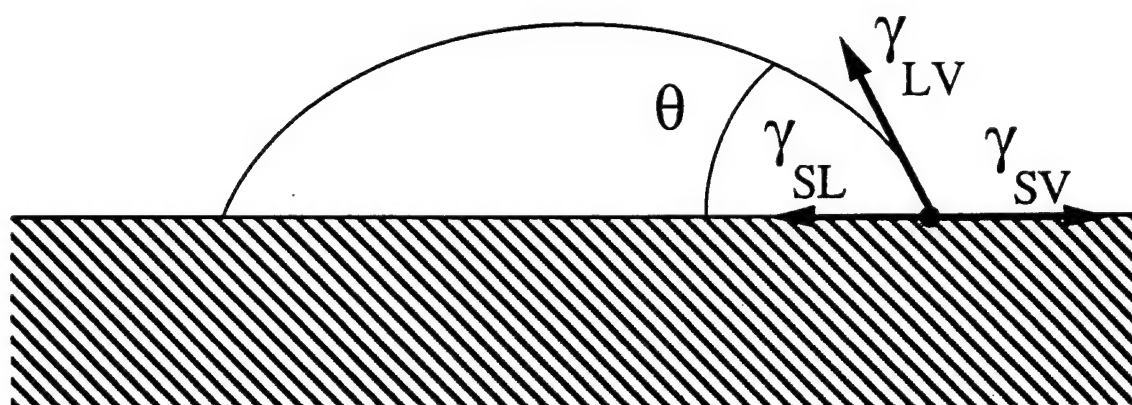
Figure 1: Sessile drop schematic diagram illustrating contact angle and relevant interfacial energies.
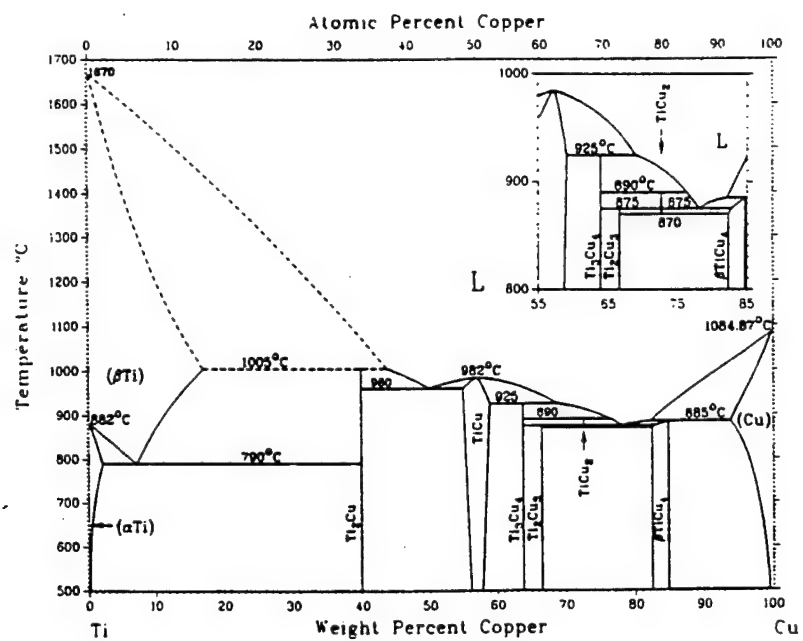
Figure 2: Copper titanium phase diagram (Massalski)
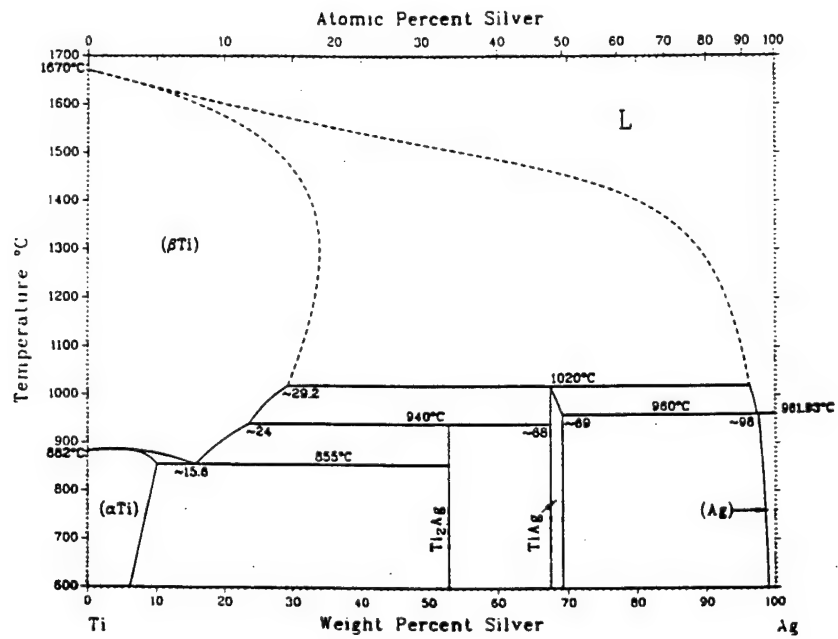
Figure 3: Silver titanium phase diagram (Massalski)
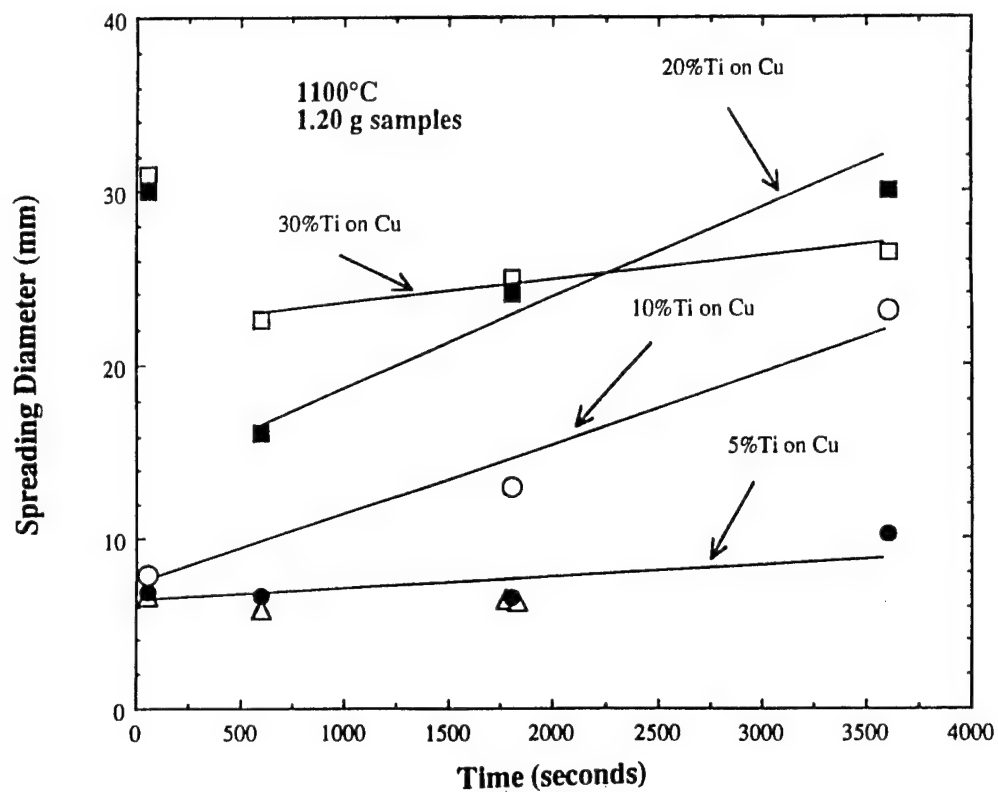
Figure 4: Initial vacuum furnace spreading data for copper-titanium alloys on
alumina.
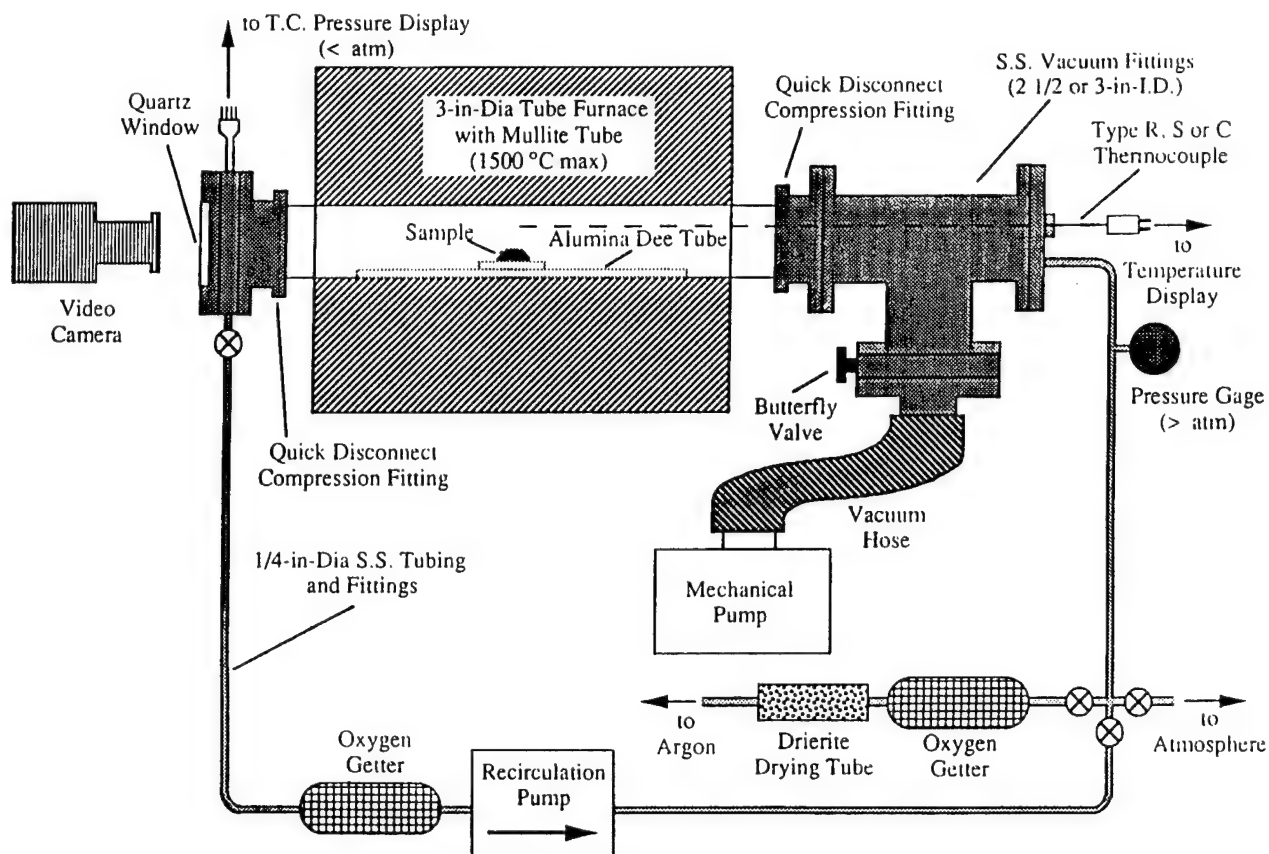
Figure 5: Schematic diagram of experimental set-up used for spreading kinetics data measurements.
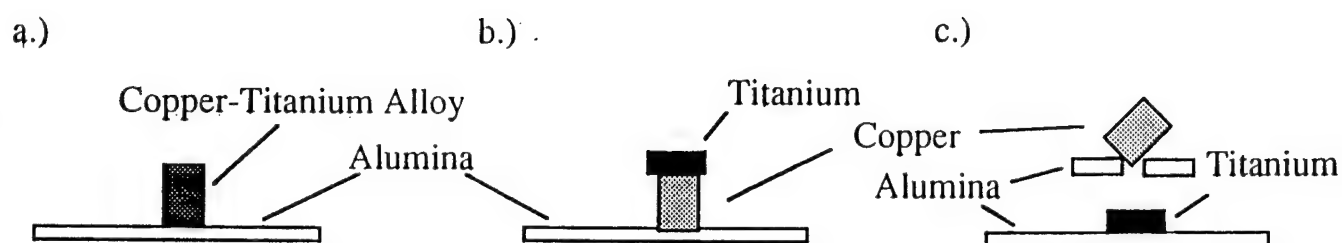
Figure 6: Initial room temperature sample configurations for sessile drop
        experiments(copper-titanium alloys on alumina), a.) pre-alloyed copper-
        titanium on alumina, b.) stacked titanium on copper on alumina, and c.)
        titanium on alumina with copper suspended above titanium.
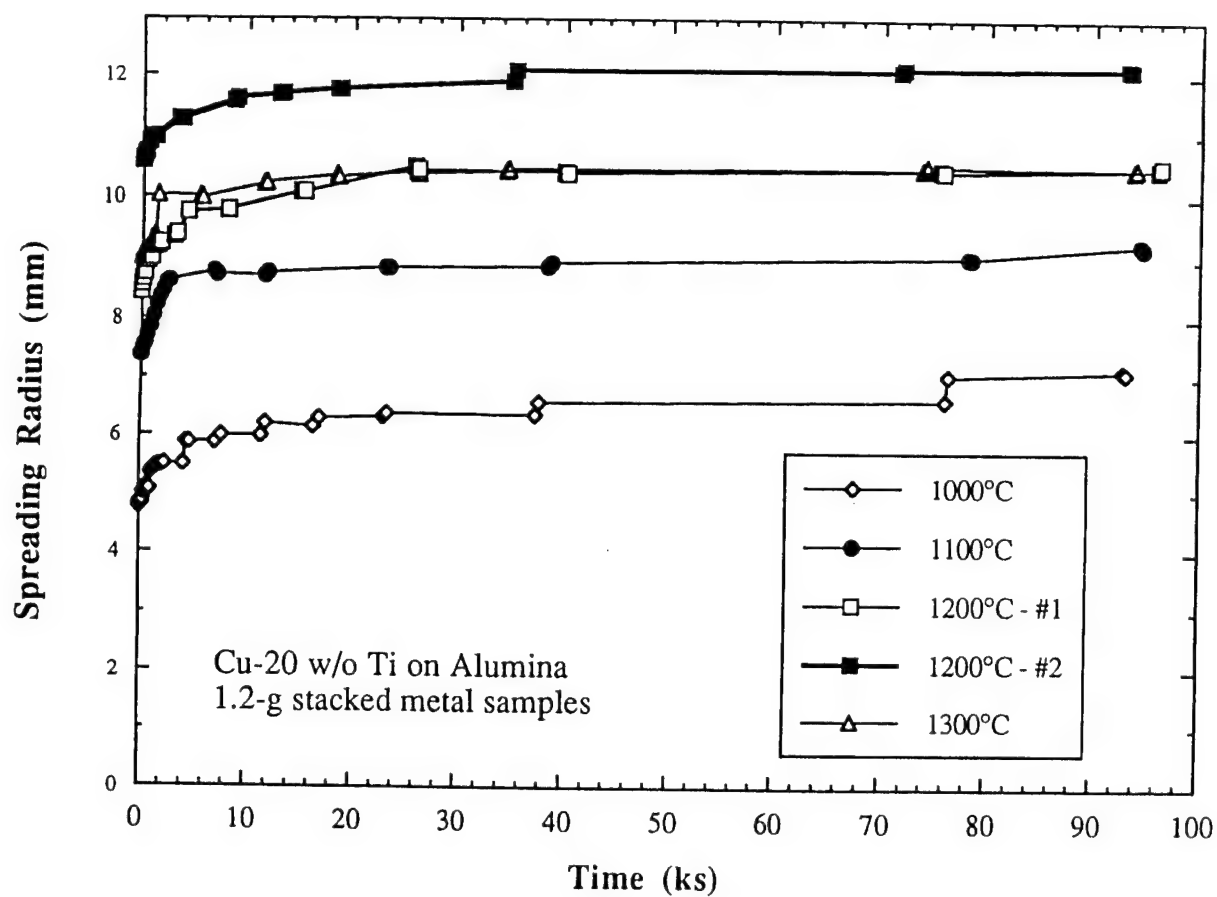
Figure 7: Spreading radius versus time for Cu-20 w/o Ti alloys on polycrystalline
alumina at 1000, 1100, 1200, and 1300°C. The initial sample configuration
was titanium stacked on copper stacked on alumina.
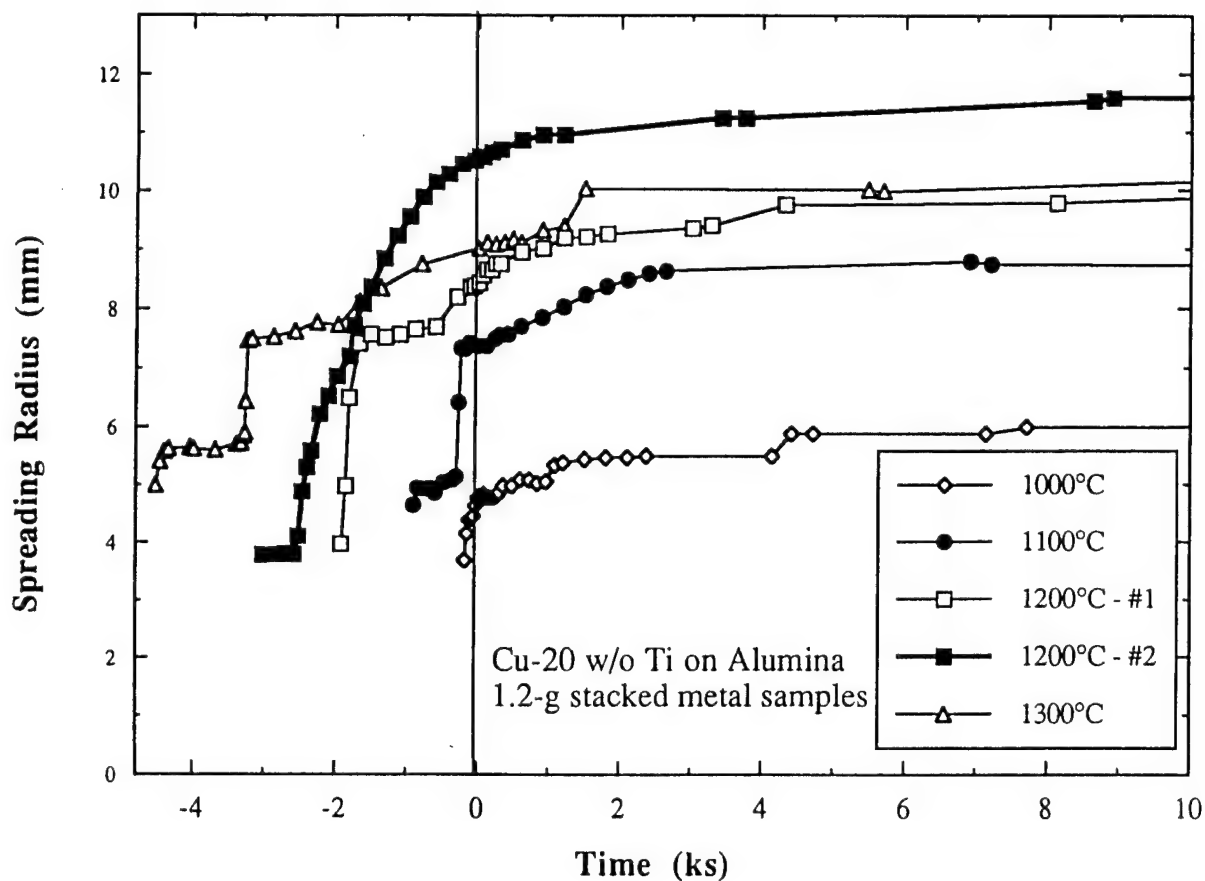
Figure 8: Spreading radius versus time for Cu-20 w/o Ti alloys on polycrystalline
alumina at 1000, 1100, 1200, and 1300°C. The negative times represent the
time required to heat the samples from the temperature at which the first liquid
forms to the isothermal testing temperature. The initial sample   configuration
was titanium stacked on copper stacked on alumina.
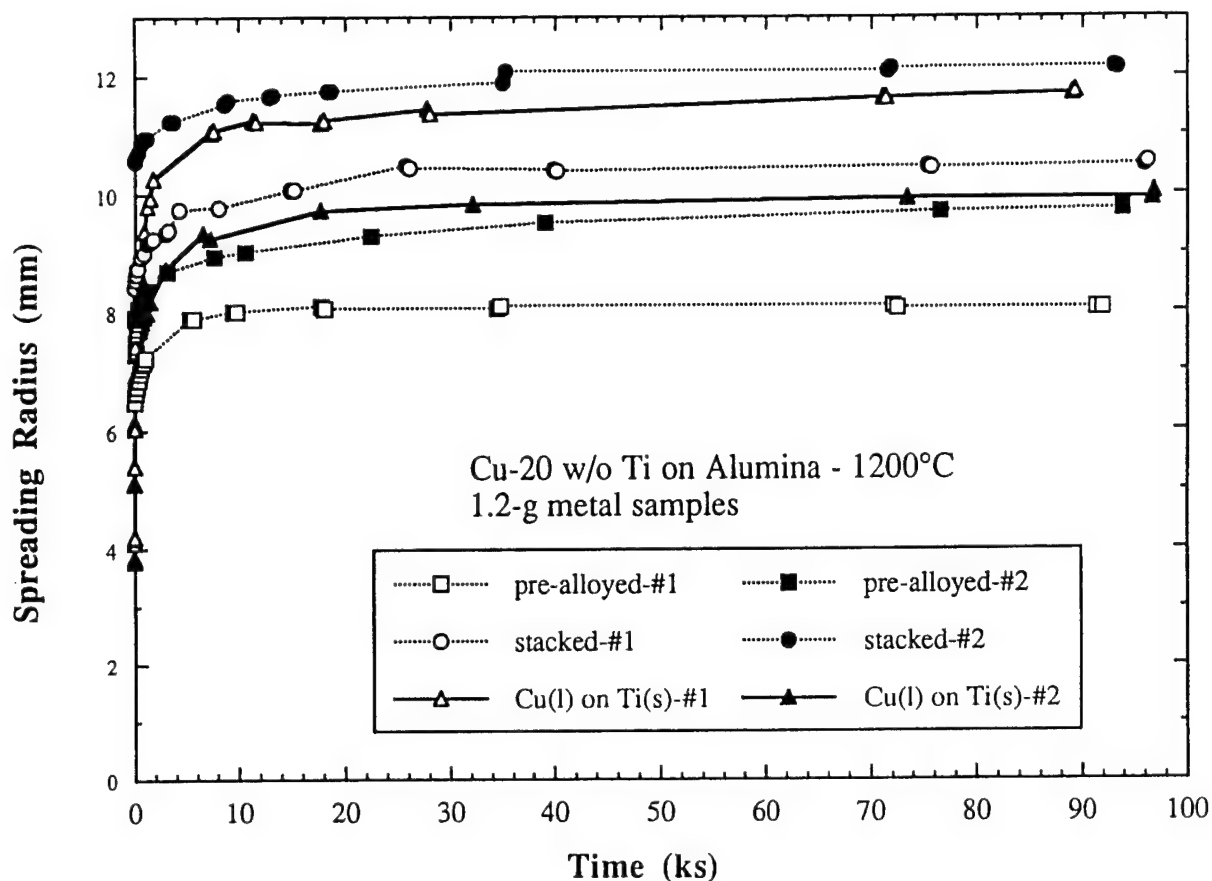
Figure 9: Spreading radius versus time for Cu-wo w/o Ti alloys on polycrystalline alumina at 1200°C. Three starting configurations are plotted: 1) prealloyed Cu-Ti (see Figure 6a), 2) Ti stacked on Cu (Figure 6b), and 3)   Cu(l) on Ti(s) (Figure 6c).
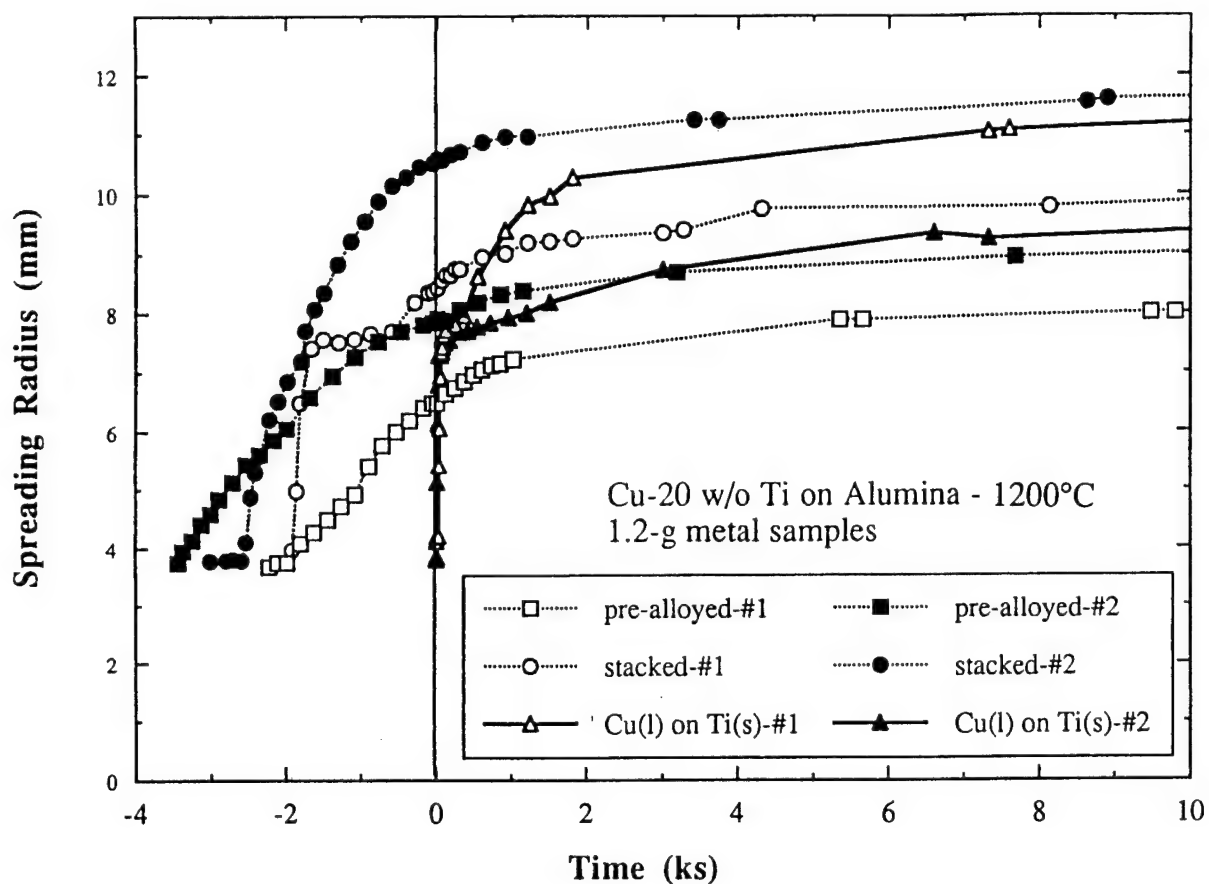
Figure 10: Spreading radius versus time for Cu-20 w/o Ti alloys on polycrystalline
alumina at 1200°C. The negative times represent the time required to heat t
he samples from the temperature at which the first liquid forms to the
isothermal testing temperature. Three starting configurations are plotted: 1)
pre-alloyed Cu-Ti (see Figure 6a), 2) Ti stacked on Cu (Figure 6b), and 3)
Cu(l) on Ti(s) (Figure 6c).
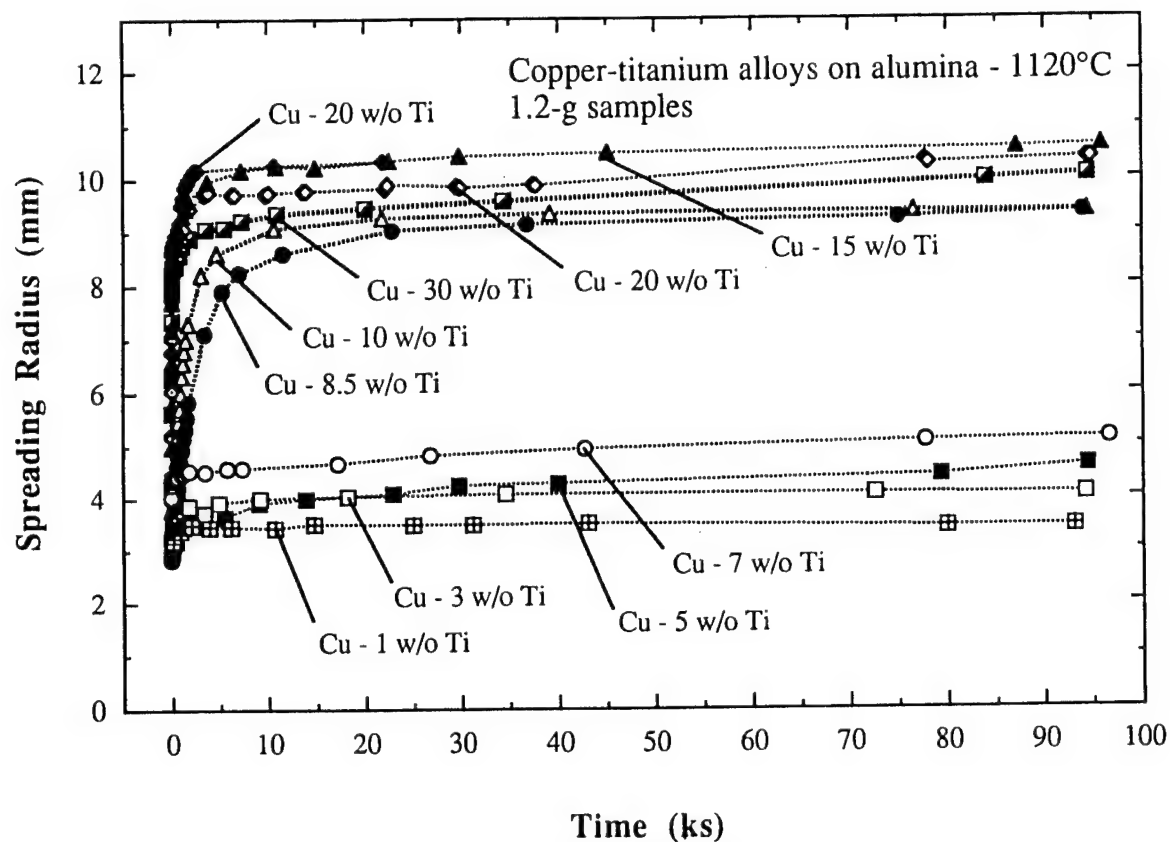
Figure 11: The spreading radius versus time as a function of composition for copper-titanium alloys on alumina at 1120°C. The starting configuration shown in Figure 6c was used.
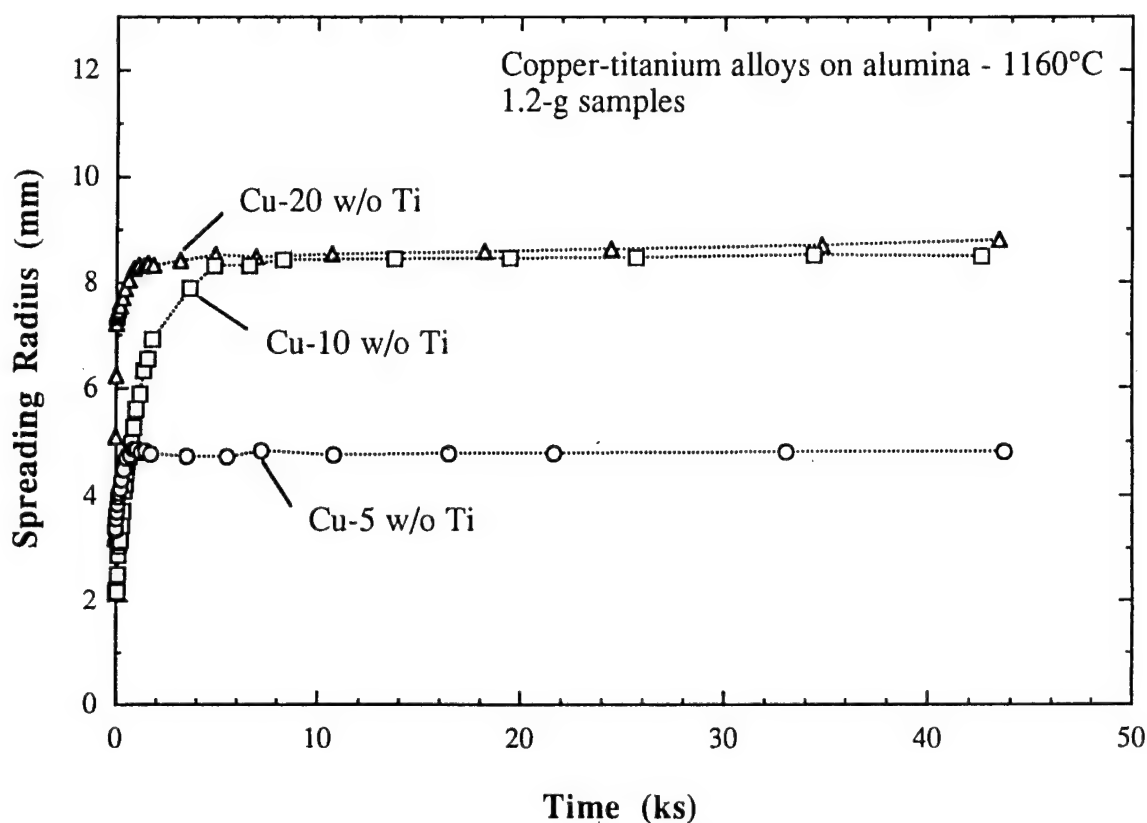
Figure 12: The spreading radius versus time as a function of composition for copper-titanium alloys on alumina at 1160°C. The starting configuration shown in Figure 6c was used.
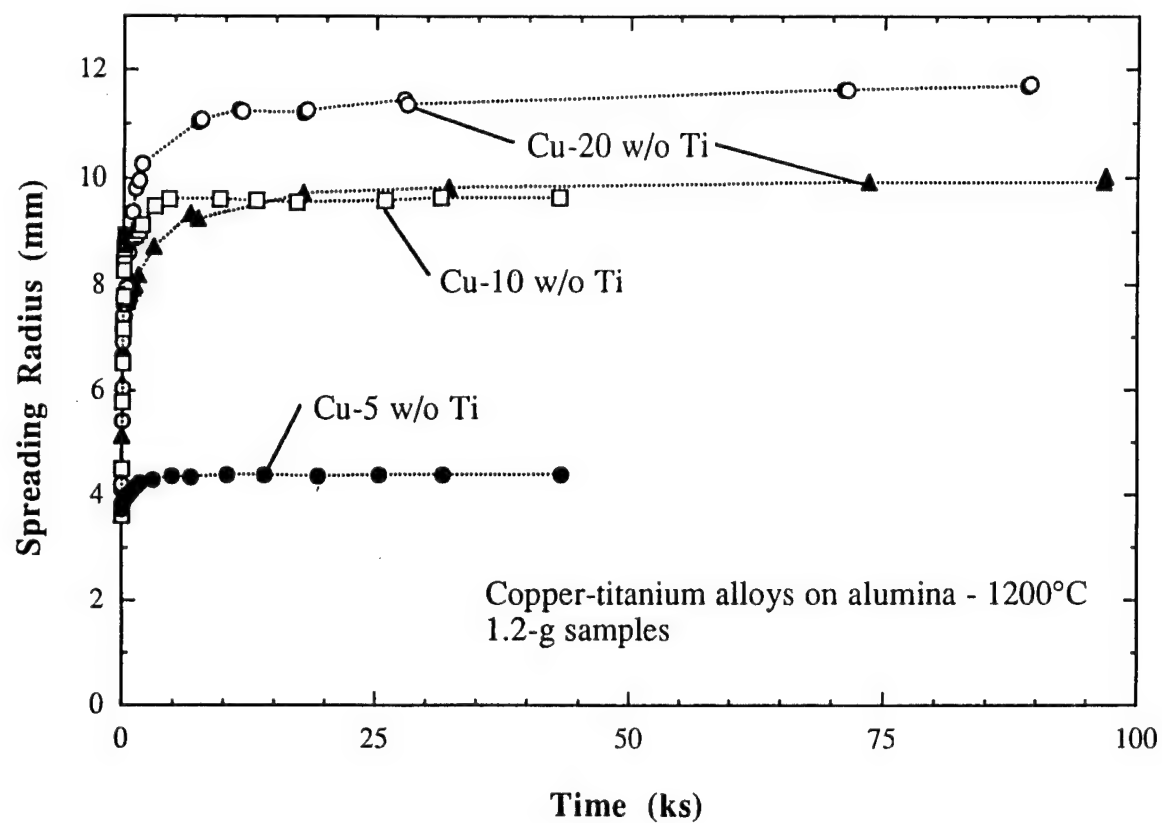
Figure 13: The spreading radius versus time as a function of composition for copper-
titanium alloys on alumina at 1200°C. The starting configuration shown in
Figure 6c was used.
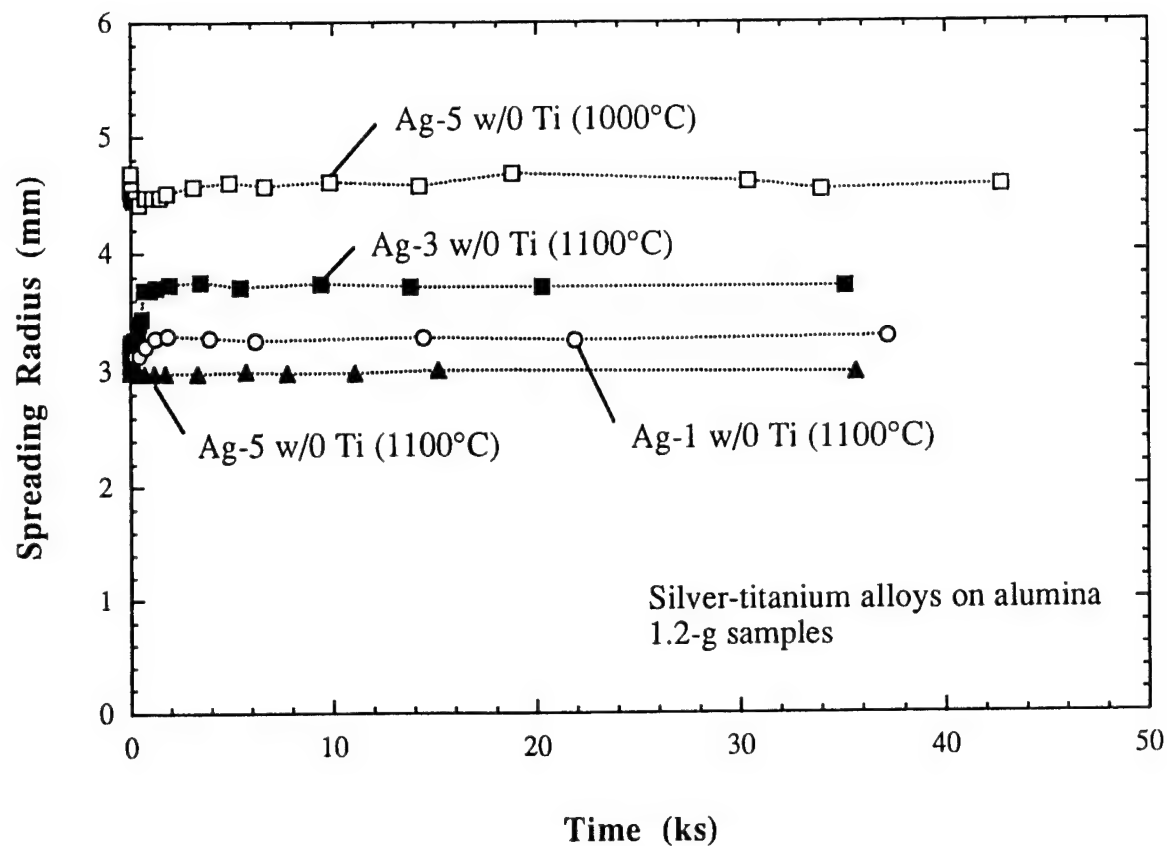
Figure 14: The spreading radius versus time as a function of composition for silver-titanium alloys on alumina at 1000 and 1100°C. The starting configuration shown in Figure 6c was used.
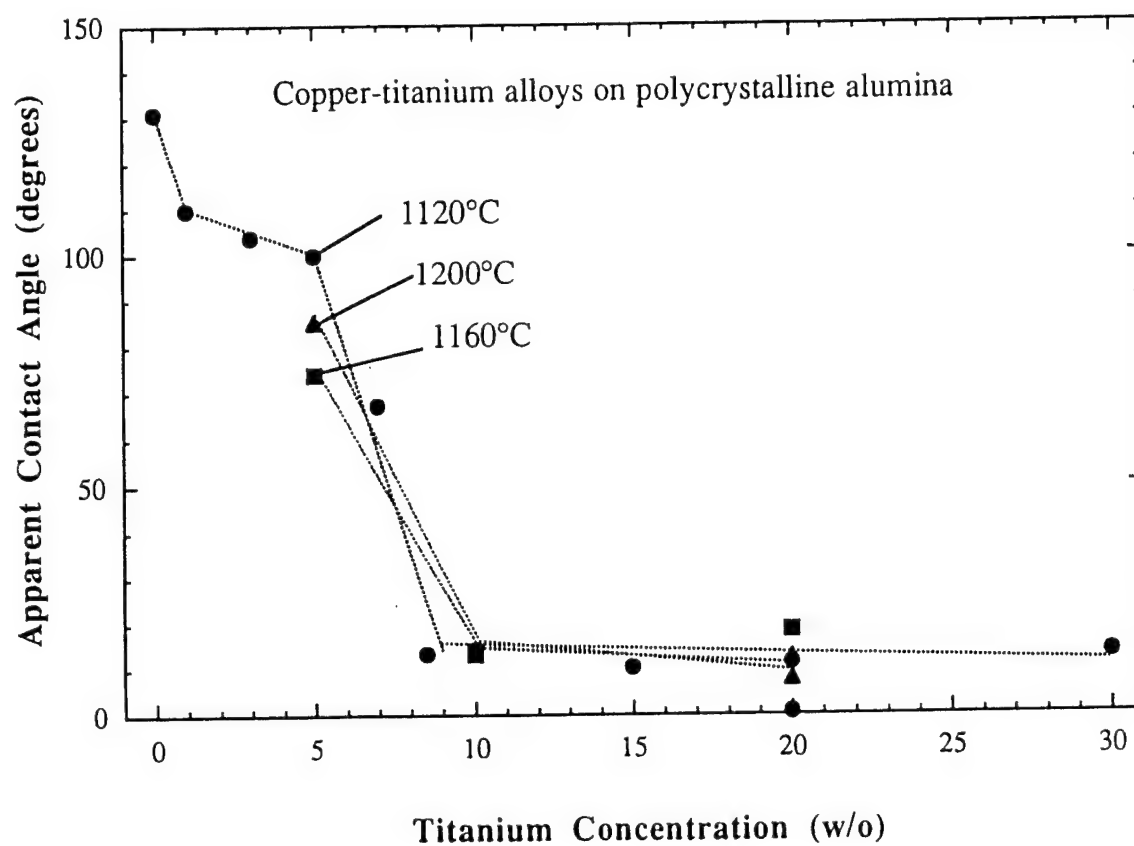
Figure 15: The apparent equilibrium contact angle (q) versus titanium concentration for copper-titanium alloys on alumina.
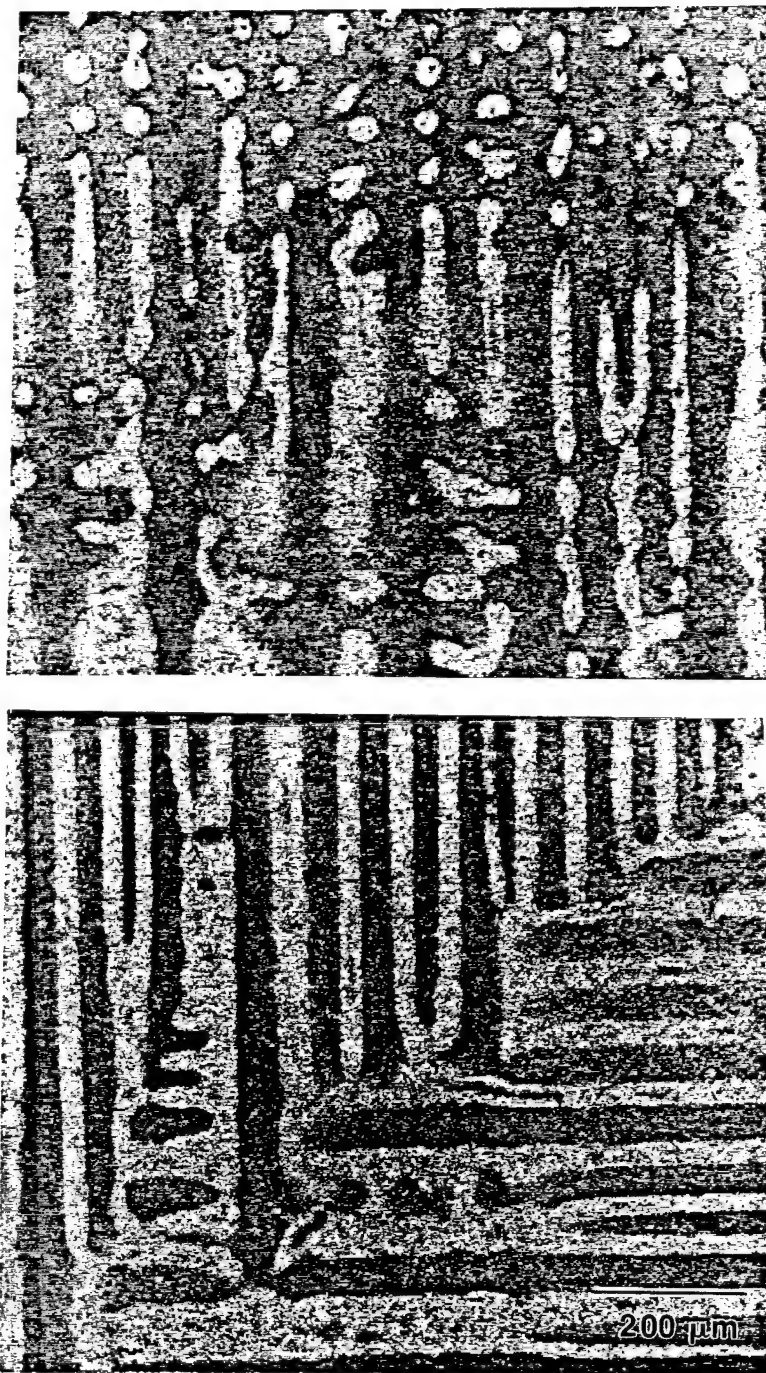
Figure 16: Micrograph of alumina surfaces after reaction showing dual product
formation and preferred growth directions (copper-3w/o titanium on alumina)
(100x).
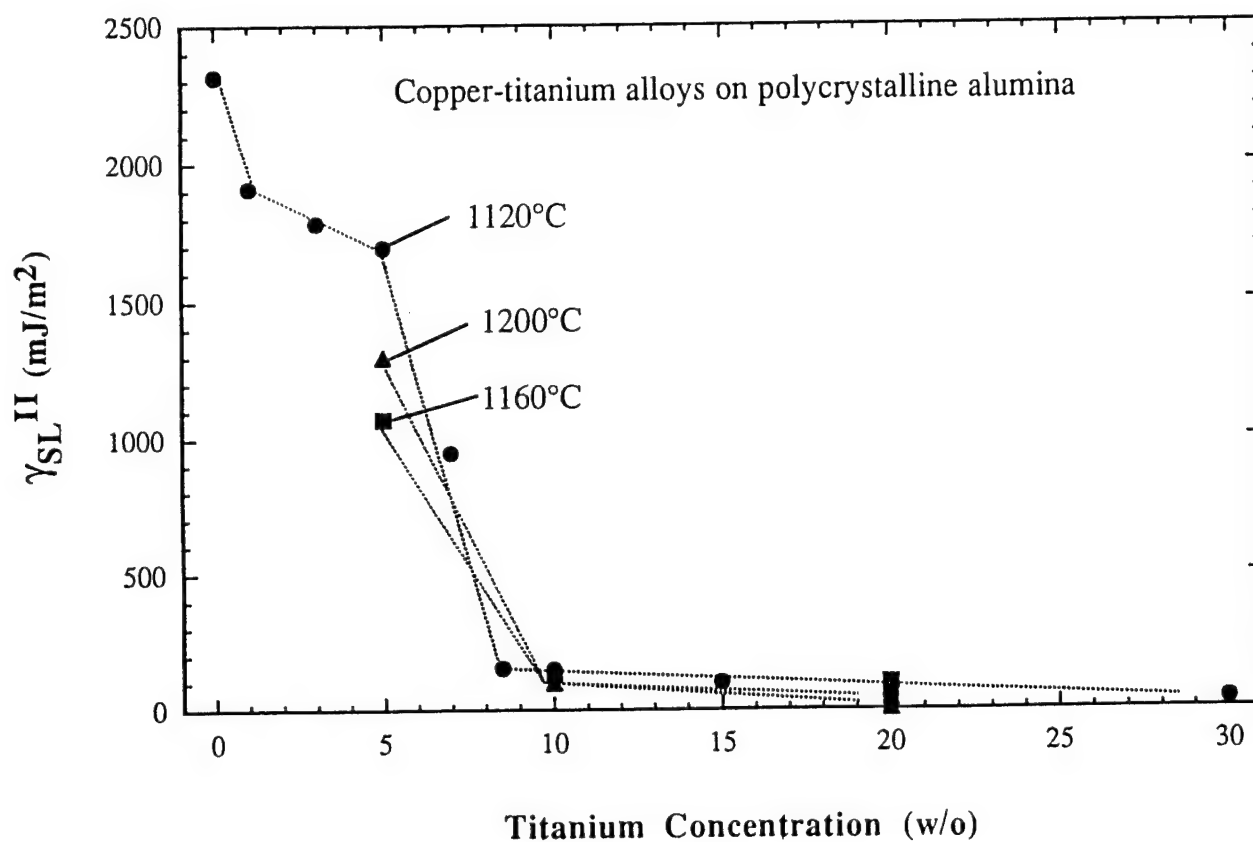
Figure 17: The equilibrium solid-liquid interfacial energy (γ_{SL}^{II}) versus composition or copper-titanium alloys on alumina.
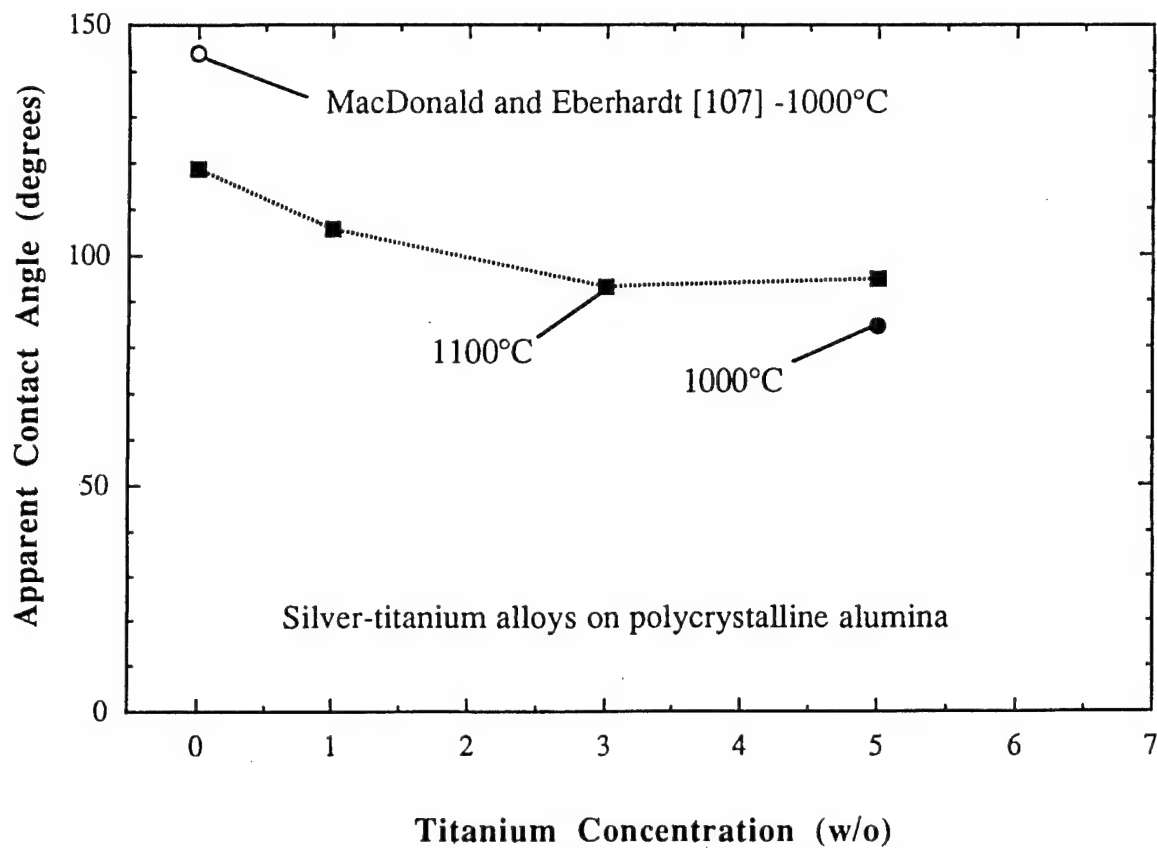
Figure 18: The apparent equilibrium contact angle (θ) versus titanium concentration for silver-titanium alloys on alumina.
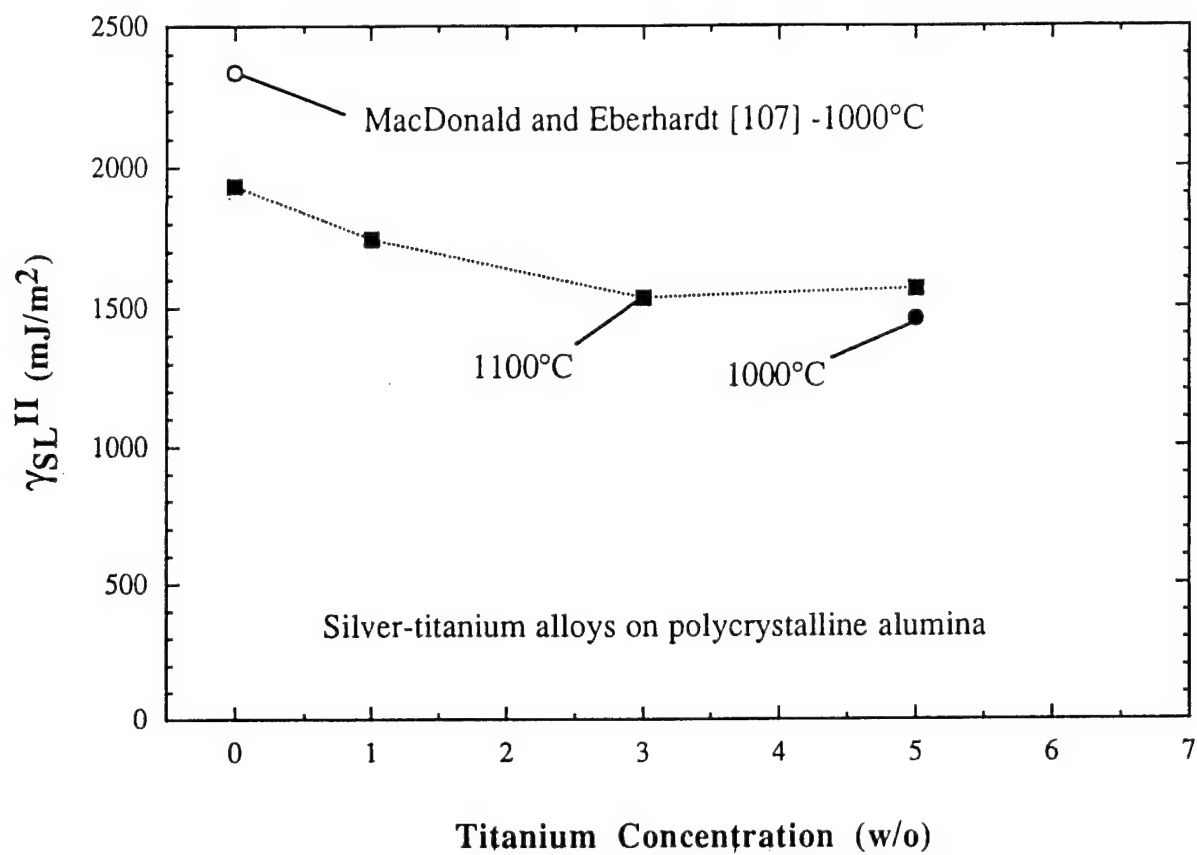
Figure 19: The equilibrium solid-liquid interfacial enerty (γ_{SL}) versus composition for silver-titanium alloys on alumina

58
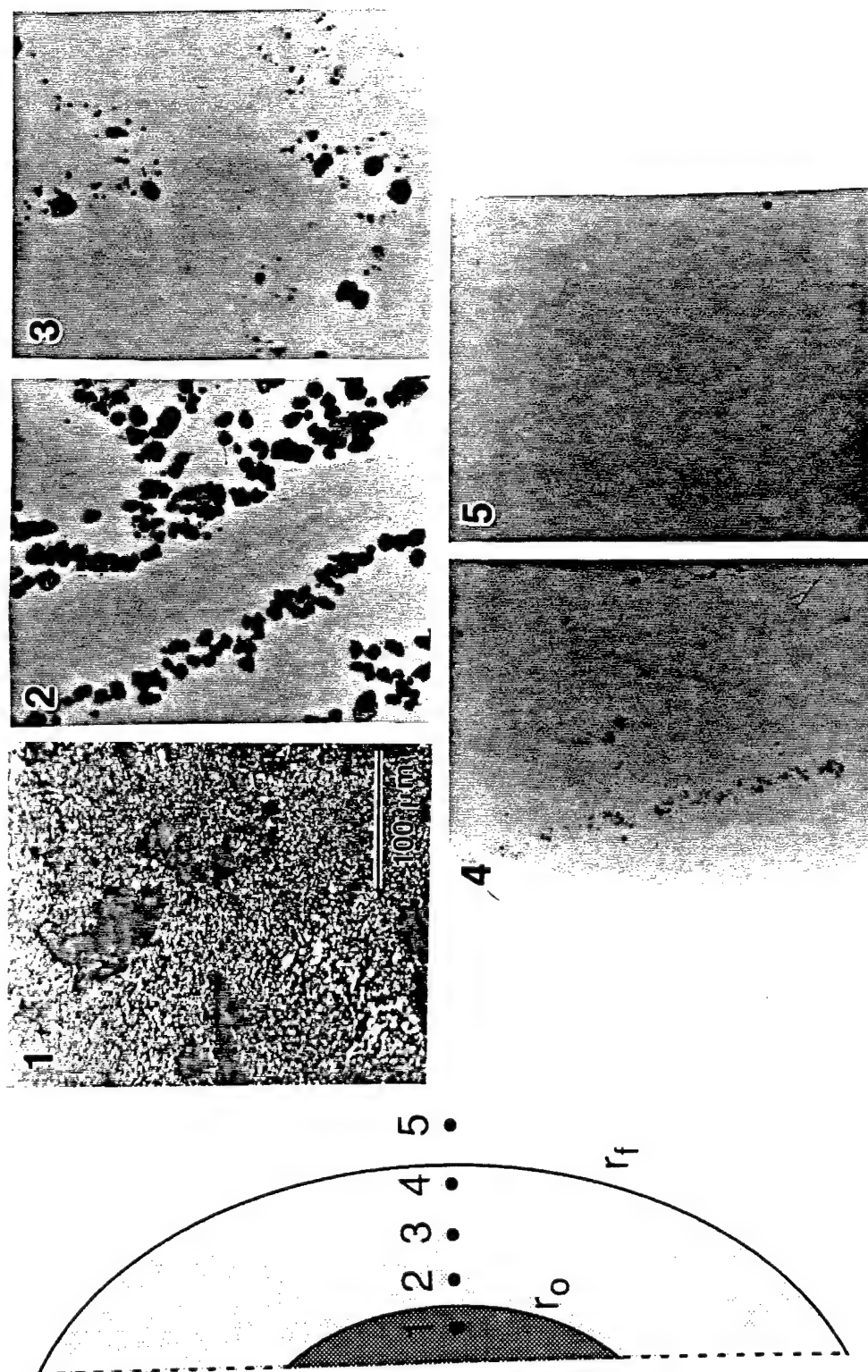
Figure 20: Microstructure of alumina surface after dissolution of copper-titanium drop (200X). The initially covered area, $r > r_o$, is completely covered with reaction product (1). Reaction product islands are observed in the spreading region, $r_o < r < r_f$, (2-4). No reaction product is observed outside of the spreading area, $r > r_f$ (5).
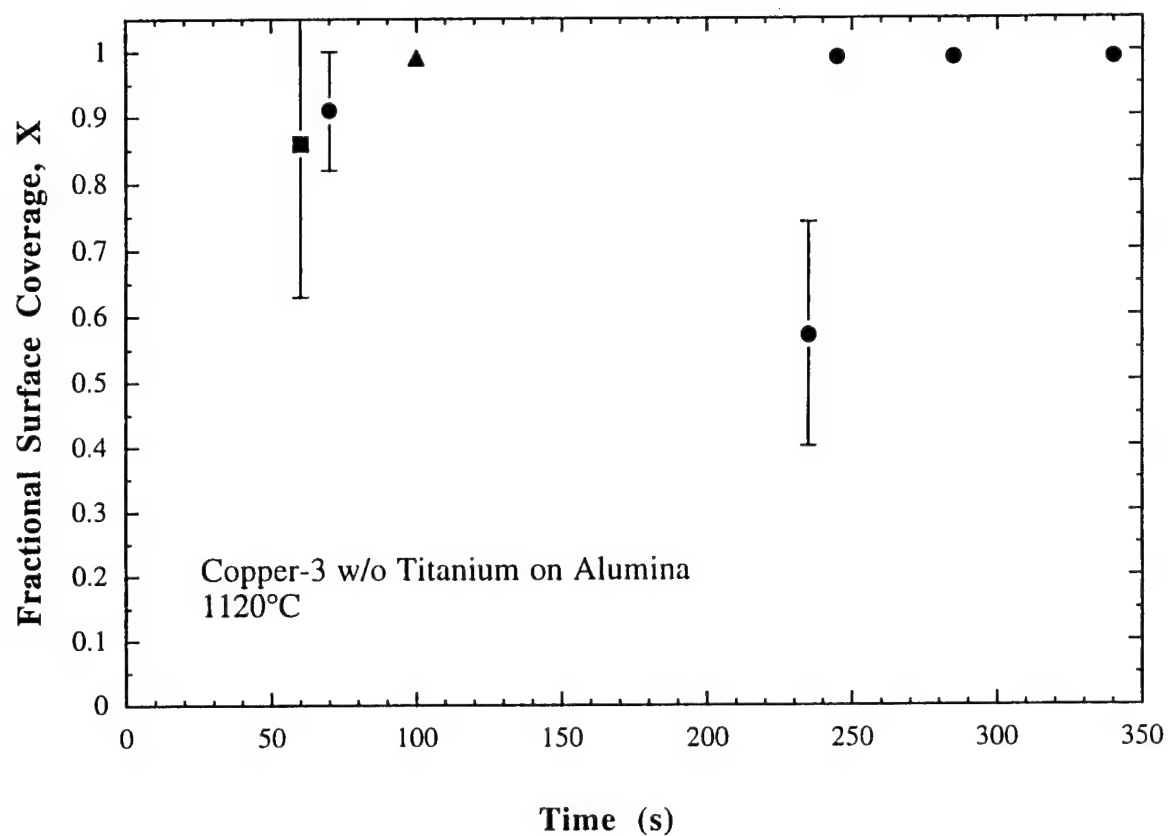
Figure 21: Fractional coverage of reaction product on alumina surface as a function of time for a copper-3 w/o titanium alloy at 1120°C. The 3 different symbols represent 3 independent sample runs. The error bars are the standard deviation of the mean for ten measurements.
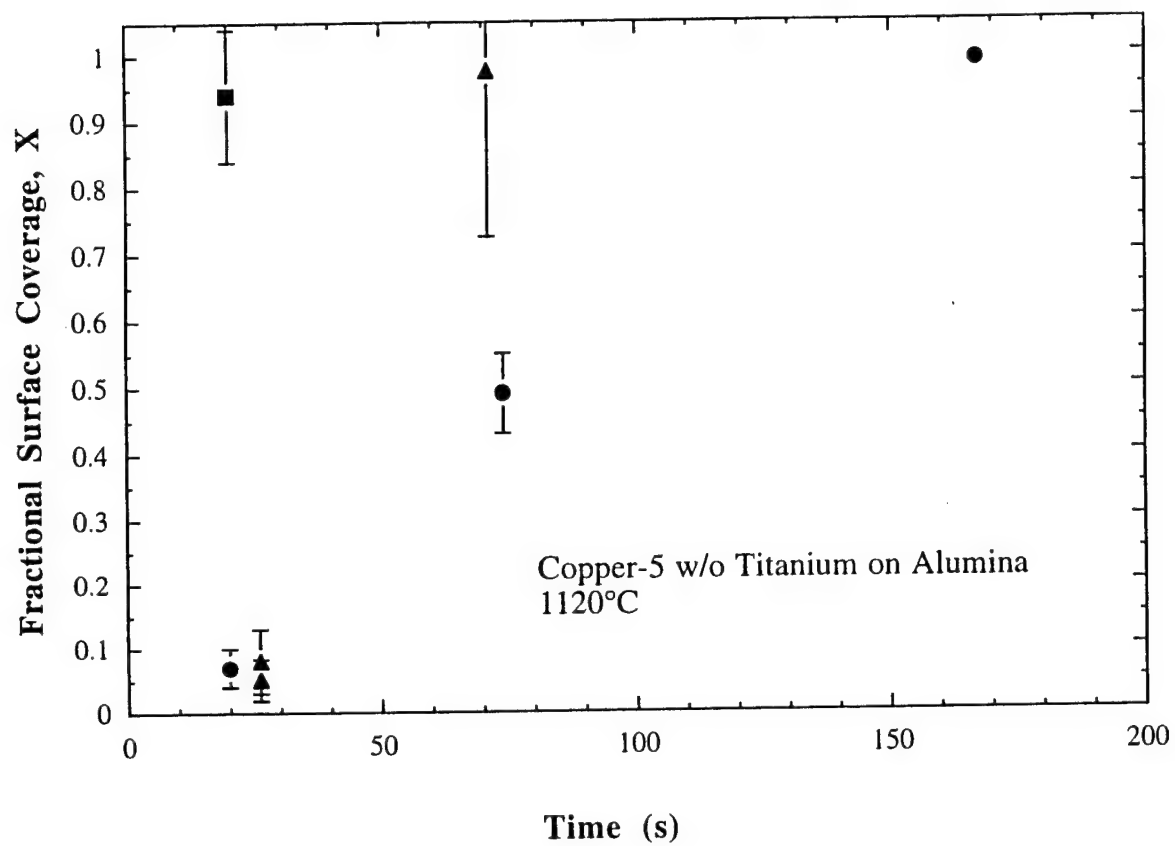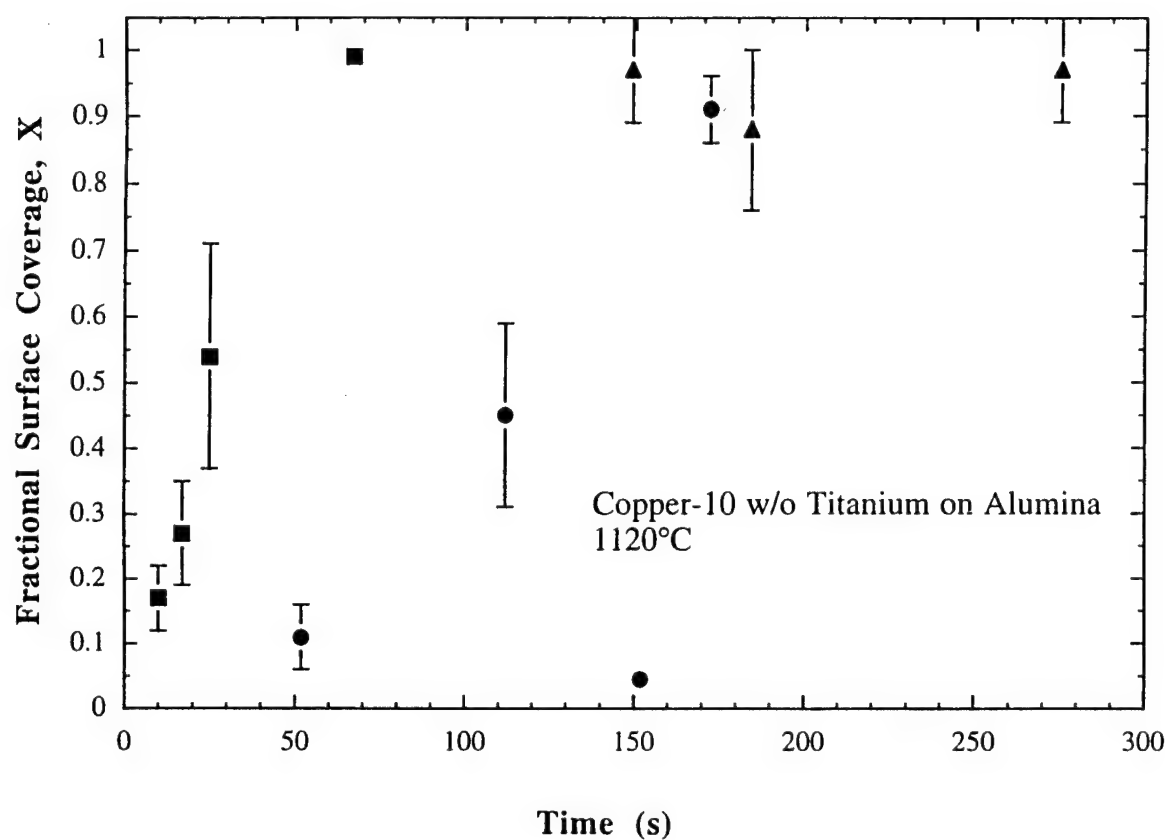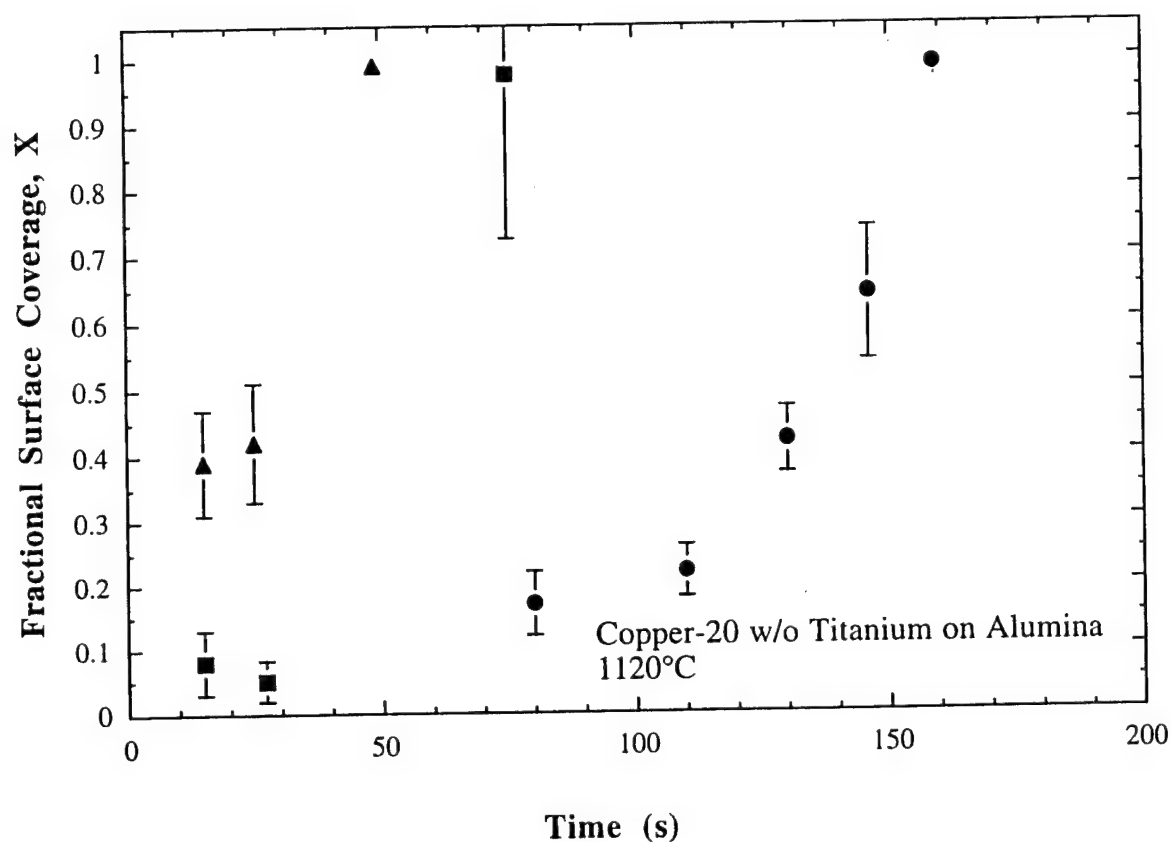
Figure 22: Fractional coverage of reaction product on alumina surface as a function of time for a copper-5 w/o titanium alloy at 1120°C. The 3 different symbols represent 3 independent sample runs. The error bars are the standard deviation of the mean for ten measurements.
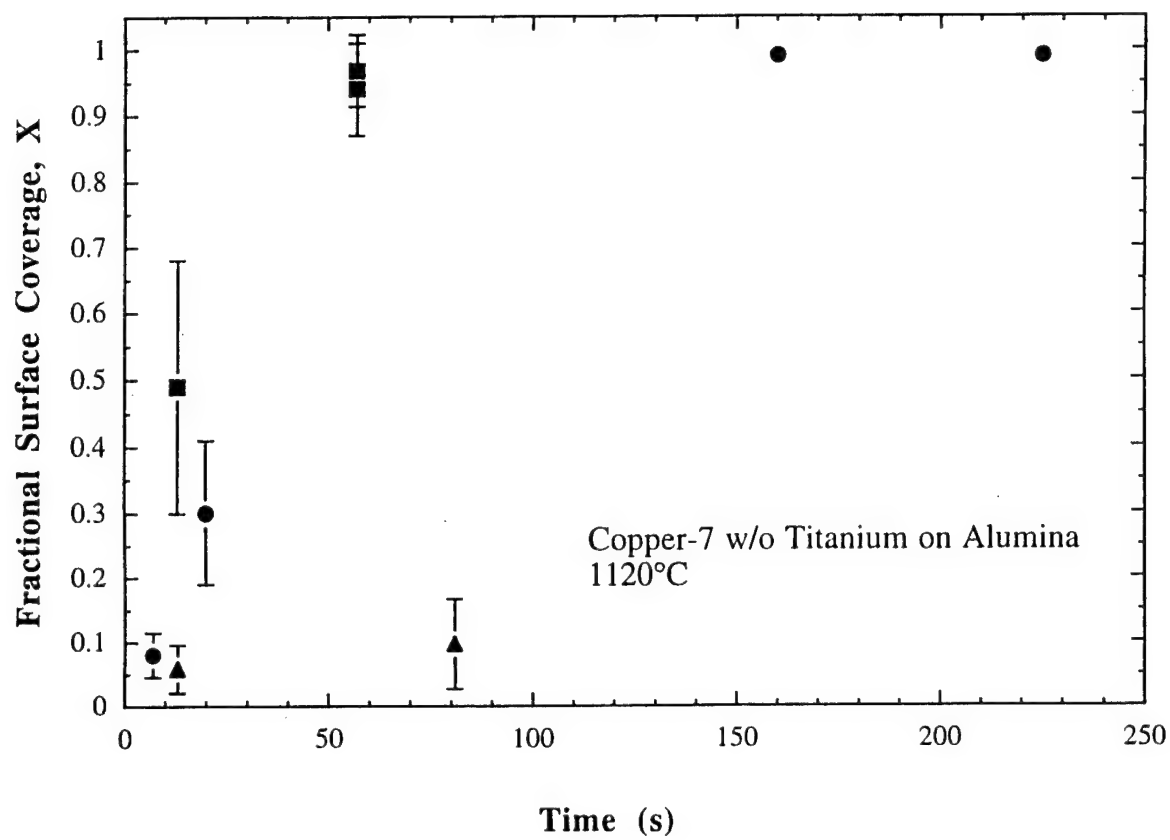
Figure 23: Fractional coverage of reaction product on alumina surface as a function of time for a copper-7 w/o titanium alloy at 1120°C. The 3 different symbols represent 3 independent sample runs. The error bars are the standard deviation of the mean for ten measurements.
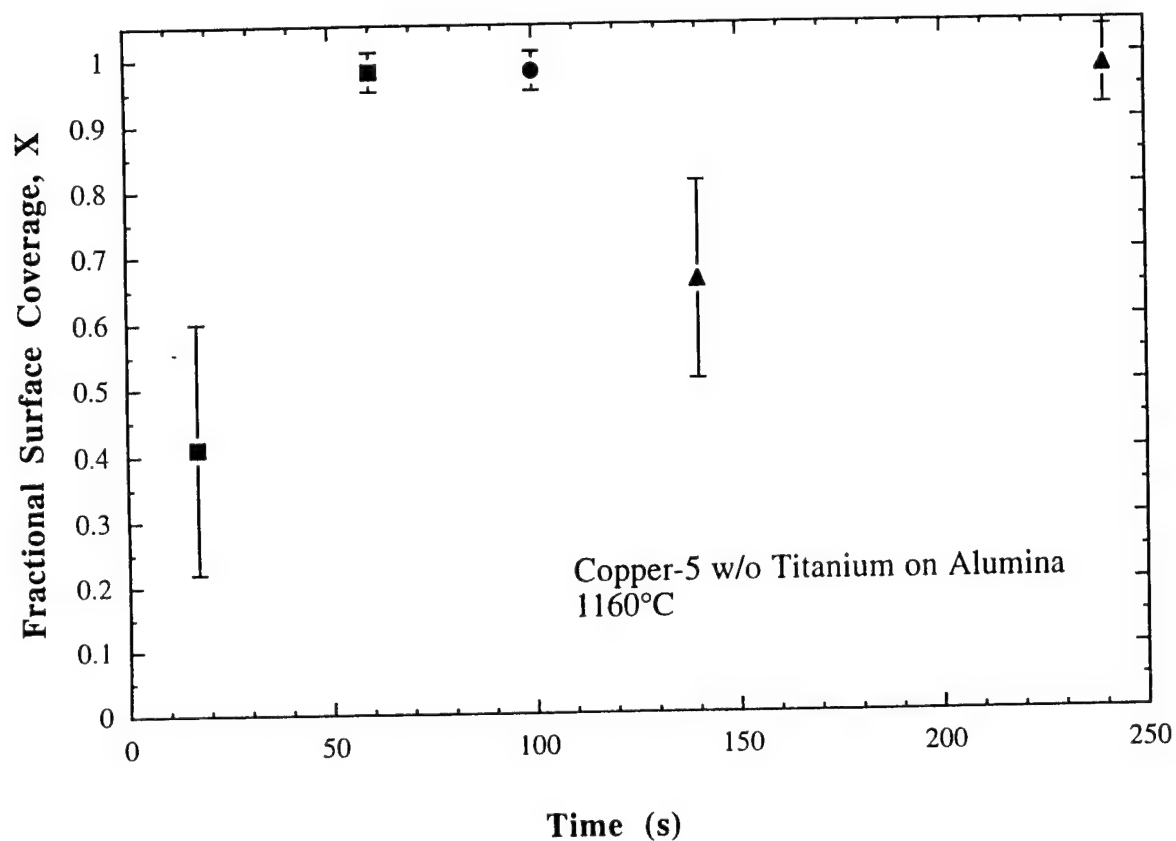
Figure 24: Fractional coverage of reaction product on alumina surface as a function
of time for a copper-10 w/o titanium alloy at 1120°C. The 3 different
symbols represent 3 independent sample runs. The error bars are the
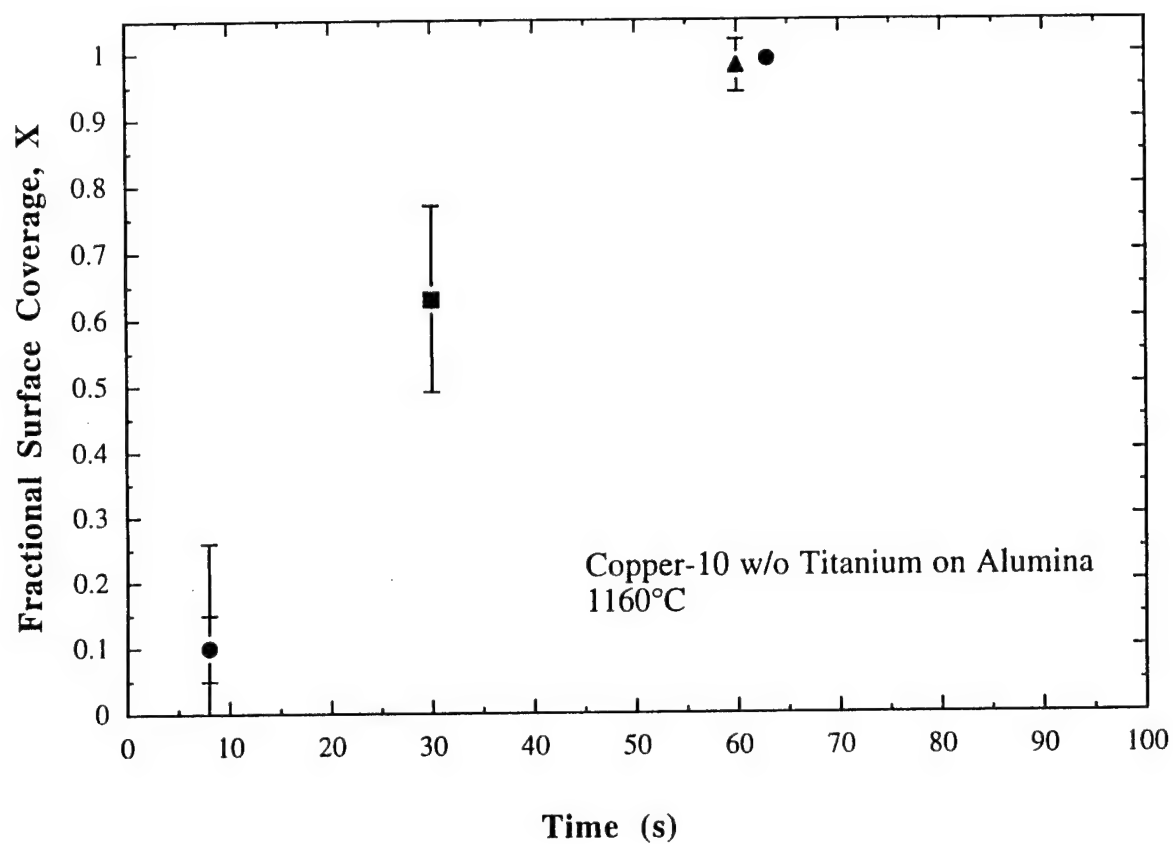standard deviation of the mean for ten measurements.

Figure 25: Fractional coverage of reaction product on alumina surface as a function of time for a copper-20 w/o titanium alloy at 1120°C. The 3 different symbols represent 3 independent sample runs. The error bars are the standard deviation of the mean for ten measurements.

Figure 26: Fractional coverage of reaction product on alumina surface as a function of time for a copper-5 w/o titanium alloy at 1160°C. The 3 different symbols represent 3 independent sample runs. The error bars are the standard deviation of the mean for ten measurements.
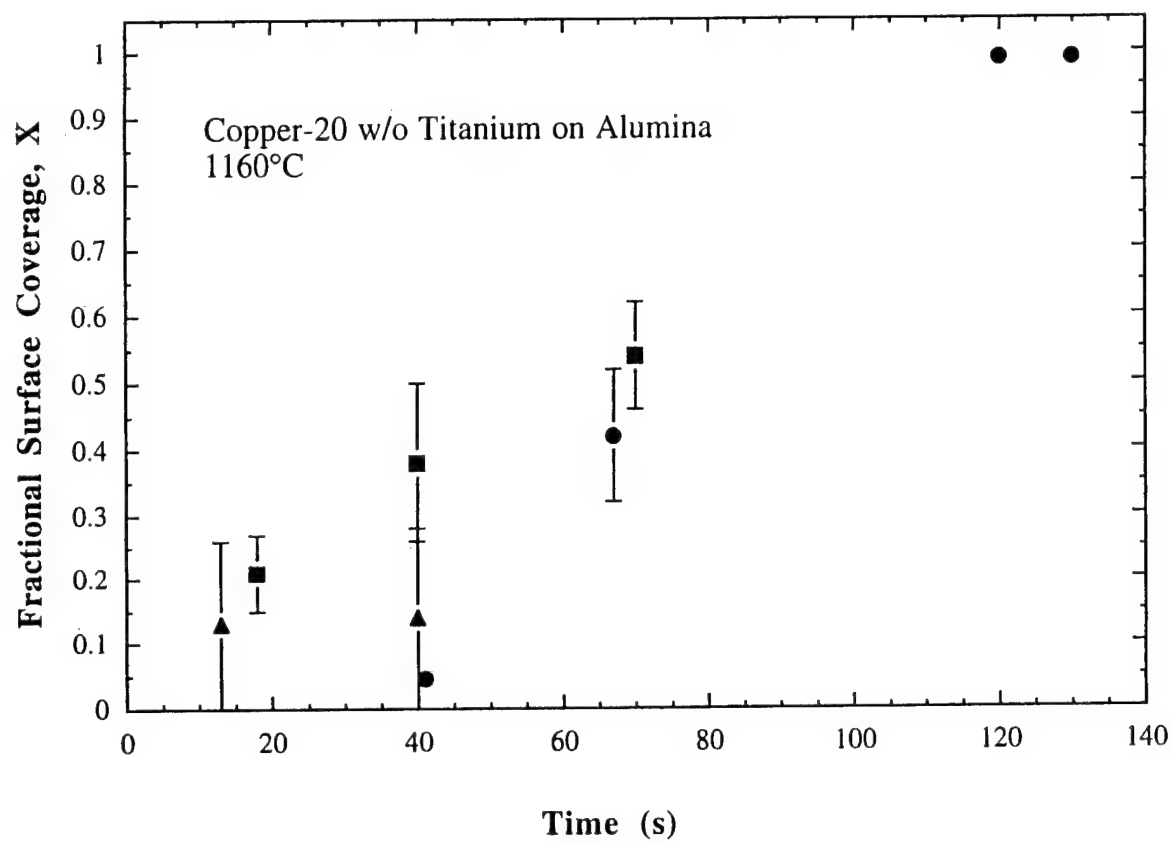
Figure 27: Fractional coverage of reaction product on alumina surface as a function of time for a copper-10 w/o titanium alloy at 1160°C. The 3 different symbols represent 3 independent sample runs. The error bars are the standard deviation of the mean for ten measurements.
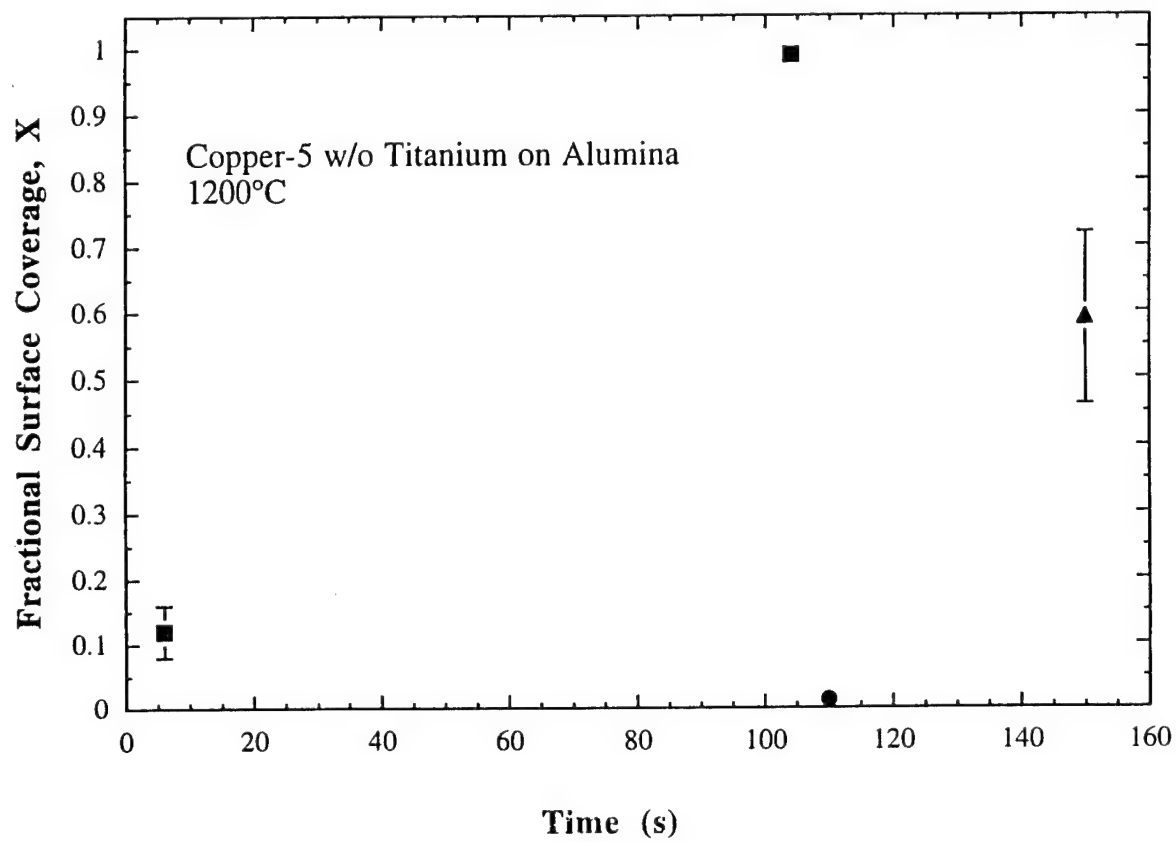
Figure 28: Fractional coverage of reaction product on alumina surface as a function of time for a copper-20 w/o titanium alloy at 1160°C. The 3 different symbols represent 3 independent sample runs. The error bars are the standard deviation of the mean for ten measurements.

Figure 29: Fractional coverage of reaction product on alumina surface as a function of time for a copper-5 w/o titanium alloy at 1200°C. The 3 different symbols represent 3 independent sample runs. The error bars are the standard deviation of the mean for ten measurements.
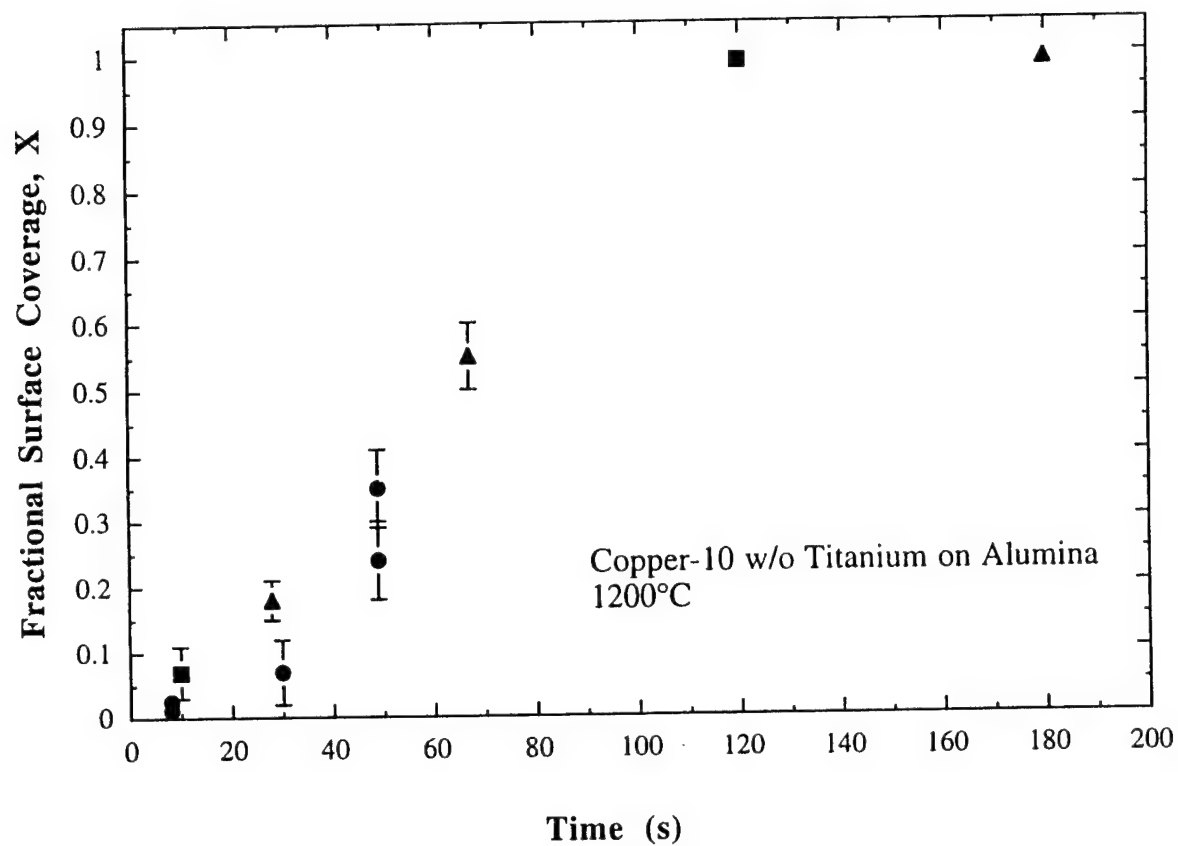
Figure 30: Fractional coverage of reaction product on alumina surface as a function of
time for a copper-10 w/o titanium alloy at 1200°C. The 3 different
symbols represent 3 independent sample runs. The error bars are the
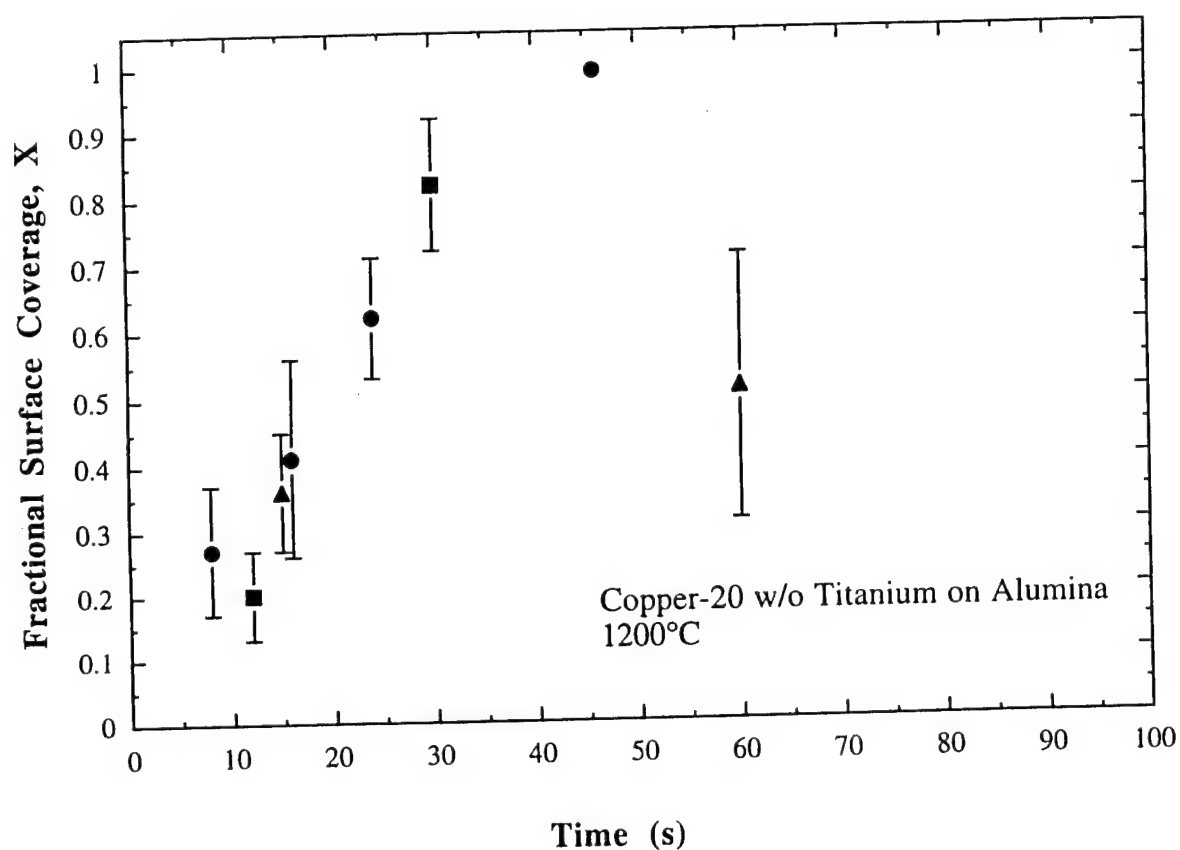standard deviation of the mean for ten measurements.

Figure 31: Fractional coverage of reaction product on alumina surface as a function of
time for a copper-20 w/o titanium alloy at 1200°C. The 3 different
symbols represent 3 independent sample runs. The error bars are the
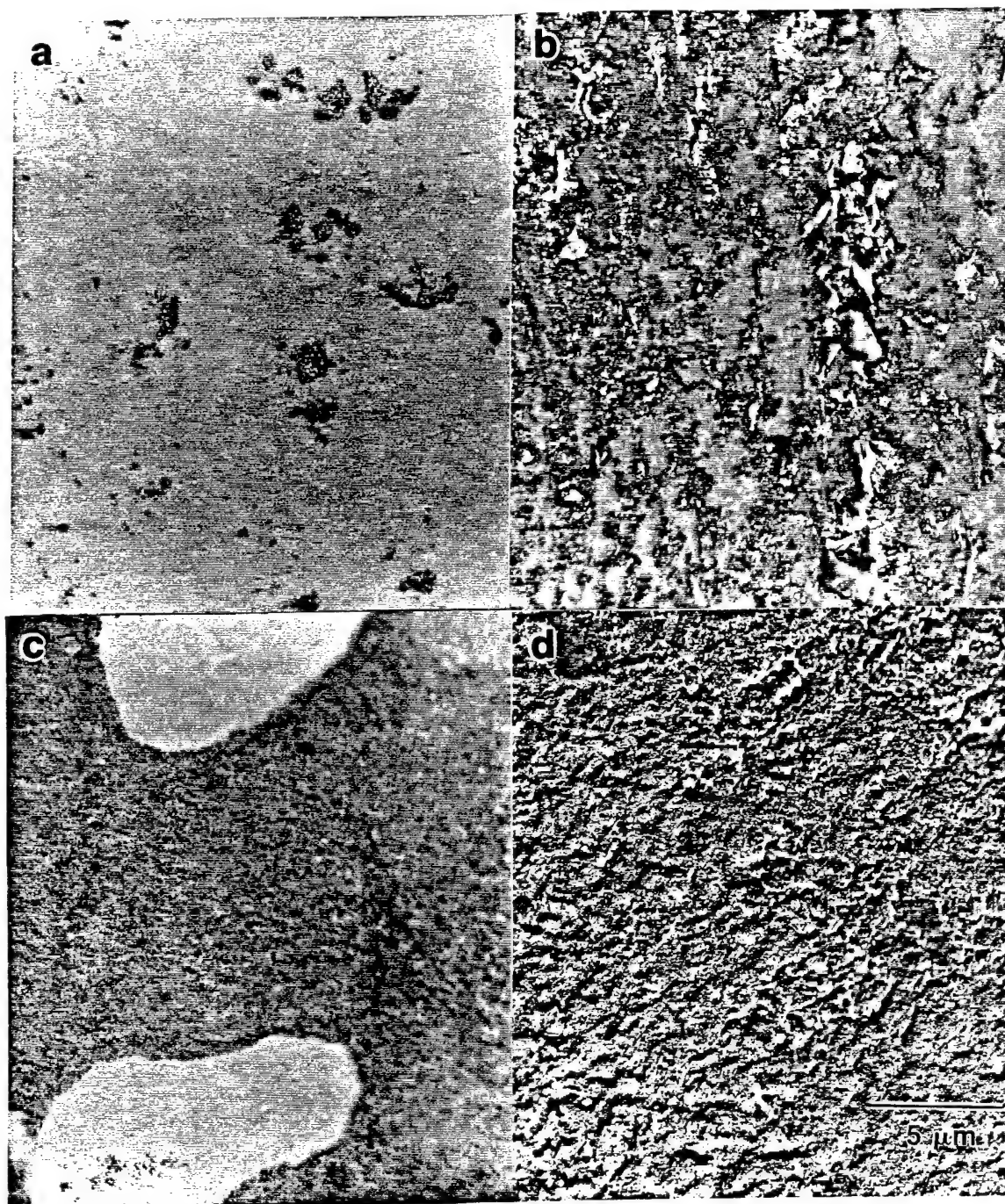standard deviation of the mean for ten measurements.

Figure 32:   Micrographs of fractional coverage of reaction product on alumina
surfaces for copper-titanium alloys (400x), a.) initial islands form, b.) islands
grow together, c.) alumina islands are left, and d.) complete coverage is
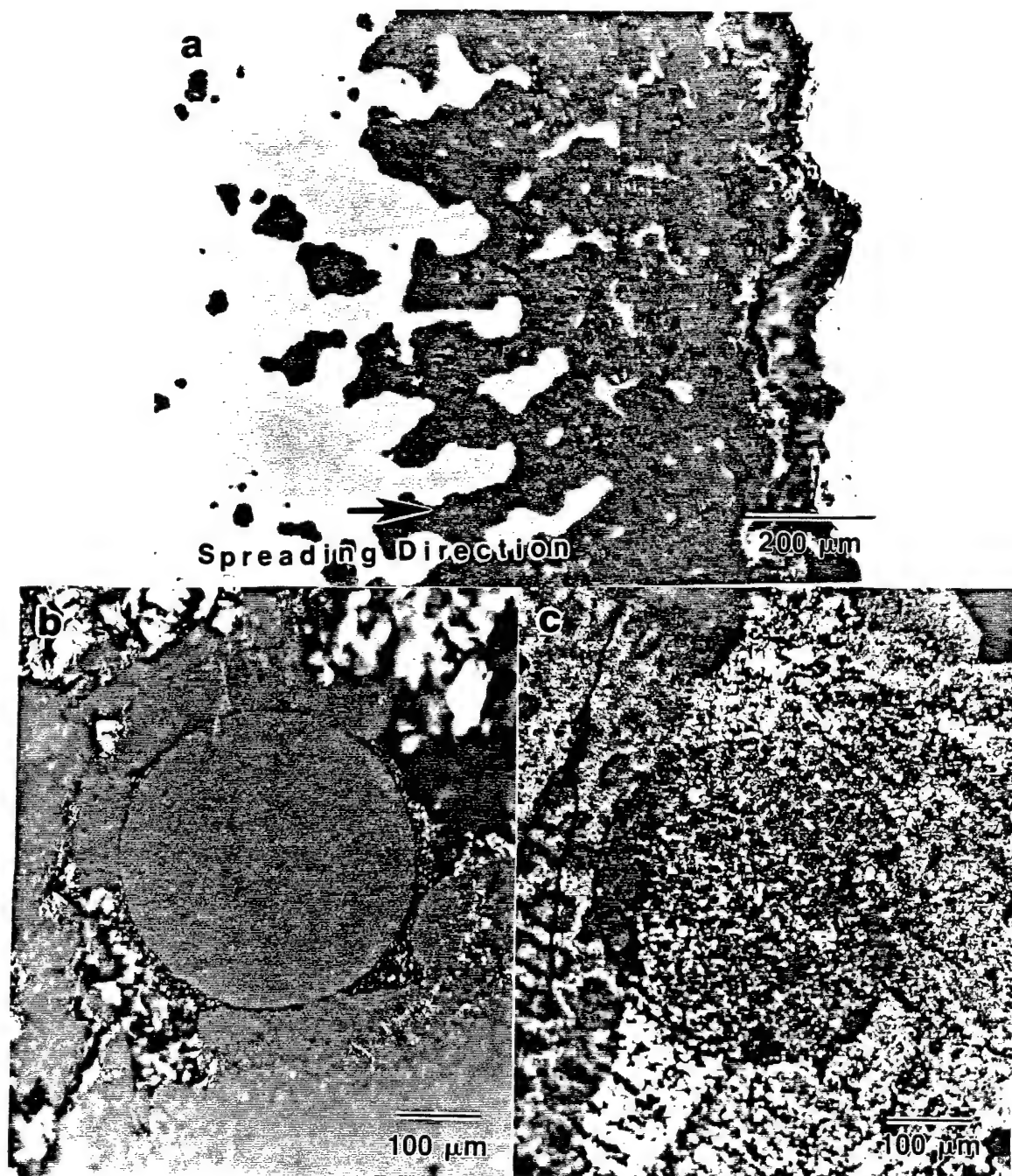obtained.

Figure 33: Anomolous spreading behavior for copper-titanium alloys on alumina, a.) enhanced reaction at the edge of the drop (100x), and b.), c.) circular region with non-uniform product formation (125x).
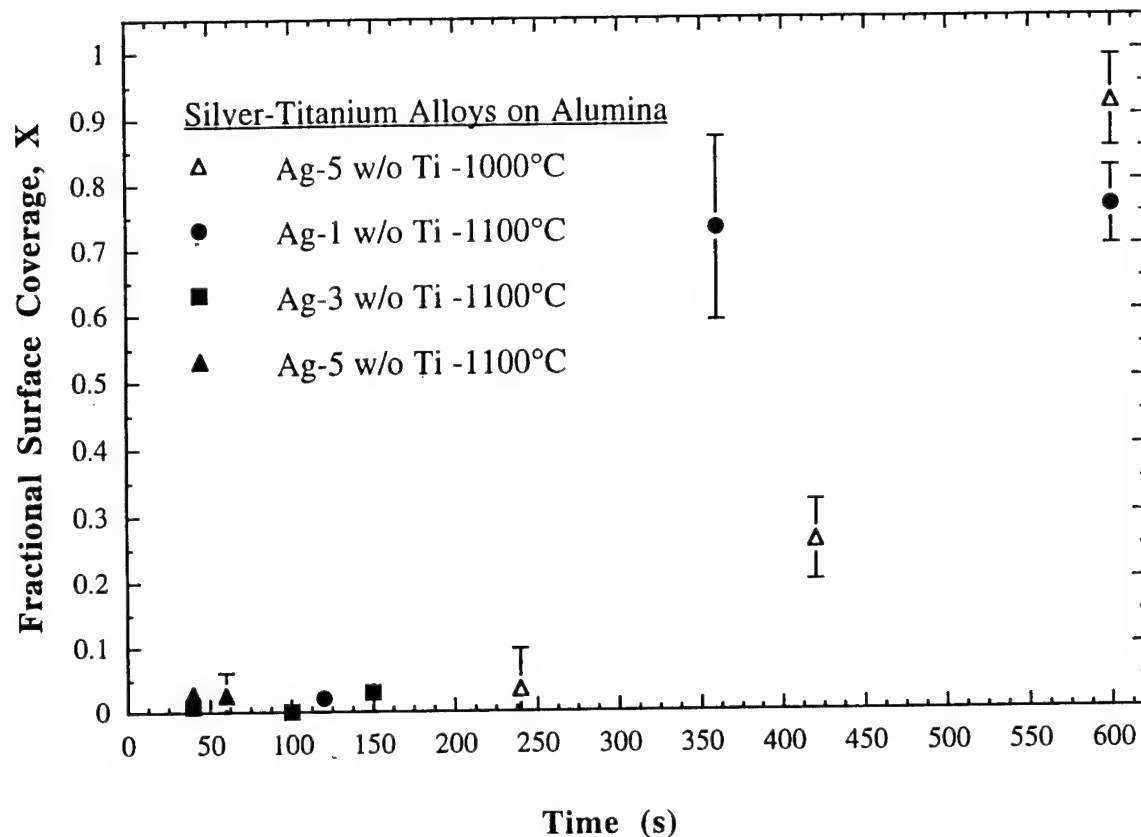
Figure 34: Fractional coverage of reaction product on alumina surface as a function of time for silver-titanium alloys at 1000 and 1100°C. The error bars are the standard deviation of the mean for fifteen measurements.
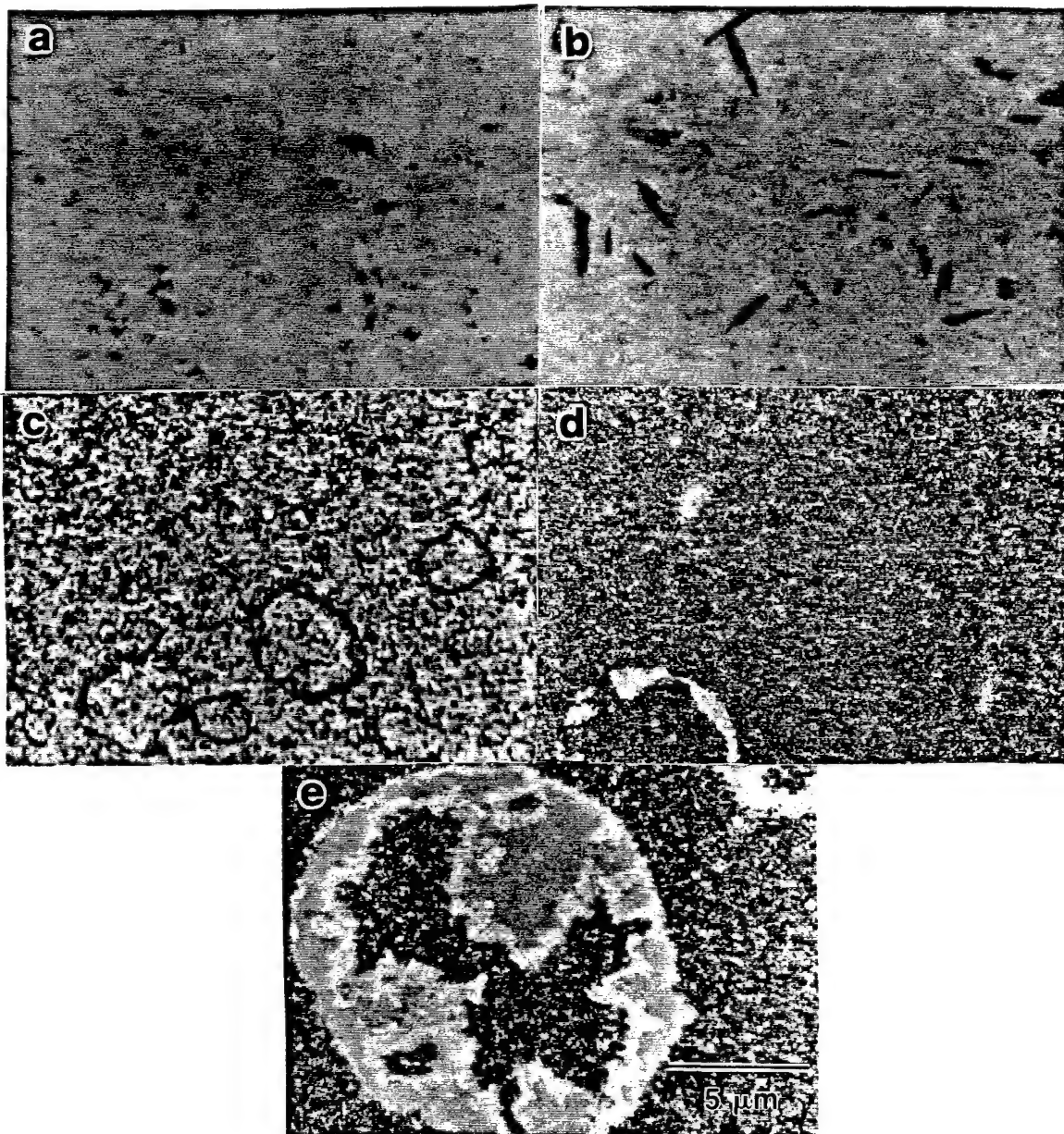
Figure 35: Micrographs of fractional coverage of reaction product on alumina surface for silver-titanium alloys (400x): a.) small islands of reaction product form, b.) in some cases, needle-like product islands grow with time, c.) the islands grow together until d.) the surface is nearly covered with reaction product, e.) large unreacted islands are sometimes observed in nearly completely reacted regions.

Figure 36: Theoretical spreading radius curves and experimental data for copper-3 w/o titanium on alumina at 1120°C. The error bars on the experimental data represent the uncertainty in the radius measurements.

Figure 37: Theoretical spreading radius curves and experimental data for copper-5 w/o titanium on alumina at 1120°C. The error bars on the experimental data represent the uncertainty in the radius measurements.
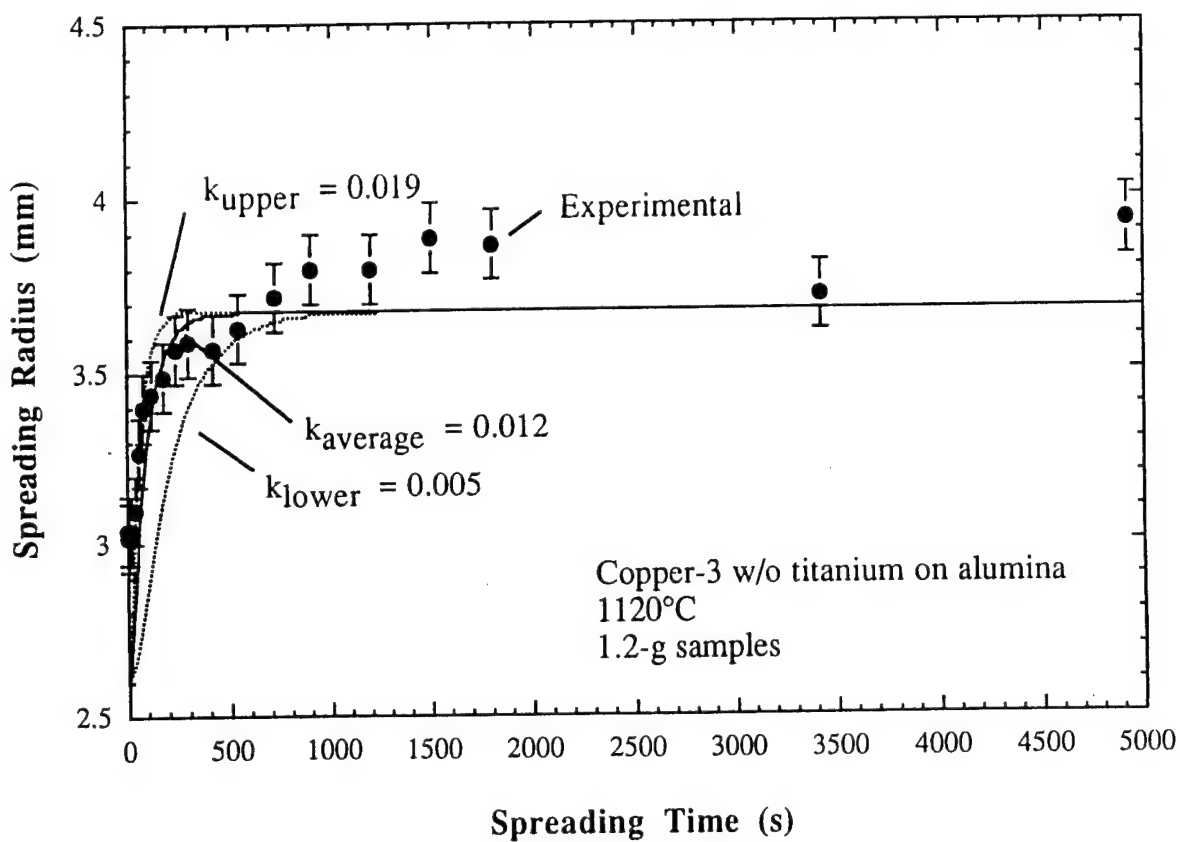
Figure 38: Theoretical spreading radius curves and experimental data for copper-7 w/o
titanium on alumina at 1120°C. The error bars on the experimental data
represent the uncertainty in the radius measurements.

Figure 39: Theoretical spreading radius curves and experimental data for copper-10 w/o titanium on alumina at 1120°C. The error in the radius measurement is smaller than the data point height.

Figure 40: Theoretical spreading radius curves and experimental data for copper-20
w/o titanium on alumina at 1120°C. The error in the radius measurement is
smaller than the data point height.

Figure 41: Theoretical spreading radius curves and experimental data for copper-5 w/o
titanium on alumina at 1160°C. The error bars on the experimental data
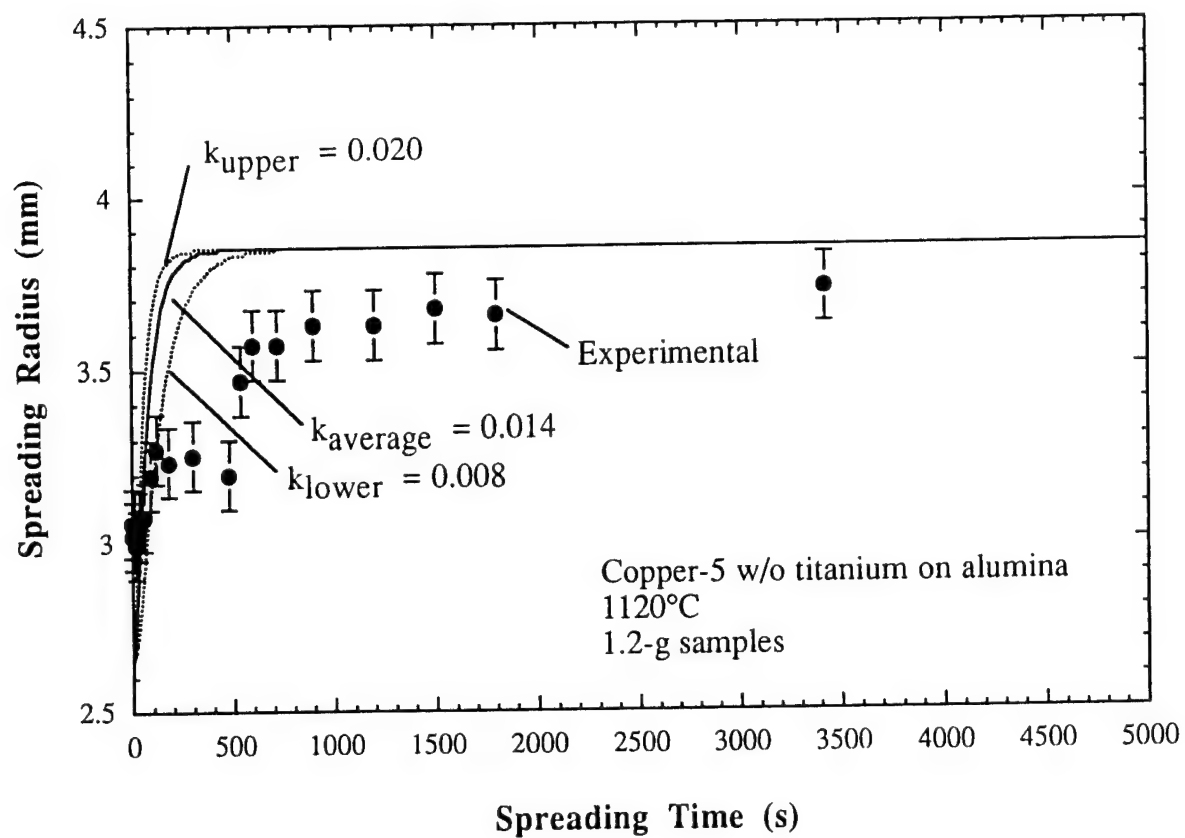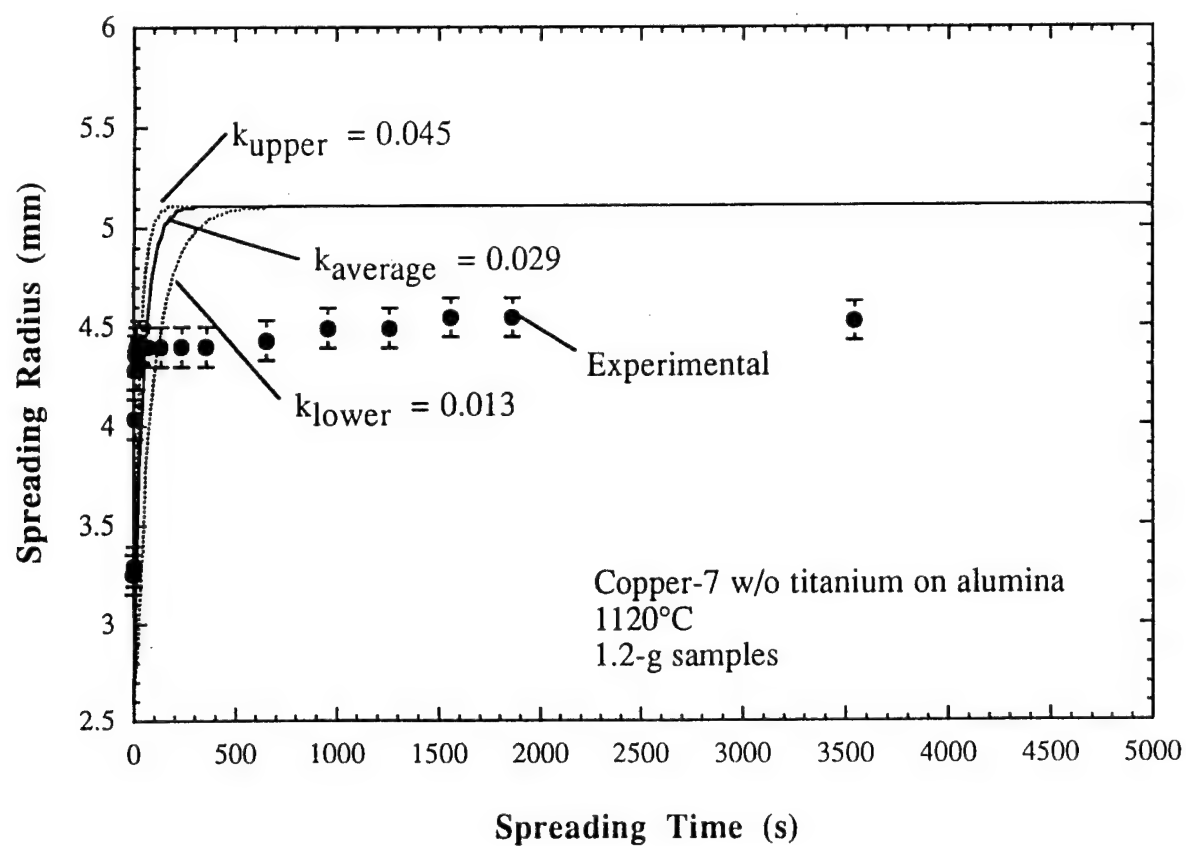represent the uncertainty in the radius measurements.
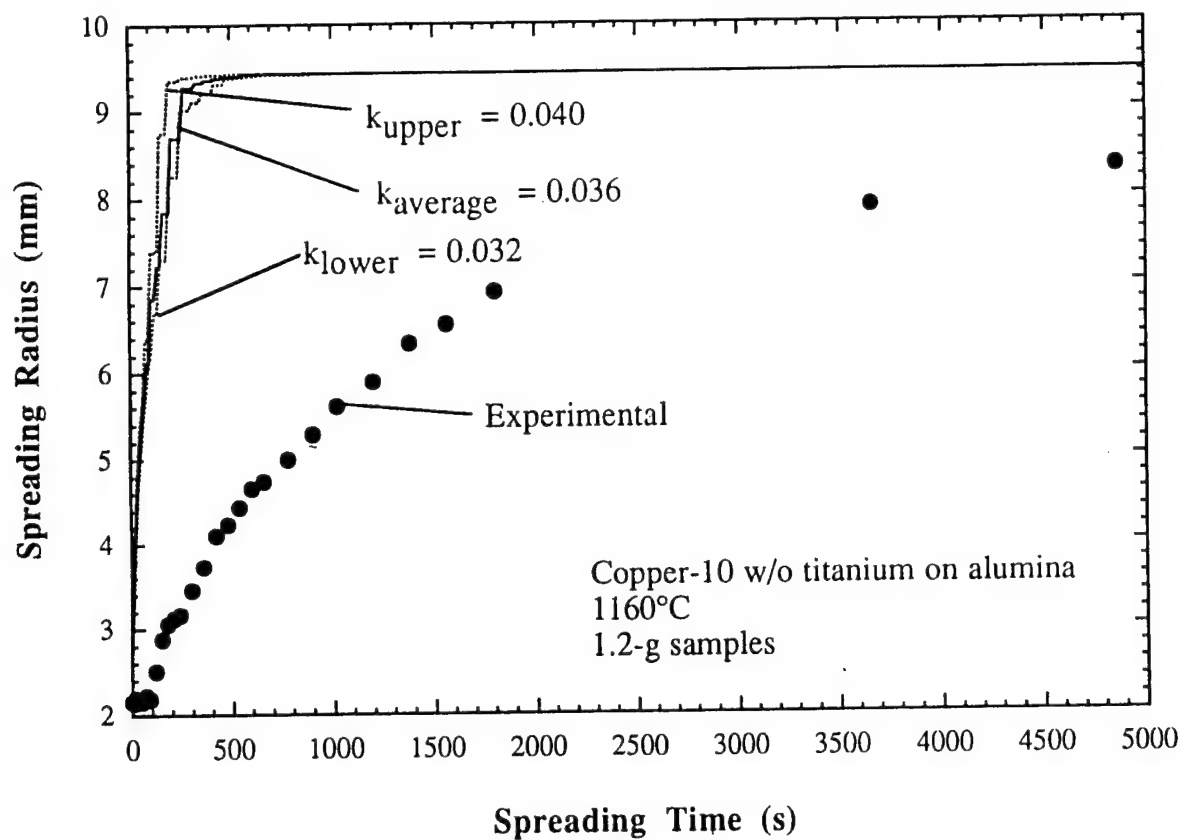
Figure 42: Theoretical spreading radius curves and experimental data for copper-10 w/o titanium on alumina at 1160°C. The error in the radius measurement is smaller than the data point height.
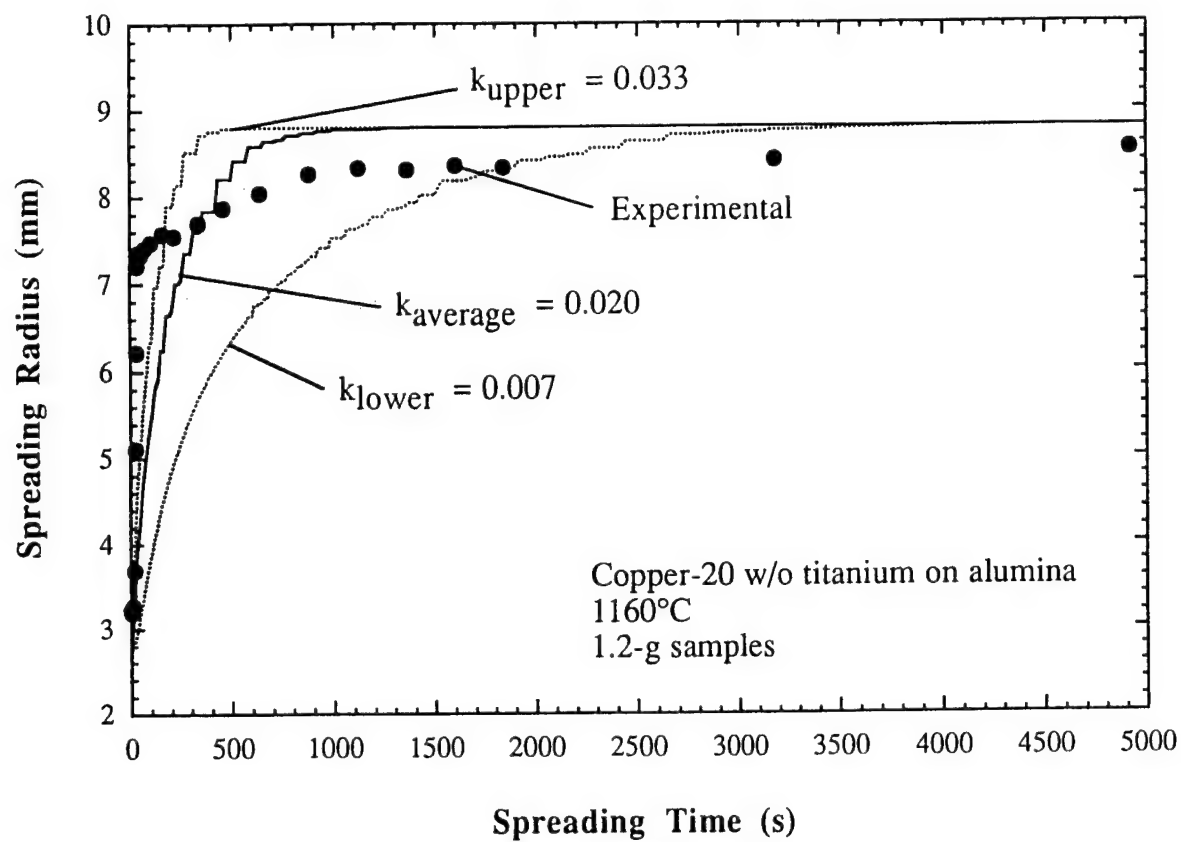
Figure 43: Theoretical spreading radius curves and experimental data for copper-20
w/o titanium on alumina at 1160°C. The error in the radius measurement
is smaller than the data point height.
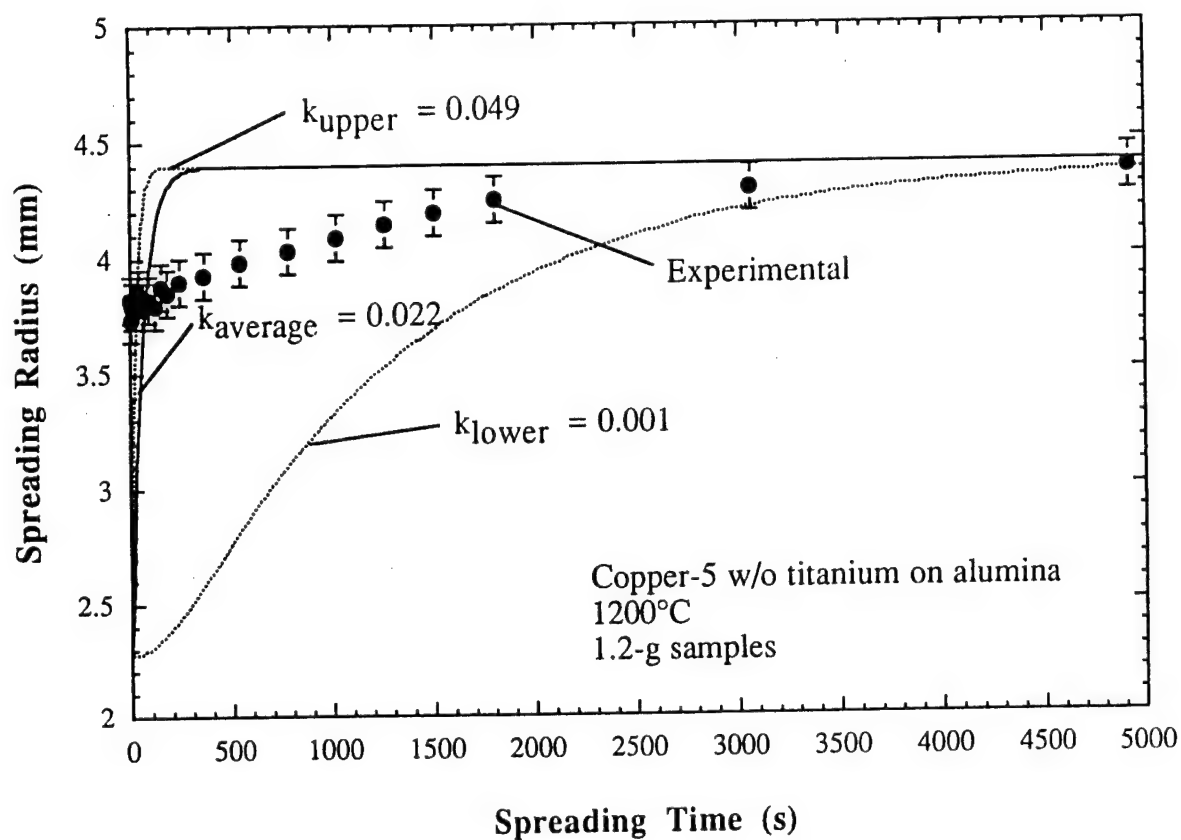
Figure 44: Theoretical spreading radius curves and experimental data for copper-5 w/o titanium on alumina at 1200°C. The error bars on the experimental data represent the uncertainty in the radius measurements.
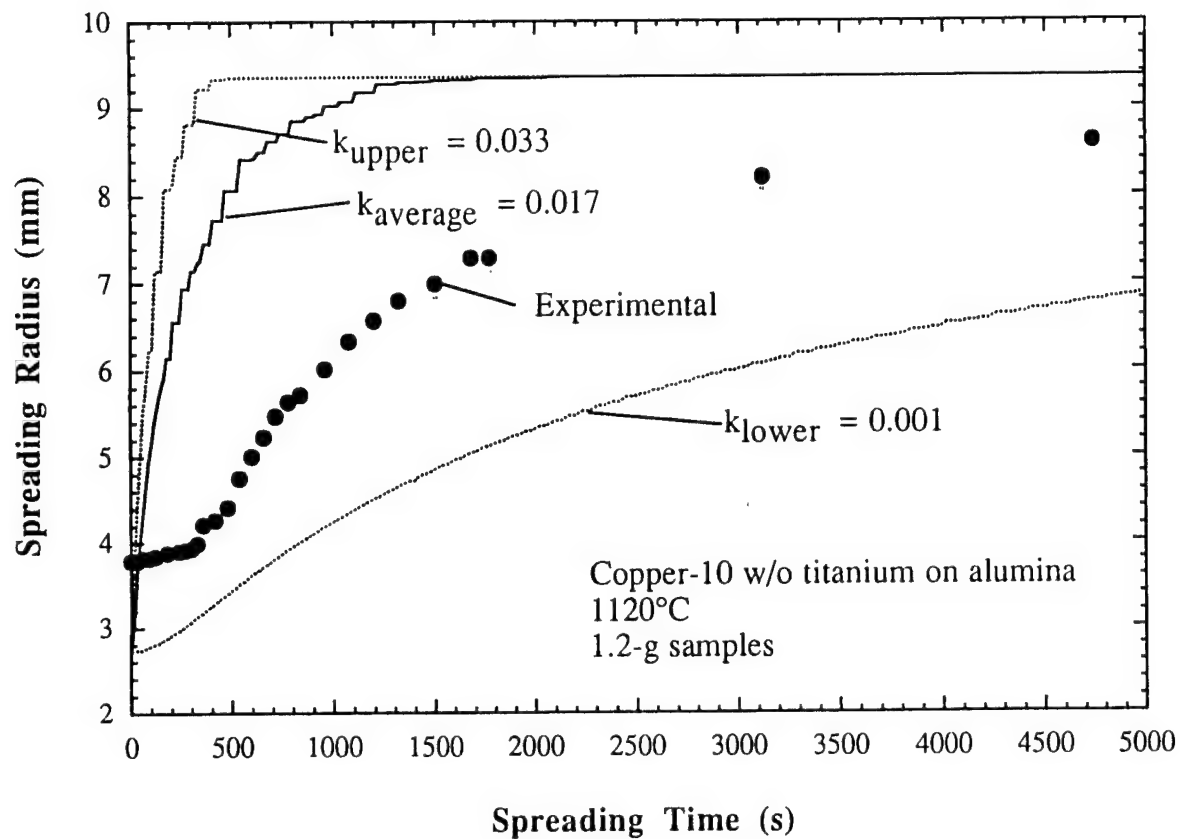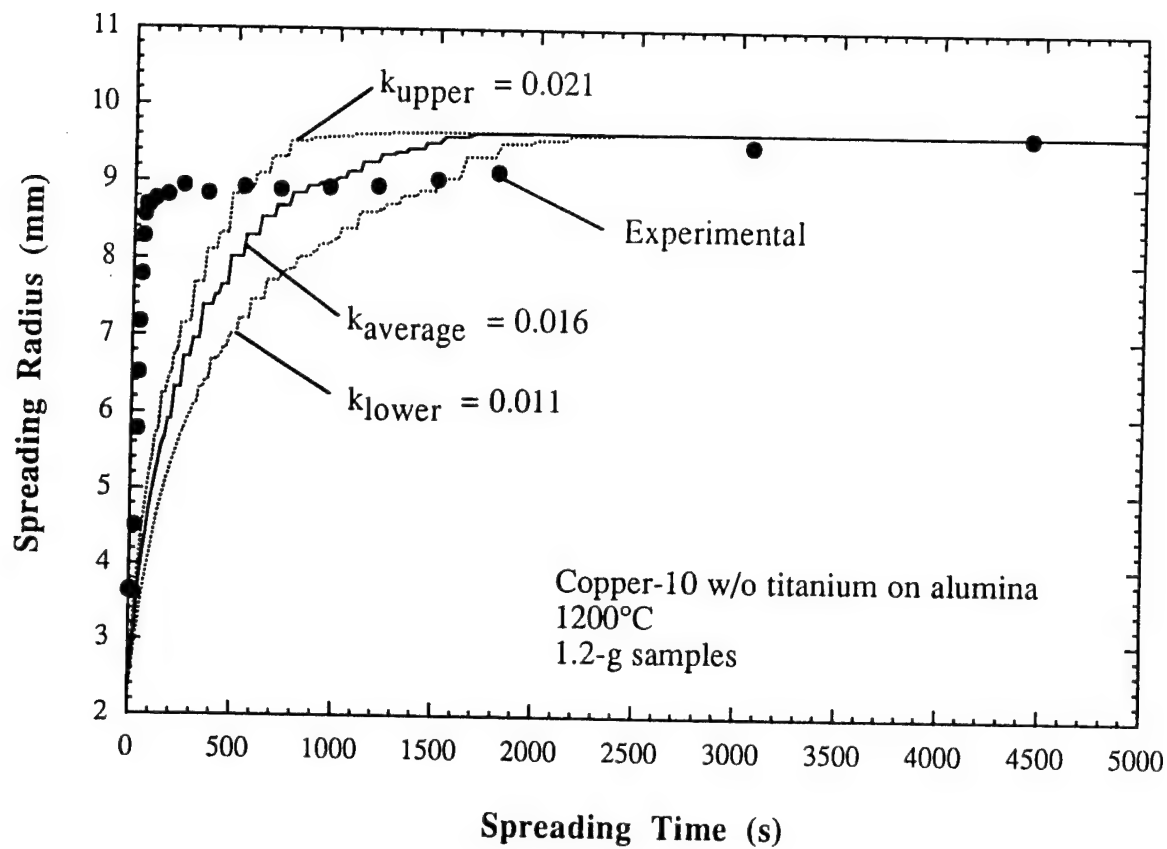
Figure 45: Theoretical spreading radius curves and experimental data for copper-10 w/o titanium on alumina at 1200°C. The error in the radius measurement is smaller than the data point height.
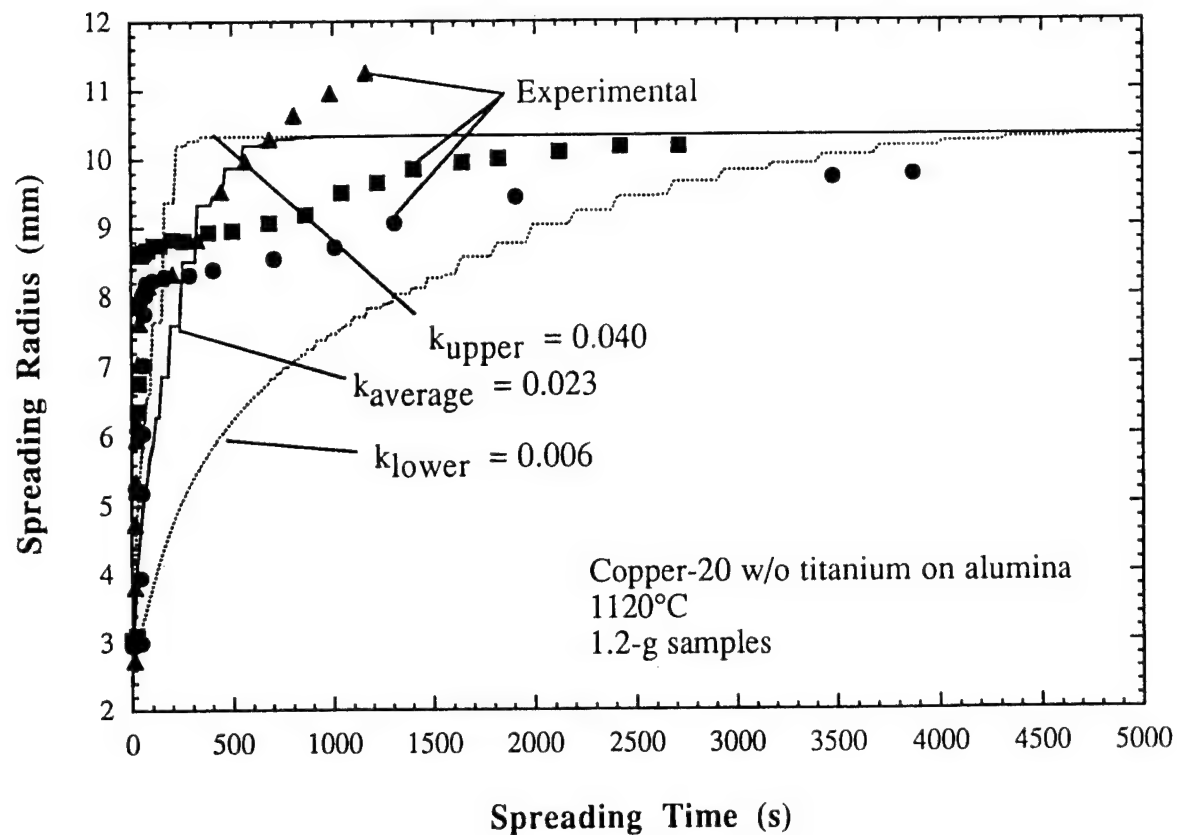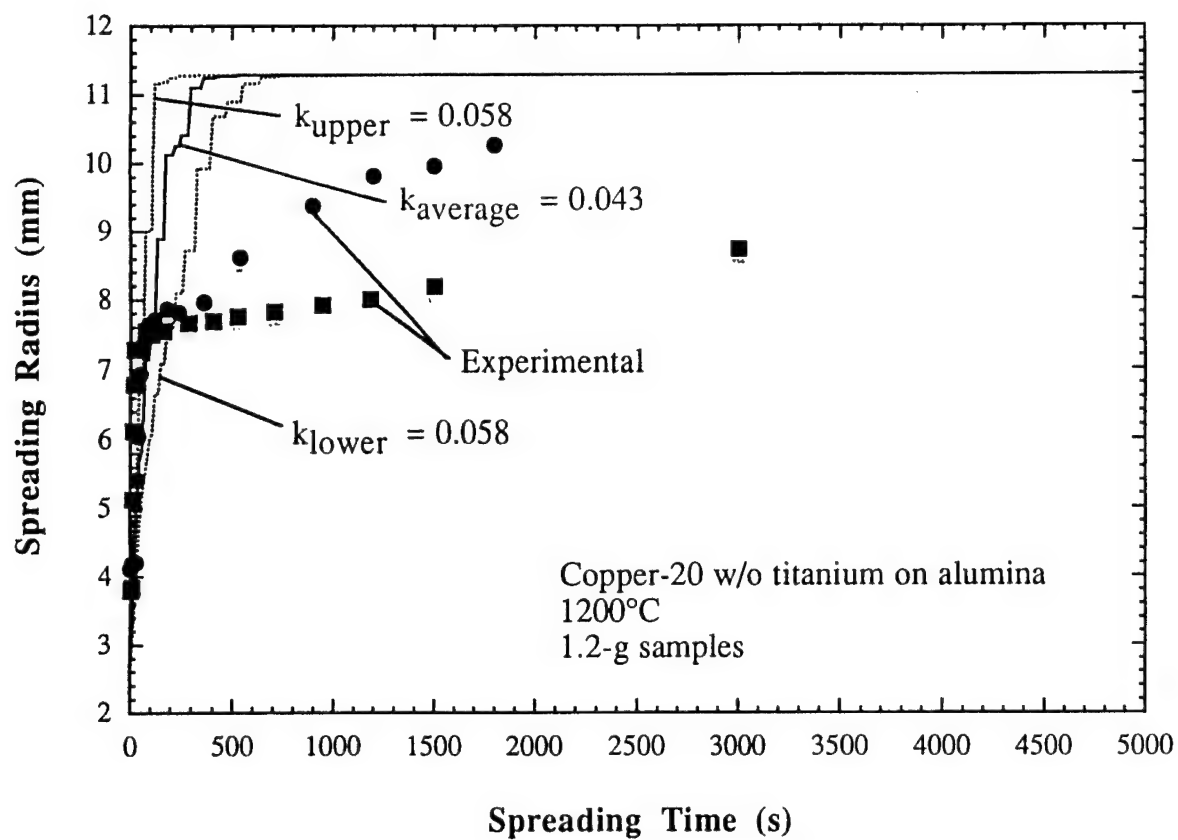
Figure 46: Theoretical spreading radius curves and experimental data for copper-20
w/o titanium on alumina at 1200°C. The error in the radius measurement
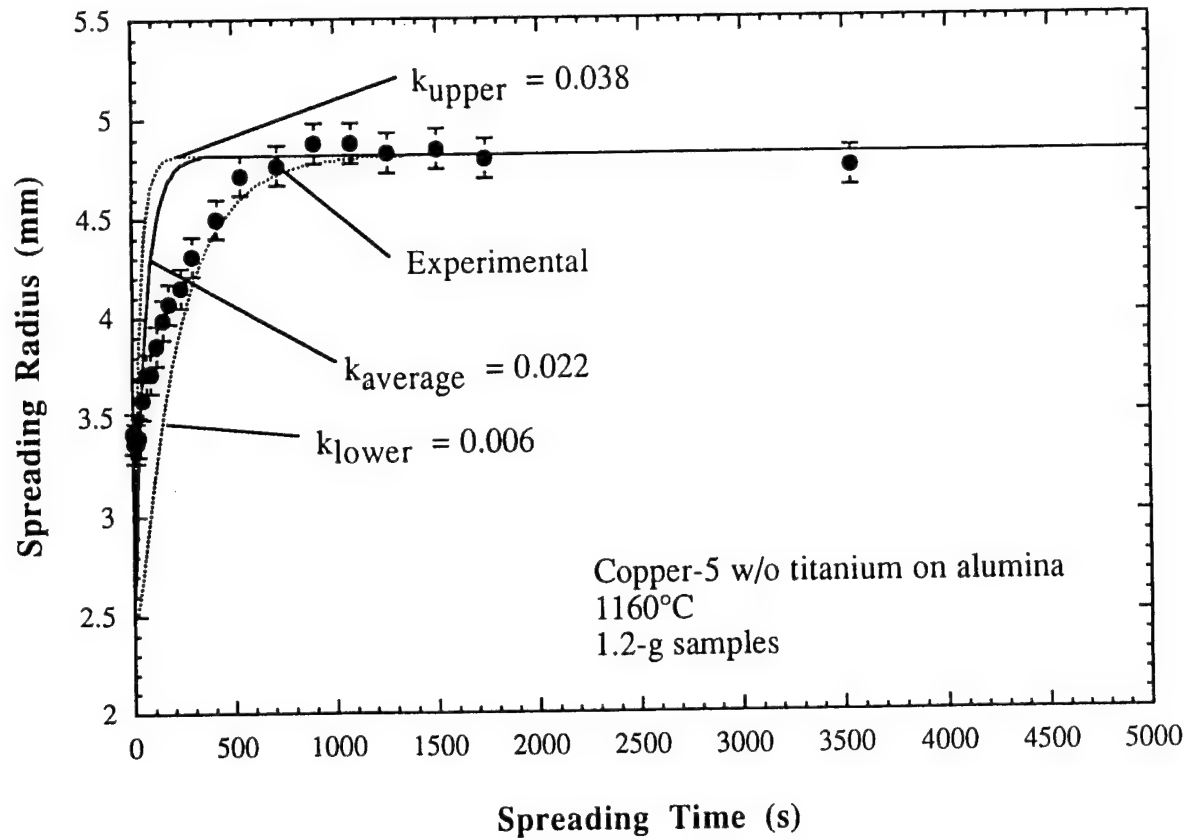is smaller than the data point height.
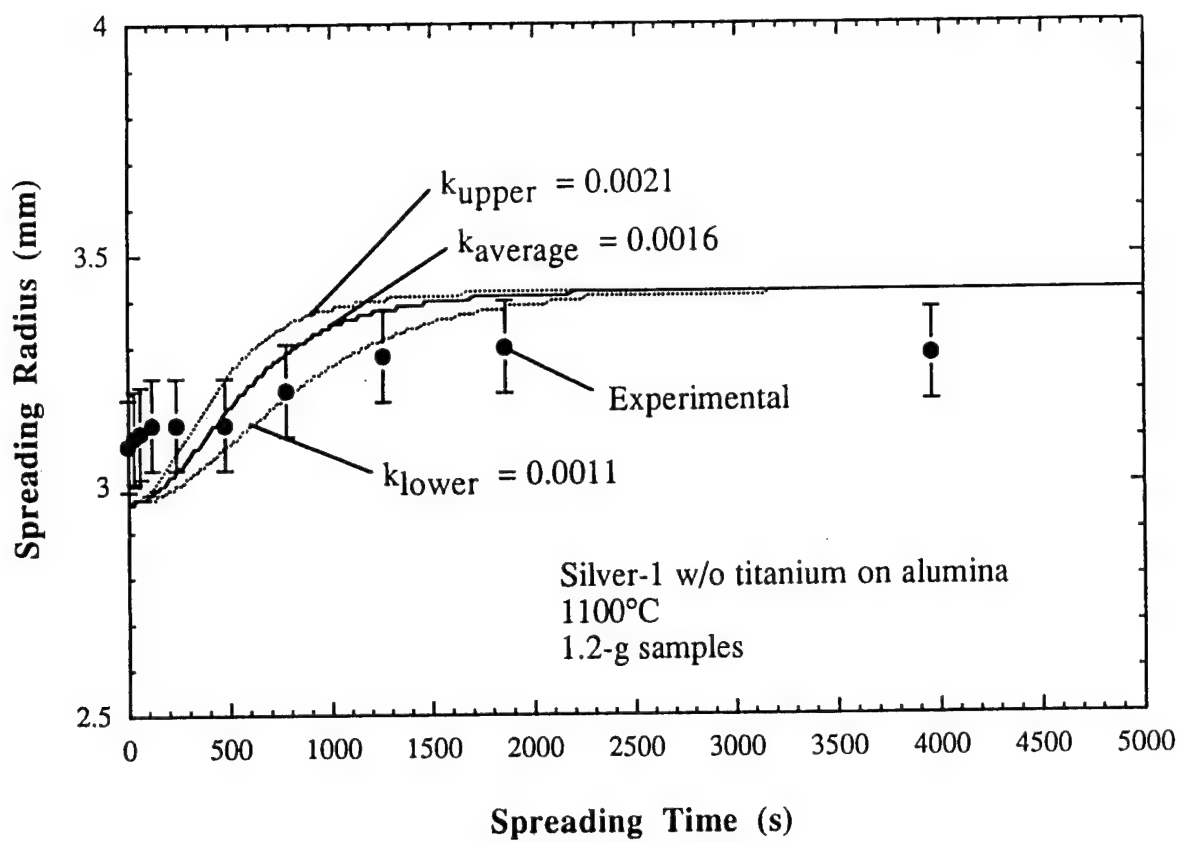
Figure 47: Theoretical spreading radius curves and experimental data for silver-1 w/o titanium on alumina at 1100°C. The error bars on the experimental data represent the uncertainty in the radius measurements.
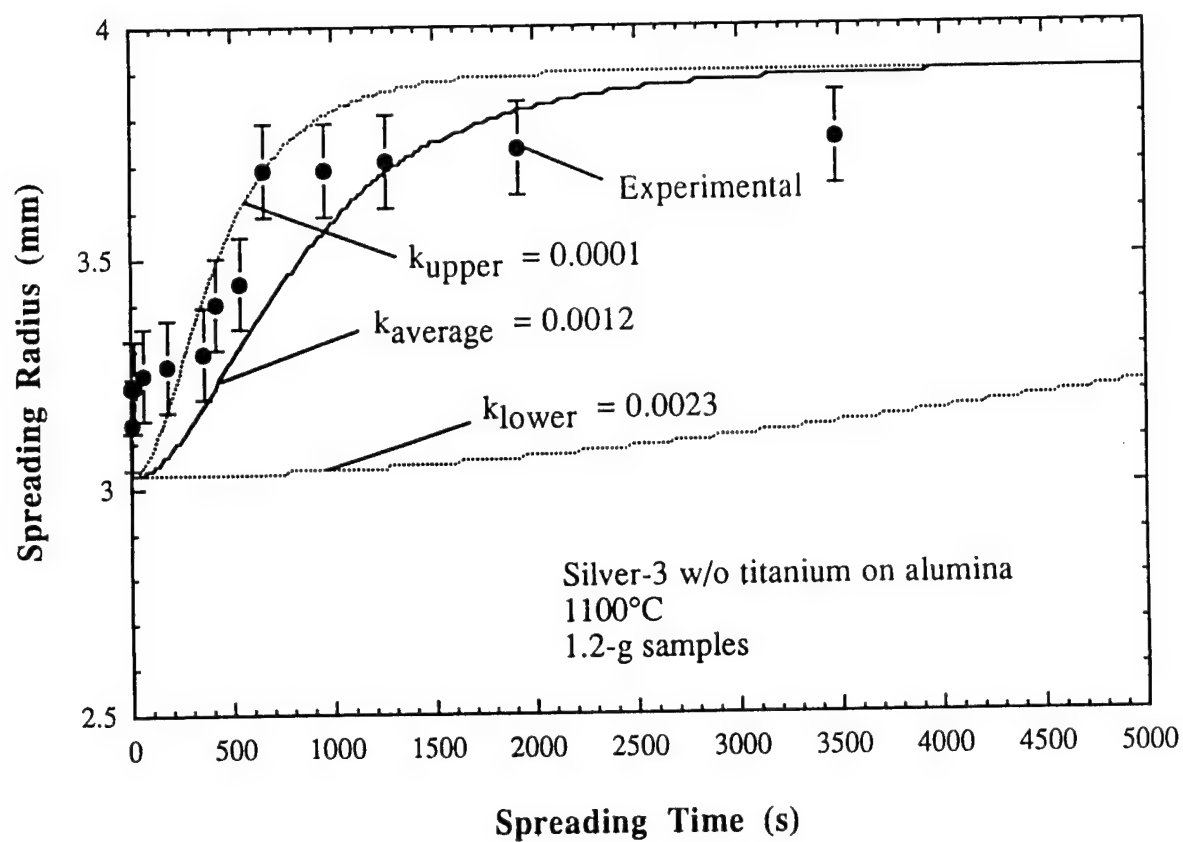
Figure 48: Theoretical spreading radius curves and experimental data for silver-3 w/o titanium on alumina at 1100°C. The error bars on the experimental data represent the uncertainty in the radius measurements.
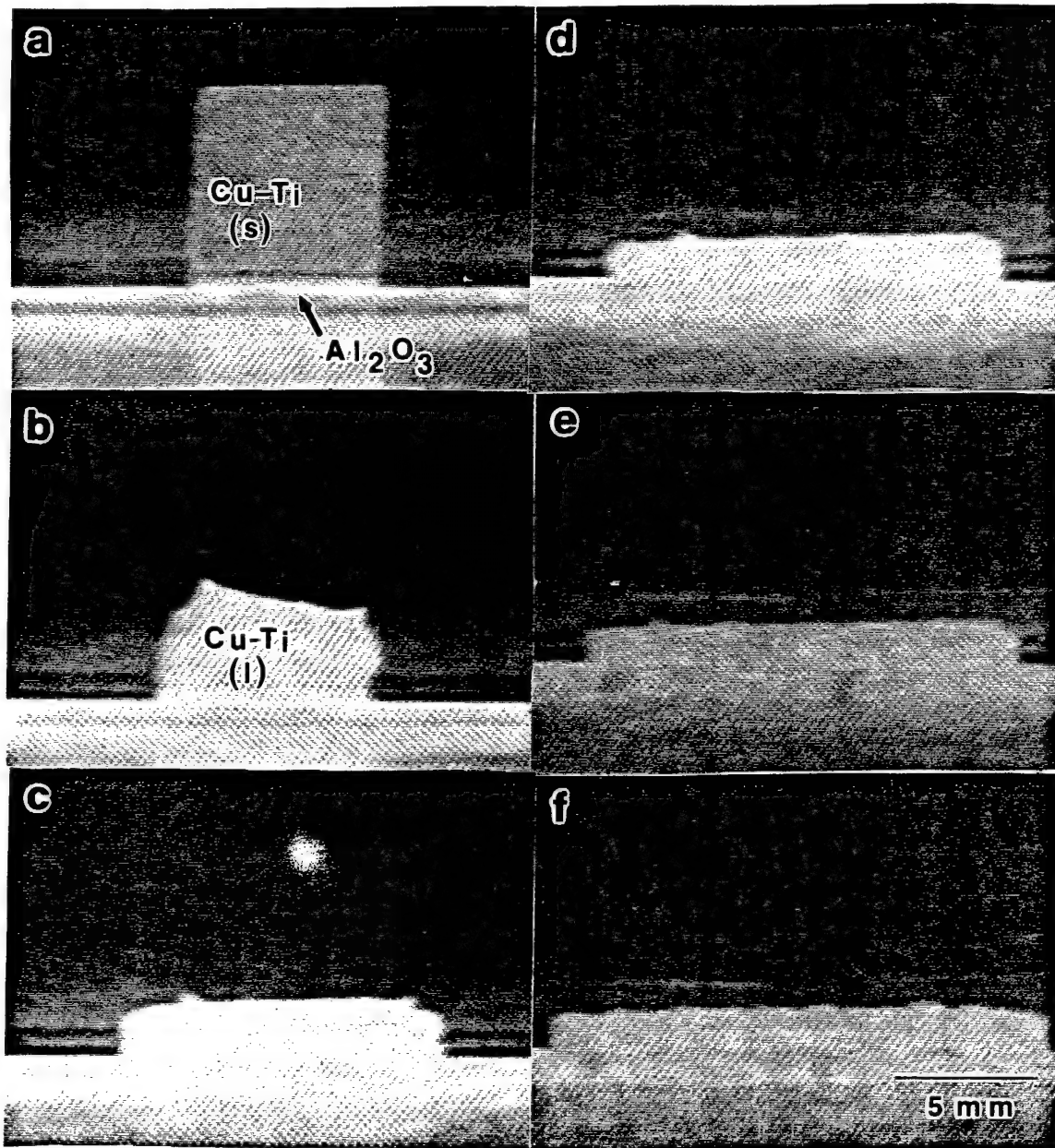
Figure 49: Spreading of a pre-alloyed copper-20 w/o titanium alloy on alumina at 1200°C: a.) initial configuration, b.) alloy melting (≈1010°C), c.) significant spreading during the heat-up cycle (1100°C), d.) 1150°C, e.) upon reaching 1200°C, and f.) after holding at 1200°C for 7 ks, very little spreading has occurred.
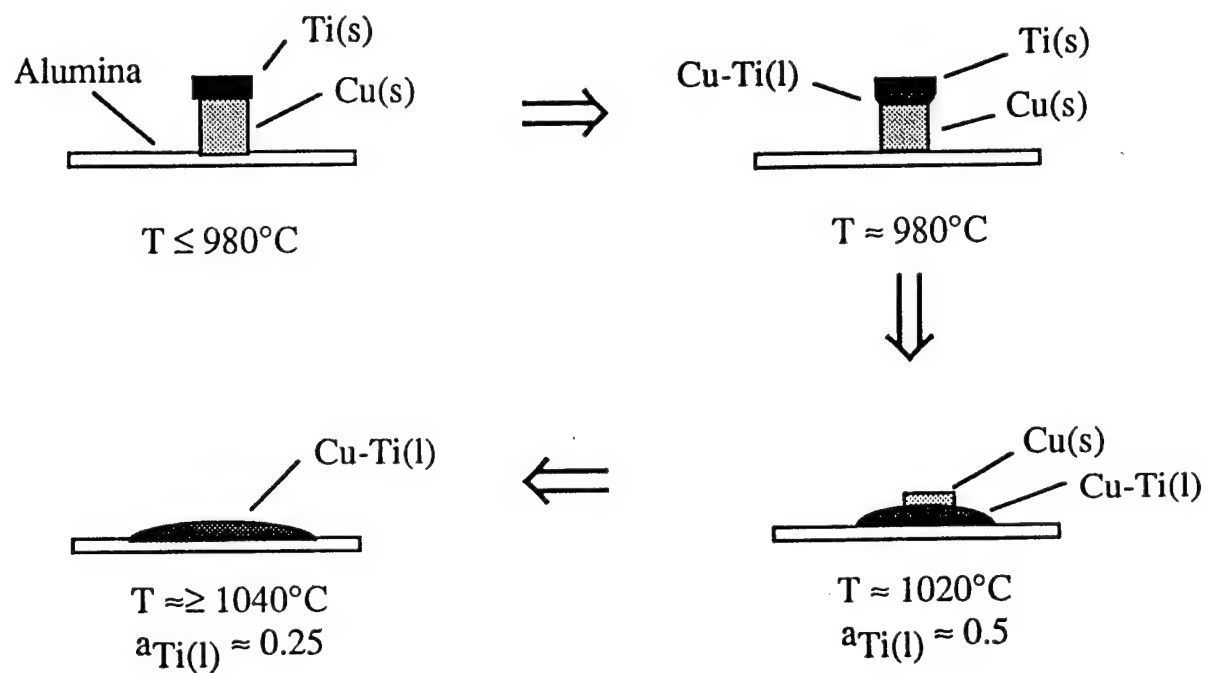
Figure 50: Schematic diagram of the changes which occur when a
titanium/copper/alumina stack is heated from room temperature to
1200°C.
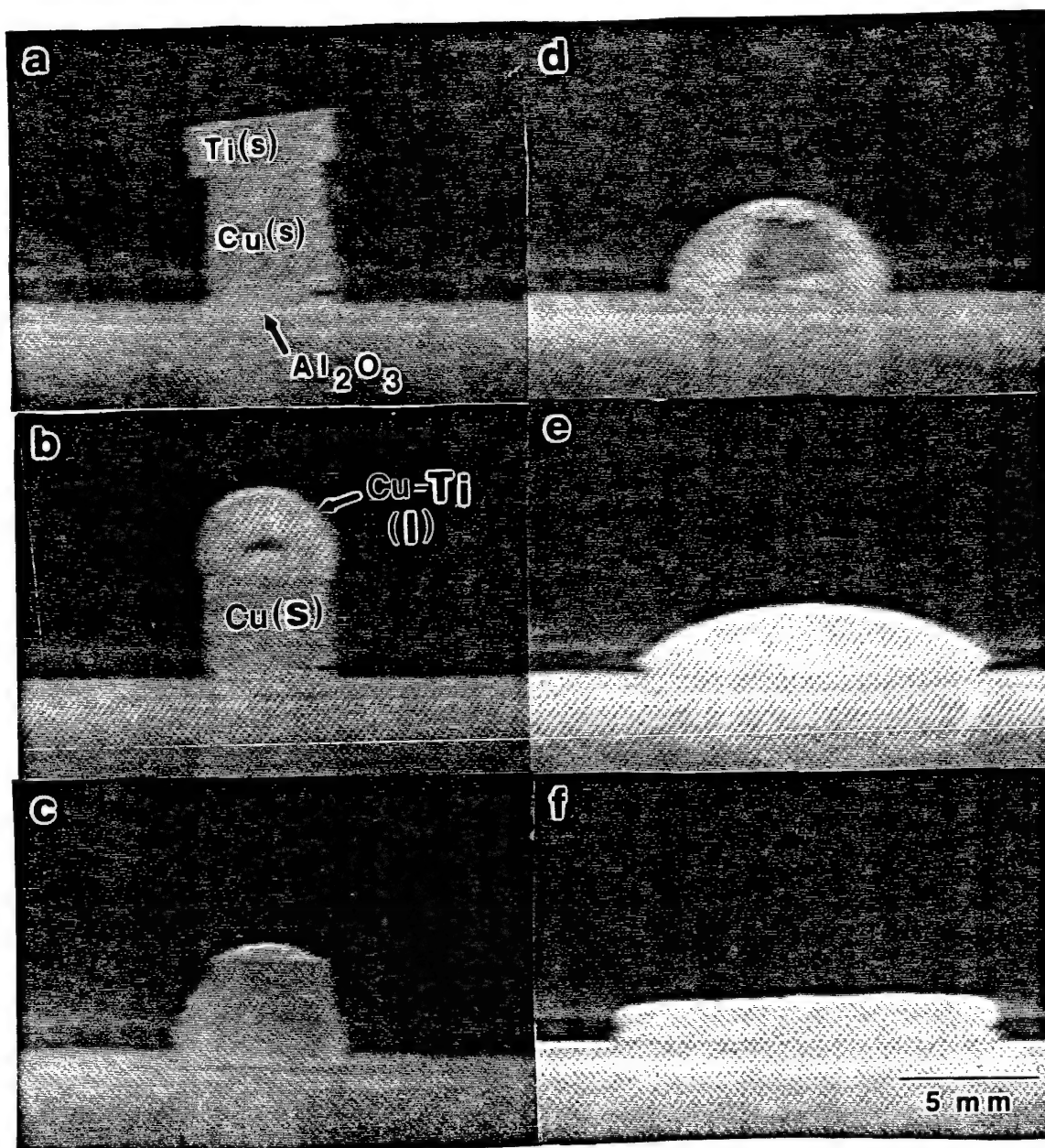
Figure 51: Spreading of a copper-20 w/o titanium alloy on alumina at 1200°C for the
titanium stacked on copper starting configuration: a.) initial configuration,
b.) high Ti concentration liquid forms (≈975°C), c.) the high-Ti liquid falls
onto the slumina substrare (≈990°C), d.) the liquid spreads before the Cu
is completely dissolved (≈1005), e.) spreading continues during the heat-
up cycle (1100°C), and f.) spreading is nearly complete when 1200°C is
attained.
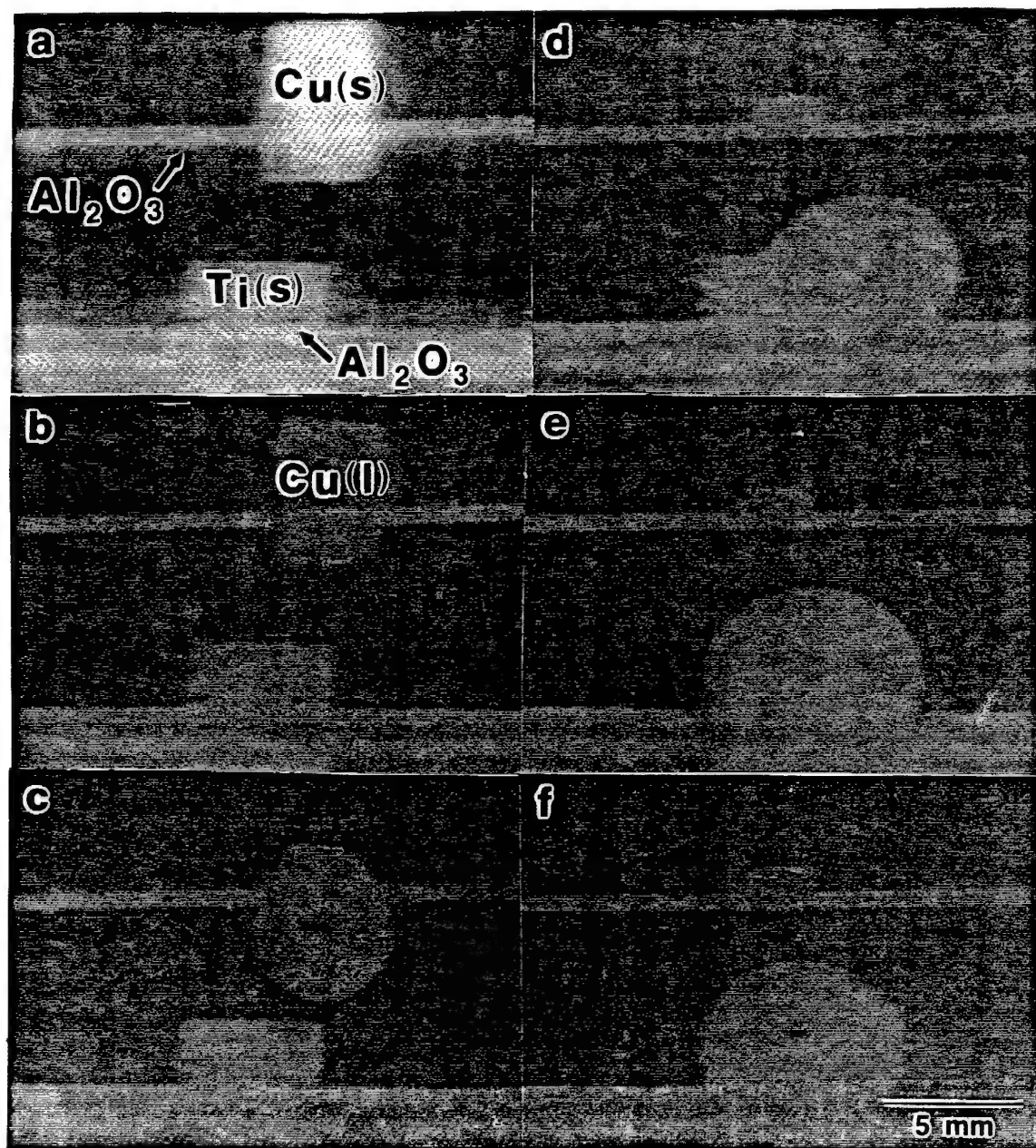
Figure 52: Formation of copper-20 w/o titanium alloy using the improved sessile drop
configuration: a.) initial configuration, b.) copper melts ($\approx$1100°C), c.) liquid
copper creeps through gap between plates, d.) copper falls onto Ti (1200°C),
e.) Cu dissolves Ti (~8s after contact), and f.) dissolution is complete (~24s
after contact).
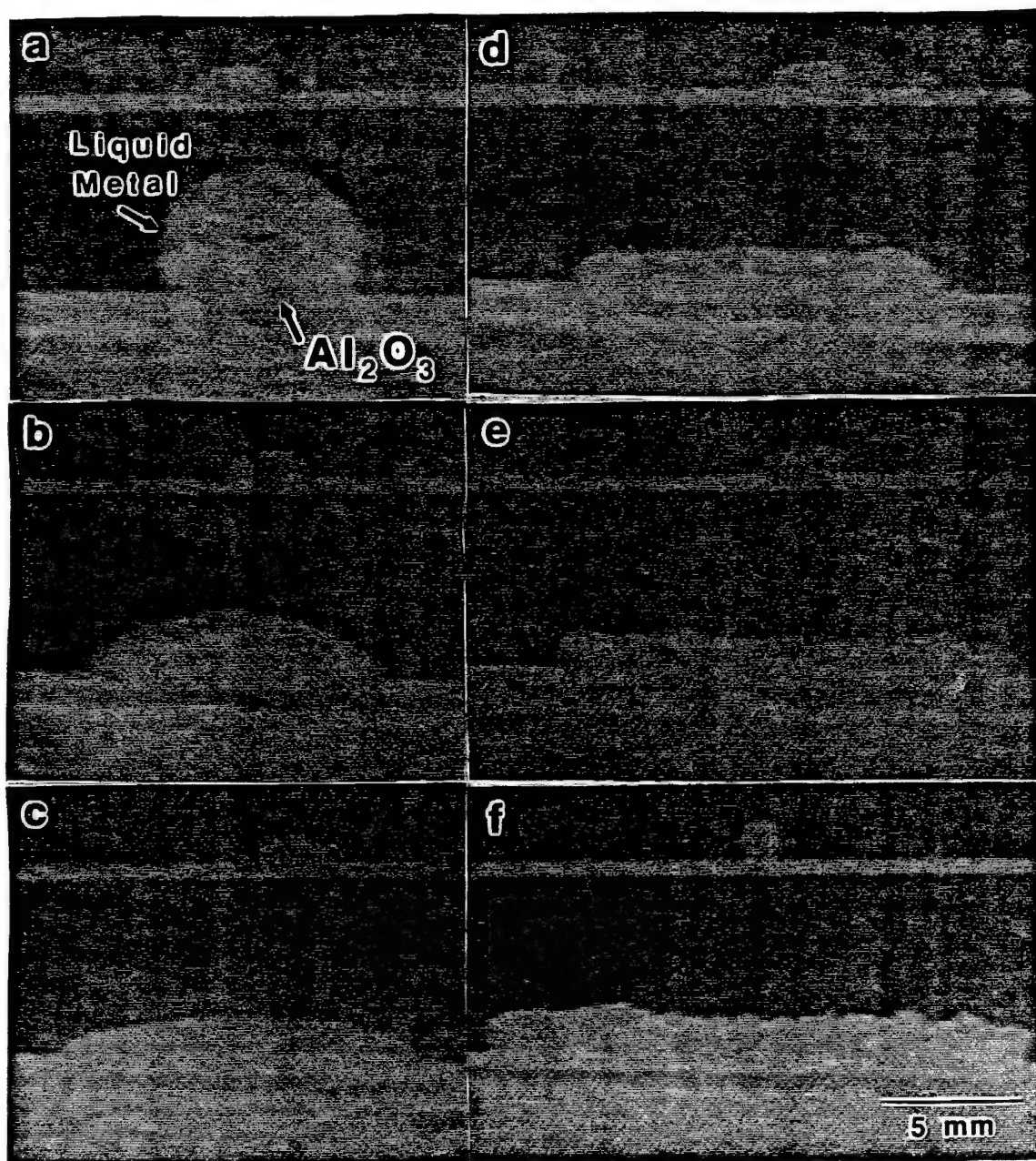
Figure 53:   Spreading of copper-20 w/o titanium alloys on alumina at 1200°C for the
mproved sessile drop configuration: a.) at 1200°C (t = 0 s), b.) t = 40 s, c.)
t = 300 s, e.) t = 1200 s, and f.) t = 10 ks.

D.   REFERENCES

1   "Thin Film Substrate Technical Specifications 10-2-0692", Coors Ceramics Company-Electronics, Golden, CO 80401.

2   Loehman, R., "Interfacial Reactions in Ceramic-Metal Systems", Ceram Bull 68 [4] (1989), pp. 891-896.

3   Loehman, R.E., and A.P. Tomsia, "Reactions of Ti and Zr with AlN and Al_2O_3", Acta Metall Mater 40 (suppl 1992), pp. 575-583.

4   Laurent, V., D. Chatain, and N. Eustathopoulos, "Wettability of SiO_2 and oxidized SiC by Aluminum", Mat Sci Eng A135 (1991), pp. 89-94.

5   Xue, X.M., J.T. Wang and M.X. Quan, "Wettability and Spreading Kinetics of Liquid Aluminum on Boron Nitride", J Mater Sci 26 (1991), pp. 6391-6395.

6   Shimbo, M., M. Naka, and I. Okamoto, "Wettability of Silicon Carbide by Aluminum, Copper and Silver", J Mat Sci Letters 8 (1987), pp. 663-666.

7   Kristalis, P., L.Courdier, and N. Eustathopoulos, "Contribution to the Study of Reactive Wetting in the $CuTi/Al_2O_3$ System", J Mat Sci 26 (1991), pp. 3400-3408.

8   Ambrose, J.C., M.G. Nicholas and A.M. Stoneham, "Dynamics of Braze Spreading", Acta Metall Mater 40 [10] (1992), pp. 2483-2488.

9   Kim, D.H., S.H. Hwang, and S.S. Chun, "The Wetting, Reaction and Bonding of Silicon Nitride by Cu-Ti Alloys", J Mat Sci 26 (1991), pp. 3223-3234.

10 Rhee, S.K., "Critical Surface Energies of Al_2O_3 and Graphite", J Amer Cer Soc 55 (1972), pp. 300-303.

11 Nikolopoulos, P., "Surface, Grain Boundary and Interfacial Energies in Al_2O_3 and Al_2O_3-Sn, Al_2O_3-Co Systems", J Mat Sci 20 (1985), pp. 3993-4000.

12 Ambrose, J.C., M.G. Nicholas, N. Young, and S.L. Jenkins, "Wetting and Spreading of Ni-P Brazes: Effects of Workpiece and Braze Composition", Mat Sci Technol 6 (Oct 1990), pp. 1021-1031.

13 Nicholas, M.G., D.A. Mortimer, L.M. Jones, and R.M. Crispin, "Some Observations on Wetting and Bonding of Nitride Ceramics", J Mat Sci 25 (1990), pp. 2679-2689.

14   Xue, X.M., J.T. Wang, and Z.T. Sui, "Wettability and Interfacial Reaction of alumina and Zirconia by Reactive Silver-Indium Base Alloy at Mid-Temperatures", J Mat Sci 28 (1993), pp. 1317-1322.

15   Fujii, H., H. Nakae, and K. Okada, "Interfacial Reaction Wetting in the Boron Nitride/Molten Aluminum System", Acta Met Mater 41 [10] (1993), pp. 2963-2971.

16   Fujii, H., H. Nakae, and K. Okada, "Four Wetting Phases in AlN/Al and AlN Composites/Al Systems, Models of Nonreactive, Reactive and Composite Systems", Met Trans 24A [10] (1993), pp. 1391-1397.

17   Naidich, Yu.V., "Wettability of Solids by Liquid Metals", Prog in Surf Membrane Sci 14 (1988), pp. 353, 388.

18   Ip, S.W., M. Kucharski, and J.M. Toguri, "Wetting Behavior of Aluminum and Aluminum Alloys on Al_2O_3 and CaO", J Mat Sci Letters 12 (1993), pp. 1699-1702.

19   Fisher, L.R., "Measurement of Small Contact Angles for Sessile Drops", J Colloid Int Sci 72 [2] (1979), pp. 200-205.

20   Meier, A., M.D. Baldwin, PR. Chidambaram, and G.R. Edwards, "The Effect of Large Additions on the Wettability and Work of Ahhesion of Copper-Oxygen Alloys on Polycrystalline Alumina", accepted for publication in: Mat Sci Eng A.

21   Li, J.G., L. Courdurier and N. Eustathopoulos, "Work of Adhesion and Contact-Angle Isotherm of Binary Alloys on Ionocovalent Oxides", J Mater Sci 24 (1989) pp. 1109-1116.

22   MacDonald, J.E., and J.G. Eberhardt, "Adhesion in Aluminum Oxide-Metal Systems", Trans AIME 233 [3] (1965) pp. 512-517.

23   Iida, T. and R.I.L. Guthrie, The Physical Properties of Liquid Metals Clarendon Press, Oxford (1988), pp. 70, 134 and 183.

24   Kristalis, P., B. Drevet, N. Valignat, N. Eusthathopoulos, "Wetting Transitions in Reactive Metal/Oxide Systems", Scripta Met 30 [9] (1994), pp. 1127-1132.

25   Deneker, S.P., "Cohesion in Refractory Moncarbides Mononitrides and Monoxides", J Less Common Metals 14 (1968), pp. 1-22.

26   Mehorta, S.P., and A.C.D. Chaklader, "Interfacial Phenomena between Molten Metals and Sapphire Substrate", Met Trans 16B (Sept 1985), pp. 567-585.

27   Nogi, K., K. Oishi, and K. Ogino, "Wettability of Solid Oxides by Liquid Pure Metals", <u>Mat Trans JIM</u> <u>30</u> [2] (1989) pp. 137-145.

28   Masslaski, T.B. (Ed.), <u>Binary Alloy Phase Diagrams</u> Vol. 1 and 2, ASM International, Materials Park, OH (1990), pp. 106 and 1495.

II.   Role of Oxygen in the Cu-O-Ti/Sapphire Interfacial-Region Formation

In the Cu-Ti/sapphire system, modeling of the interfacial-region formed by Active Metal Brazing has traditionally been based on the reduction reaction between titanium (the active element) and oxygen (from the stoichiometric decomposition of the sapphire) to form TiO as the intermediate oxide layer that bridges between the filler metal and the ceramic substrate. Several investigations have been devoted to identifying possible contributions for the total Gibb's free energy change of the reaction which would validate this proposed path for the interfacial region formation.

However, the oxygen concentrations of the precursor alloy and gas phase are normally ignored in these investigations. Additionally, titanium atoms in solution are not known to be surface active in liquid copper and the observed titanium segregation to the metal/sapphire interface can only be attributed to a coadsorption phenomenon involving oxygen participation. Therefore, instead of accepting sapphire decomposition as the only source of oxygen in the brazing system, this research task has been devoted to elucidate the mechanistic role of the readily available oxygen in the Cu-Ti alloy and in the gas phase, in the formation of the Cu-Ti/sapphire interfacial region.

Sapphire single crystals were contacted with three Cu-Ti-O alloys containing 4 at. pct. titanium and 100, 860 and 2,400 ppm of oxygen in controlled oxygen partial pressure atmospheres (between 10^{-7} and 10^{-30} atm).

The Ti-O system stability diagram was extended to include all possible solid and gaseous oxides species. $TiO_{(g)}$ was shown to be a predominant gaseous species for the processing conditions. The development of thermodynamic equations describing the segregation of titanium in the Cu-O-Ti system indicated that the surface enrichment of titanium occurs simultaneously with oxygen. This observation of Ti-O coadsorption and the identification of the gaseous $TiO_{(g)}$ species were then used to model the formation of a sessile drop with Cu-Ti alloy in static equilibrium with the sapphire substrate. In this model, the

reaction layer responsible for bonding between sapphire and Cu-Ti alloy is postulated to be the result of a solution reaction between the Ti-O coadsorbed interphase and the sapphire, and not the direct reaction between titanium and sapphire. XPS analyses conducted on the metal/gas atmosphere and metal/sapphire interfaces corroborate the proposed model. Measurements obtained by SEM analyses showed that the thickness of the Ti-O coadsorption interphase increased dramatically with increase in the bulk oxygen concentration from 100 to 2,400 ppm. These results provide definitive validation that the titanium segregation to the interfacial region is controlled by the bulk oxygen concentration.

A. Experimental

1. Ceramic-to-Oxide Bonding: Background

Oxygen is an inherent species in the Cu-Ti/Sapphire system. It is present in the sapphire (Al_2O_3), in the reaction interphase region, in the Cu-Ti filler alloy, and in the brazing atmosphere. Consequently, the demand for improvements in the performance and reliability of metal alloy-sapphire joints, when operating under extreme conditions, can be best achieved by developing a basic understanding of the role of oxygen in the complex interactions that occur at the metal/sapphire interface, in the bulk metal, and at the metal/gas atmosphere interface.

Oxide-metal interfaces of commercial and scientific interest are typically obtained by the formation of a reaction interphase region at the interface. As such, thermodynamics becomes the tool of choice for the development of models that would predict the possible formation (stability) of ceramic/metal interfaces and provide insight into the possible mechanisms. The first investigations based on equilibrium (thermodynamic) approach were conducted by Humenik and Kingery [1], and, McDonald and Eberhart [2] who proposed that bonding of Al_2O_3 to a metal could be directly established between the oxygen anions at the ceramic surface and the metal cations. The stability of this bond could be evaluated by a direct relation between the work of adhesion (W_{AD}) and the standard Gibb's free energy of formation of the metal oxides (ΔG^o). The direct bonding model between metals and sapphire is supported

by the theoretical quantum-mechanical calculations conducted by Johnson and Pepper [3] and Ohuchi et al. [4](1991).

Blackburn [5] showed that wetting of Al_2O_3 by metals and subsequent adherence could be promoted through metal oxidation in slightly oxidizing atmospheres, followed by the dissolution of this oxide in Al_2O_3, even for metals that do not possess the necessary thermodynamic "potential" to reduce sapphire (e.g. copper and nickel). The strength of the interface is related to the reaction between this metal-oxide interlayer and Al_2O_3 to form a complex oxide.

The understanding of the role of oxygen in the interface region formation has advanced substantially with the advent of modern surface analysis techniques. In the system $Cu-Al_2O_3$ system, Ohuchi et al. [6,7] showed that when oxygen is absent in the atmosphere (under UHV conditions, with estimated oxygen partial pressures lower than 10^{-40} atm) copper will bond directly, even though weakly, to sapphire. This result was the first experimental confirmation of the direct bonding between copper and the oxygen atoms at the surface of Al_2O_3 as proposed by Johnson and Pepper [3]. In contrast, the deposition of copper in the presence of oxygen showed a much larger number of atoms involved in the interfacial bonding phenomenon, which also increased the adhesion significantly [8]. The same trend was also found in the Ni/Al_2O_3 system, where the expected formation of nickel aluminate spinel $(NiAl_2O_4)$ [9] only occurred when oxygen partial-pressure was high enough to stabilize the spinel [7]. Under UHV conditions, however, an Ni-Al intermetallic compound was observed to form at the Ni/Al_2O_3 interface.

The results obtained from the surface analytical techniques clearly demonstrated that bonds with entirely different characteristics can be obtained depending on the amount of oxygen available in the system. In contrast, the differences in the nature of the interfaces observed in active metal brazing promoted two different thermodynamic approaches in modeling the oxide ceramic/filler metal interfacial reactions. The first approach considered the solution reaction, where the presence of oxygen (in a form of a surface oxide film) is required

for the formation of an interphase [10,11]. The second approach is more applicable to metals with great affinity for oxygen (e.g. titanium, vanadium, chromium, yttrium, and niobium). In this case, the development of an interfacial product is considered to be the result of a reduction reaction, where the active element reacts directly with the ceramic oxide, establishing a bond between the two components.

In the case of the solution reaction, the presence of an initial oxide interlayer, such as would be formed under an oxidizing atmosphere is not essential. Instead, segregation of oxygen may occur as a result of coadsorption of metal atoms with the residual oxygen atoms (commonly found in copper and other metals) to form metal oxygen complexes. This coadsorption phenomenon has been identified with the simultaneous surface segregation of two species through an attractive interaction mechanism [12]. Thus, coadsorption refers to the process by which a non-surface active solute segregates to an interface because of its strong interaction with oxygen, which is surface active, in the liquid metal. In the case of Cu-Ti-O system, it is well documented in the literature that oxygen is highly surface active in liquid copper [13,14,15]. On the other hand, quantum-mechanical theoretical calculations such as those carried out by Mukherjee [16] have shown that titanium is not surface active in molten copper. Also, the very large negative interaction parameter for Ti-O [17] reflects the strong interaction between the titanium and oxygen atoms, which is consistent with the expectation of strong coadsorption of titanium-oxygen in liquid copper.

The concept of reduction reaction is easily incorporated in the active metal brazing process and consists of the addition of an active element, at low concentrations, to a metal solvent to promote the reduction of the oxide ceramic at the interface. However, even for those elements known as "reactive metals", the standard Gibb's free energy changes for the reduction of Al_2O_3 are positive, which implies that the reduction reactions are not thermodynamically feasible. This dilemma has been the focus of several investigations in search of favorable contributions to the total free energy change for the reduction reaction, which

would then provide explanations for the experimentally observed interface formation, thereby validating the reduction reaction as the actual path for the interfacial region formation [18].

In the Cu-Ti/Al_2O_3 system, the formation of TiO has been identified by many authors as the interfacial product associated with the bonding process [19,15,20,21]. In fact, soon after Naidich and Zuralev [22] identified TiO as the only titanium oxide to be wetted by copper, the thermodynamic requirement for the stability of TiO in the interfacial-region has been used interchangeably as the conditions for the promotion of wetting in systems using titanium as the active element. The proposed path for the interface formation is as follow:

$$Al_2O_3 + \underline{Ti} \Leftrightarrow \underline{Al} + TiO \qquad \Delta G_R^o$$
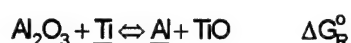
where $\underline{Al}$ and $\underline{Ti}$ represent element solution in the copper matrix. Several investigators have shown that the above reaction can be stable if the contributions of the dissolution of the active elements such as oxygen and aluminum in the solvent metal are considered [20,21].

However, direct reduction of the ceramic oxide may not necessarily be the only path for the interphase region formation. In fact, several limitations to the direct reduction approach exists. For example, if the stoichiometric dissociation of the ceramic oxide is considered as the only source of oxygen, the initial oxygen content of the alloy, which could have a dramatic influence on the thermodynamic activity of the active element in the melt would be ignored. This limitation becomes even more apparent when it is recognized that all active elements interact readily with oxygen, and that the presence of oxygen at residual levels is common in most metals.

Additionally, the titanium concentration at the metal/Al_2O_3 interface can be much higher than that within the bulk liquid phase [15], indicating segregation of the element. Since titanium is not a surface-active element in copper [16], the observed surface enrichment can only be attributed to coadsorption of (Ti-O) complexes.

Ultimately, the separation between solution reaction and reduction reaction can only be considered academic, since there are no clear criteria that define the boundaries between the two approaches. The most compelling reason for refuting this division is that even in the most

controlled brazing environments, the presence of oxygen can not be completely excluded from the system. Thus, there is the need of better understanding of the mechanism(s) of interfacial reaction layer formation.

2. Thermodynamic Considerations

a. Equilibrium Al-O-Ti Phase Distribution

In the Cu-Ti/Sapphire system, the formation of TiO, with 1 to 2 at. pct. dissolved aluminum, has been identified by several investigators [15,20,21,23,24,], in sessile drop experiments or in actual active-metal brazing experiments carried out in protective atmospheres or vacuum. This consistency in the identification of TiO as the reaction product is, in fact, surprising if one considers that the formation of TiO alone is not supported by the most recent isothermal section of the Al-O-Ti ternary diagram shown in Figure 1 [25]. This diagram shows tie-lines radiating from Al_2O_3 to all other phases present in the diagram, indicating that Al_2O_3 can be in equilibrium with any phase but the β-Ti. Using basic rules such as the charge and mass balance, and chemical potential gradient considerations, [25] showed that the phase distributions for the $Ti-Al_2O_3$ reaction can only follow the two sequences below:

$$\beta - Ti/\alpha - Ti(Al,O)/Ti_3Al(O)/TiAl(O)/Al_2O_3$$

or

$$\beta - Ti/\alpha - Ti(Al,O)/Ti_3Al(O)/Al_2O_3$$
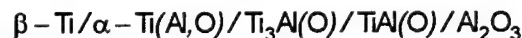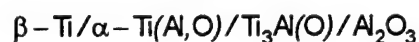
depending on the oxygen activity in the system. In addition to the α- and β-Ti solution, intermetallic compounds such as Ti_3Al and $TiAl$, with oxygen in solution, are the phases identified. These sequences of reaction products agree with the results of [26,27], and with the analyses conducted by Ohuchi [4], Chaug et al. [28], using advanced surface-sensitive techniques under extremely well controlled conditions.

The interfacial reaction products reported by the investigators engaged in phase diagram determination, $Al_2O_3/Ti_3Al(O)$ or $TiAl(O)/TiO$, are clearly different from that determined in active-metal brazing experiments, TiO. The distinction between the two

processes is traced to fact that the phase diagram determination experiments were conducted at 1100°C with no melting of the alloys, while the brazing process involved the melting of the filler metal. In the solid-state reactions, oxygen may not be readily available for the reactions at the interface. The presence of coadsorbed Ti-O complexes in the interfacial regions in active-metal brazing is, most likely, the explanation for the different reaction products identified in the two experiments.

The controversy on the nature of the interfacial products extends also to the duplex layer (Ti$_3$Al(O) and TiAl(O)) identified in the solid-state diffusion couples and phase diagram experiments which is not always found in the reported interfacial analyses of active-metal brazed joints. Nevertheless, Kritsalis et al. and Bang [20,21] reported the presence of Cu$_2$Ti$_2$O and Ti$_3$Cu$_3$O between the reaction layer of TiO and the bulk filler metal.

b. Titanium-Oxygen Phase Stability

In addition to the Al-O-Ti ternary diagram, the Ti-O stability diagram is also useful in the investigation of interfacial reactions in Cu-Ti/Al$_2$O$_3$ bonding since it provides supplemental information on the stability of the different titanium oxides as a function of the partial pressures of gaseous species in the temperature range of interest. In the Ti-O system, vaporization experiments such as those conducted by Wahlbeck and Gilles [29] revealed that the non-stoichiometric TiO$_{(g)}$ is the main gaseous oxide species in the system, and should, therefore, be included in the calculations. Also, TiO$_{(s)}$ features a large range of nonstoichiometry and several phase transformations. Therefore, thermodynamic calculations of the partial pressures of oxygen, TiO$_{(g)}$ in equilibrium with TiO$_{(s)}$ and other titanium oxides (considered as stoichiometric line compounds) can provide semi-quantitative information on the interactions between the solid and gaseous species in the system. The final Ti-O equilibrium diagram, described in detail elsewhere [30], is shown in Figure 2. The calculations were made using the thermodynamic data provided by Pankratz [31] and considering the solid phases as in their standard state. The solid lines represent the calculated boundaries that define the stability

regions of the different titanium oxides as a function of the temperature and oxygen partial pressure. The $TiO_{(g)}$ partial pressures in equilibrium with oxygen and the various titanium oxides are represented in Figure 2 in the form of isobar lines (dashed lines) ranging from 4.6 x 10^{-10} to 2.5 x 10^{-15} atm. These isobars must be interpreted by parts. In the region of the stability of $TiO_{(s)}$, the partial pressure of $TiO_{(g)}$ is obviously independent of the oxygen partial pressure and the isobars are represented by vertical lines. In the stability regions of the oxygen-rich oxides, however, the partial pressure of $TiO_{(g)}$ depends on the partial pressure of oxygen, with the isobars assuming a negative slope. This change in slope means that as the oxygen partial pressure increases in those regions, the system shifts to a new equilibrium position at higher temperatures to provide the same $TiO_{(g)}$ partial pressure. In a similar way, it can be said that for the same temperature, the $TiO_{(g)}$ partial pressure decreases significantly as the system moves to regions of stability of oxygen-rich titanium oxides. Also, it is important to notice that the $TiO_{(g)}$ partial pressures in equilibrium with $TiO_{(s)}$ (e.g. 10^{-14} to 10^{-10} atm), are many orders of magnitude higher than the corresponding equilibrium oxygen partial pressures (10^{-35} to 10^{-25} atm), in agreement with the titanium oxide vaporization experiments by Gilles et al. [32]. This analysis implies that the transport of oxygen between the solid and gaseous phase may be realized basically in the form of $TiO_{(g)}$ and not as oxygen itself.

c. Oxygen-Titanium Coadsorption in Molten Copper

The concept of coadsorption of copper-oxygen, most probably Cu_2O, as being responsible for the decrease in the liquid copper surface tension is well established in the literature [13,14,33]. More recently, the coadsorption of chromium-oxygen clusters has been invoked by Kritsalis et al. [34,35] as necessary to explain the wetting behavior of Cu-Cr and Ni-Cr alloys on sapphire under variable oxygen activities in the metallic alloy.

The modeling of interfacial segregation based on the regular solution type model for the thermodynamic equilibrium between the bulk and surface phases has been popular for quite some time [36]. Recently, Plessis and van Wyk [37] revisited the regular solution model for

segregation in multicomponent alloys in terms of macroscopic thermodynamic properties and generalized the model derived by McMahon and Marchut [38] which based on the initial analysis of Guttmann [36]. The basic hypothesis of the model are as follow:

- Surface segregation is defined as the redistribution of solute atoms between the surface and bulk of a crystal which are both regarded as open systems.

- The surface region is finite and the bulk is infinite in size but the two together form a closed system for the crystal as a whole.

- Equilibrium is reached when the energy of the closed system is a minimum.

A complete and detailed derivation of the model is shown in the work of McMahon and Marchut [38]. Application of the model with detailed calculations has also been discussed recently by Camargo [30]. Here, only the final equations are presented for the determination of the equilibrium surface concentrations of the solutes in a ternary system. Species 1 and 2 are the solutes and species 3 is the solvent.

$$X_1^\Phi = \frac{X_1^B \exp\left(\dfrac{\Delta G_1}{RT}\right)}{1 - X_1^B + X_1^B \exp\left(\dfrac{\Delta G_1}{RT}\right) - X_2^B + X_2^B \exp\left(\dfrac{\Delta G_2}{RT}\right)} \tag{1}$$

and

$$X_2^\Phi = \frac{X_2^B \exp\left(\dfrac{\Delta G_2}{RT}\right)}{1 - X_2^B + X_2^B \exp\left(\dfrac{\Delta G_2}{RT}\right) - X_1^B + X_1^B \exp\left(\dfrac{\Delta G_1}{RT}\right)} \tag{2}$$

where

$$\Delta G_1 = \Delta G_1^\circ + 2\Omega_{13}\left(X_1^\Phi - X_1^B\right) + \Omega'\left(X_2^B - X_2^\Phi\right) \tag{3}$$

$$\Delta G_2 = \Delta G_2^\circ + 2\Omega_{23}\left(X_2^\Phi - X_2^B\right) + \Omega'\left(X_1^B - X_1^\Phi\right) \tag{4}$$

and

$$\Omega' = \Omega_{12} - \Omega_{13} - \Omega_{23} \tag{5}$$

In these equations, X_i^Φ and X_i^B correspond to the respective surface and bulk concentrations of the element i, the Ω_{ij} terms represent the binary interaction parameters in a quasi-chemical

manner of the corresponding binary system. The term ΔG_i^o represents the adsorption energy of the element i in the metal matrix (species 3) and it accounts for the change in non-configurational enthalpy (i.e. elastic, vibrational, etc.) when one solute atom replaces one solvent atom in the boundary [36].

The interaction parameters Ω_{12}, Ω_{13}, and Ω_{23} were obtained from the Gibb's free energy of the solution calculation considering each of the solutes in their respective solvent. The thermodynamic data for the Cu-O, Cu-Ti, and Ti-O binary systems were extracted from work of Schmid [39], Hoshino et al. [40], and Pajunen and Kivilathi [41], respectively. In addition to the binary interaction parameters, the adsorption energies of oxygen and titanium (as solutes) in the Cu-O and Cu-Ti binary systems (ΔG_1^o and ΔG_2^o) were determined. In particular, the adsorption energy in the Cu-Ti system was estimated using the Miedema [42] model, with the prediction of -47,500 J/mole for the adsorption of titanium in copper. For the adsorption of oxygen in copper, an adsorption energy of +420,000 J/mole was provided by Gerasimov [43] who based his calculation on experimental measurements and theoretical predictions. This value is an indication of the strong surface activity of oxygen in copper and correlates very well with the value of + 458,964 J/mol reported by Toyoshima and Somorjai [44]. Figure 3 shows the chemical composition profile for a system that contains 0.01 at. pct. oxygen and 1.0 at. pct. titanium. Note that approximately 50 to 100 ppm oxygen are typically found in OFHC copper and 1.0 at. pct. titanium represents the typical upper limit of the active metal in most commercial brazing alloys. Despite that titanium is not surface active in copper, it can cosegregate to the free surface due to the strong interaction with oxygen. Also, the equilibrium free surface composition is basically composed of oxygen with small concentrations of titanium and no copper. The complete absence of copper (the solvent) at the surface is because of the strong decrease in the total Gibb's free energy of the system promoted by the Ti-O coadsorption to the free surface. In addition, the equilibrium surface composition is temperature sensitive, with the general trend of oxygen enrichment and titanium depletion on the surface as the temperature increases. The time required to establish the equilibrium at the

interface was estimated to be only fractions of a second for a temperature just below the melting point of the Cu-Ti alloy [30]. This calculation clearly indicates that equilibrium Ti-O surface concentration in the Cu-O-Ti ternary system can be established at the free surface much earlier than any interfacial reaction between the Cu-O-Ti alloy and the sapphire. According to these calculations, the modeling of the brazed Cu-O-Ti/sapphire interfacial region as a result of the interaction between the Ti-O coadsorption layer and sapphire is well based.

The equilibrium titanium-oxygen ratio, in addition to being temperature sensitive, was found to depend strongly on the bulk titanium and oxygen concentrations. As such, the physical properties of the Cu-O-Ti/sapphire interfacial region are expected to closely relate to the equilibrium Cu-O-Ti surface composition.

3. Model Conceptualization

Based on the Ti-O coadsorption model and the characterization of $TiO_{(g)}$ as the most important gaseous species in the Ti-O system, the equilibrium situation for a sessile drop in the Cu-Ti-O/sapphire system was proposed in Figure 4. The thermodynamic equilibrium between the bulk and the surface of the Cu-O-Ti alloy is achieved by the Ti-O coadsorption to both Cu-O-Ti/sapphire and Cu-O-Ti/gas atmosphere interfaces. As indicated earlier, the actual interfacial titanium-to-oxygen ratio is determined by the processing temperature and the titanium and oxygen bulk concentrations in the Cu-O-Ti alloy. At the metal/gas interface, the adsorbed layer is in equilibrium with oxygen and $TiO_{(g)}$. It is important to notice that the formation of $TiO_{(g)}$ would imply in a loss of oxygen and titanium from the alloy, and the formation of a $TiO_{(s)}$ film ahead of the gas/liquid/solid triple point by vapor deposition. Such a film would be an ideal substrate for the Ti-Cu alloy to wet and spread. It is important to recall from Figure 2 that $TiO_{(s)}$ features the highest equilibrium partial pressure of $TiO_{(g)}$ compared to other higher oxygen titanium oxides, suggesting that $TiO_{(s)}$ would de the ideal metal/gas interfacial product. Moreover, stronger interaction with the sapphire would be expected if the reacting titanium oxide film is an oxygen-deficient TiO as compared to a titanium-rich

stoichiometric oxide such as TiO_2. The phase diagram in Figure 1 shows that TiO can be in equilibrium with Al_2O_3 and a limited solution would promote the formation of the interfacial region.

Considering that TiO represents the ideal Ti-O coadsorption product at both metal-gas and metal/sapphire interfaces, the optimal range of oxygen partial pressures for TiO stabilization is shown in Figure 2, between 10^{-27} and 10^{-35} atm at 1100°C.

In summary, the model proposes that the reaction layer, responsible for the interface formation between the Cu-Ti alloy and the sapphire, is not a result of direct reaction between titanium and sapphire. Instead, the interface formation is a result of the reaction between the adsorbed layer (Ti-O) and sapphire. At brazing temperatures, titanium aluminate ($TiAl_2O_4$) is not stable according to the Al-O-Ti ternary phase diagram presented in Figure 1. Nevertheless, a small amount of TiO may dissolve in sapphire to result in the Cu-Ti/sapphire bonding (formation of the "reaction layer" shown in Figure 4). In terms of bonding between the Cu-Ti alloy and the sapphire as a whole, TiO from Ti-O coadsorption represents the ideal surface reactant which interacts with sapphire to form the final interfacial region, and not the ideal reaction product itself as it is largely accepted in the current literature.

4. Experimental Verification

High purity copper and titanium metal were used to produce the three Cu-Ti filler metals with 4 at. pct. titanium and varying levels of oxygen (100, 860 and 2,400 ppm) for the sessile drop experiments. The substrates were high purity single crystal sapphire with (0001) orientation.

The sessile drop experiments were conducted in an environmental cell which was heated in a vertical tube furnace. The process temperatures and holding times were 1110, 1150 and 1190°C, and 5, 10 and 30 min., respectively. Details of the laboratory equipment has been described elsewhere [30]. Varying oxygen partial pressure was achieved by ppm-level hydrogen additions to the argon carrier gas and controlled by equilibrium between the

hydrogen-oxygen-water vapor in the gas phase. Measurements of oxygen partial pressures in the range of 10^{-7} to 10^{-30} atm were made using a stabilized zirconia oxygen sensor. A titanium sponge reactor was also incorporated into the system to remove trace concentrations of nitrogen in the gas phase.

The characterization of the interfacial regions was performed using three techniques: scanning electron microscopy (SEM), energy dispersive spectroscopy (EDS), and X-ray photoelectron spectroscopy (XPS). The SEM equipment (JEOL JXA-840) provided general imaging, phase characterization of the interfacial region, and X-ray dot mapping of the interfacial region (JEOL 6400-JSM SEM). These analyses provided for quantification of the size of the Ti-O coadsorption interphase as a function of the processing conditions. X-ray photoelectron spectroscopy (XPS) analyses was the most important analysis technique in this research since it has the surface sensitivity necessary to unambiguously identify the composition of the interfacial region in terms of its chemical constituents and bonding states.

B   Results and Discussion

The analysis and discussion section will be presented in two parts, based on the results obtained at the filler metal/gas atmosphere interface and the filler metal/sapphire interface.

1.   The Filler Metal/Gas Interface

The presence of concentric rings around the sessile drops that were produced by vapor deposition from $TiO_{(g)}$ was consistently observed in the sessile drop experiments. Note that $TiO_{(g)}$ was identified from the Ti-O stability diagram in Figure 2 as the most important gaseous species in this system, featuring equilibrium partial pressures that are many orders of magnitude higher than the corresponding oxygen partial pressures (Figure 2). Figures 5a and 5b show the top and bottom (through the transparent sapphire crystal) views of the metal droplet, respectively. The top view shows two distinct rings with characteristic colors: the inner ring (closer to the metal droplet) has a yellowish color that can be associated with that of TiO; the

outer ring appears bluish which is characteristic of oxygen-rich titanium oxides. These colors are quite different from the grayish color of the Cu-Ti/sapphire interface when viewed from the bottom through the sapphire lens, which is characteristic of hypostoichiometric TiO. XPS analysis on both rings showed that titanium and oxygen are present confirming the presence of titanium oxides. However, nitrogen has also been detected, particularly in the inner ring, indicating the presence of TiN. In fact, the color of the inner ring matches the color of TiN (goldish-yellow), closer than it does with TiO. Since TiN is not volatile [45] and that the nitrogen content in the Cu-Ti alloy was extremely low, it must have formed between nitrogen in the gas phase and the titanium oxide film formed by vapor deposition on the sapphire substrate. The source of nitrogen in the gas phase is argon because nitrogen can be present in argon as a trace impurity (Grade 5 Argon - between 4 to 6 ppm). While this concentration may seem to be minute, it can result in nitrogen partial pressures in the gas phase at the order of 3 to 5 x 10^{-6} atm (at 0.84 atm ambient pressure), which is orders of magnitude higher than the nitrogen partial pressure in equilibrium with TiN at 1100°C (approximately 1 x 10^{-17} atm).

The range of oxygen partial pressures more significant for the vapor deposition of $TiO_{(g)}$ appears to be in the vicinity of 1 x 10^{-18} atm, which is much higher than the pressures that would stabilize $TiO_{(s)}$ at the metal-gas interface, and therefore promote the highest equilibrium pressures of $TiO_{(g)}$ as calculated in Figure 2. This difference may be attributed to the volatilization kinetics which could lead to conditions very different from those described by thermodynamic equilibrium considerations. Also, $TiO_{(s)}$ was considered as a line compound in this investigation and the effect of its large nonstoichiometry on the equilibrium with the gas phase was not included in the stability analysis. Nevertheless, the observation of the films formed by TiO vapor deposition agrees with the model proposed in Section 3. The experimental observation clearly corroborates the significant role that $TiO_{(g)}$ plays in the early stages of interface formation, by providing a precursory $TiO_{(s)}$ film that modifies the surface of the sapphire substrate. Although the range of oxygen partial pressures that maximize the $TiO_{(g)}$ partial pressure in the system also corresponded to the region where $TiO_{(s)}$ is stable, as

discussed in Section 2, $TiO_{(g)}$ will always be present in the system, to a lesser or greater extent, depending on which titanium oxide is stabilized by the prevailing oxygen pressure.

A series of experiments were also conducted at low oxygen partial pressures, approximately 1×10^{-27} atm measured in the outlet gas leaving the environmental chamber. Surprisingly, the sessile drops processed at this level of oxygen partial pressure practically preserved the original pancake shape of the solid metal pellet and exhibited a goldish-yellow color typical of TiN. In addition, these sessile drops were only weakly bonded to the sapphire substrate after processing and could be dislodged by the application of only a moderate force. Figure 6 shows two photographs of one of these sessile drops, as seen from the top (metal side of the metal/gas interface) and from the bottom of the droplet after debonding from the sapphire substrate (metal side of the metal/sapphire interface). Both sides of the sessile drop in fact presented approximately the same color. However, the metal side of the metal-sapphire interphase region is much smoother and reflective, and appears to be much darker in the photograph than it appears on visual inspection. These results indicate that at this level of oxygen partial pressure, TiN (already identified to be present and discussed before) may control the interfacial product formation and its interaction with the sapphire substrate would not leading to bonding. This fact is readily apparent since TiN has great thermodynamic stability and is a well known diffusion barrier for many elements.

One of these sessile drops was sectioned and analyzed using an SEM. The resulting image and X-ray dot maps are shown in Figure 7. The photomicrograph of the metal side of the metal/gas interface is shown at the top of the figure where a continuous and well defined interfacial product of thickness between 1.5 and 2 μm can be observed. This continuous phase encapsulated the molten sessile drop and prevented it from flowing, acquiring the characteristic semi-spherical cap shape. The bottom part of Figure 7 shows the corresponding X-ray dot maps for titanium and copper, where it can be observed that the interface region constitutes primarily of titanium and virtually no copper. The titanium content in the bulk Cu-Ti alloy was analyzed by EDS and showed approximately the same concentration as the starting material (4

at. pct.). Titanium appears to be absent in the bulk in the X-ray map because the bulk titanium concentration is relatively low compared to the much higher (segregated) concentration at the metal/gas interfacial region.

The capability of an SEM in conducting microanalyses is limited because the equipment cannot detect elements of low atomic numbers such as oxygen and nitrogen. Nonetheless, titanium is expected to coadsorb with oxygen to the free surface as discussed in the model proposed in Section 3. The observation of titanium enrichment at the metal/gas interfacial region is an important result since it is believed, in general, that the titanium interfacial enrichment would occur only at the metal/sapphire interface and the "driving force" for such enrichment would be the "desire" of titanium to react with the sapphire [46]. In addition, the Ti-O coadsorption phenomenon to the metal/gas interfacial region demonstrates that small titanium additions in copper completely changes the metal/gas interfacial region. This fact has been largely neglected in the Cu-Ti/sapphire sessile drop experiments reported in the literature, [15,20]where the surface tension of copper is normally assumed not to be affected by small titanium additions.

The metal side of the metal/gas interfacial region of the sessile drop shown in Figure 6 was also analyzed using XPS. The overall photoemission spectra are shown in Figure 8 for the as-received and sputtered conditions. The sputtering rate was 120 Å/min during all analyses. The very "clean" spectra obtained are strikingly evident in Figure 8. Small traces of calcium and silicon, found in the as-received condition, rapidly disappeared as the first layers of the surface was removed by short-time sputtering. The presence of nitrogen in the metal/gas interfacial-region is confirmed in the photoemission spectra, with the N1s peak increasing significantly from the as-received to the 3 minutes sputtering condition. The same behavior is followed by the $Ti2p_{3/2}$ peak under the same conditions. The O1s, in contrast, showed accentuated decrease as the first layers of the surface were sputtered away.

The expanded $Ti2p_{3/2}$ photoemission spectra are shown in Figure 9. In this figure, the range of the electron binding energies, characteristic of the different compounds, is given in the

form of a label with the name and the corresponding energy range (solid black bar) as provided by Chastian [47]. For the as-received condition, Figure 9a shows that the surface titanium is in a bonding state that corresponds predominantly to TiO_2 and TiN. The formation of TiO_2 actually occurred when the sessile drop was in contact with the ambient air within the period (several days) after the sessile drop experiment and before the XPS analyses. This conclusion is also based on the fact that the gas phase oxygen partial pressure (1×10^{-27} atm) was not expected to stabilize TiO_2 in accordance with the stability diagram shown in Figure 2. The conclusion is further substantiated by the spectra illustrated in Figure 9b, where after the first surface layers are sputtered away, the $Ti2p_{3/2}$ peak shifts to lower binding energies indicating the presence of TiO and TiN, predominantly. The actual quantitative composition analyses are shown in Table 1. These data confirm that titanium is the major metallic element at the interface, with a virtual absence of copper as predicted in Figure 7.

Table 1 - Quantitative analysis corresponding to spectra shown in Figure 9(b).

Element	Area (cts-ev/s)	Sensitivity Factor	Concentration (at. pct.)
Ti2p	549000	168.731	60.04
N1s	58970	44.949	24.21
O1s	51710	66.598	14.33
Cu2p	28340	367.737	1.42

The identification of the titanium compounds at the interface can be further characterized by the expanded photoemission-spectra for nitrogen as shown in Figure 10. The nitrogen peak presents a very limited shift in the N1s electron binding energy for all possible nitrides. However, titanium forms only the line compound TiN with nitrogen and therefore, the nitrogen spectra displayed in Figure 10 can be interpreted as being all associated with the titanium. The

spectra corresponding to $Ti2p_{3/2}$ and $N1s$ also support the conclusion that the interfacial region is constituted primarily of TiN and TiO. Since TiN can be considered as a line compound, nitrogen can be related to titanium using the atomic ratio of 1:1. This estimation shows TiN as accounting for 40% of the interfacial atomic composition. The remaining titanium would then be associated with oxygen to form oxygen-deficient $TiO_{0.4}$ which would account for approximately 60% of the interfacial atomic composition.

The simultaneous surface enrichment of titanium and oxygen identified here clearly confirms the predictions of the Ti-O coadsorption in the Cu-O-Ti ternary system as proposed by the model presented in Section 3. The premise that the Ti-O coadsorption would be restricted to a monolayer is obviously not realistic in this system, since the Ti-O adsorbed interfacial region observed in Figure 7 was between 1 to 2 μm thick. The bulk oxygen concentration of 0.086 at. pct. in this experiment is close to that used to predict the Ti-O coadsorption in the Cu-O-Ti ternary system presented earlier in Figure 3 (0.1 at. pct. Oxygen). The difference between the experimental results ($TiO_{0.4}$) and the prediction from Figure 3 at 1150°C (approximately 10%) is due to the lower titanium concentration used in the calculations (titanium 1 at. pct.). It is important to remember that the titanium concentration in the Ti-O coadsorption predictions in Section 2 were limited to 1 at. pct. because of the limitation in the validity of the thermodynamic data.

Obviously, the presence of $TiO_{(s)}$ at the metal/gas interface can also be interpreted as being due to the oxidation of the bulk titanium by oxygen in the gas phase, since the prevailing oxygen partial pressure (1×10^{-27} atm) was in the TiO stability-range as indicated by Figure 2. However, titanium is a solute in copper and the virtual absence of copper at the surface would be inconsistent with the direct reaction of titanium with oxygen in the gas phase. Moreover, if reaction occurs between titanium and the gas phase, only TiN would be expected to be found at the surface since the nitrogen partial pressure in the gas phase (4 to 6×10^{-6} atm) is about ten orders of magnitude higher than the nitrogen partial pressure in equilibrium with TiN at the processing temperature used in these experiments. Therefore, the presence of TiO at the

metal/gas interface provides supporting confirmation of the Ti-O coadsorption prediction in the Cu-O-Ti ternary system, as proposed in the model for the Cu-O-Ti/sapphire sessile-drop equilibrium presented in Section 3. It is relevant to note that, due to the high intrinsic rate of the adsorption phenomenon, the Ti-O coadsorption at the metal/gas interface, followed by the reaction of this adsorbed interphase with nitrogen, occurs in a time interval short enough such that no significant change in the original shape of the metal alloy occurs during the sessile drop experiment.

The analytical results for the metal side of the Cu-Ti alloy/gas interface indicate that when the oxygen partial pressure is decreased below a certain level, the nitrogen present in the Grade 5 argon would adversely affect the metal-sapphire interaction, including spreading of the molten filler metal over the sapphire substrate. While it may be tempting to interpret this finding as indicating that the oxygen partial pressure should be maintained at a level that is above the minimum where nitrogen would control the interface formation. However, within the context of exploring the mechanisms of the interfacial-region formation, it indicates instead that the nitrogen can have a confounding effect on the process and should be maintained at much lower levels than those found in standard commercial Grade 5 argon.

It is clear from the results presented above that the control of the nitrogen partial pressure in the system is mandatory. Because of this, a titanium sponge bed was incorporated into the gas train to getter the nitrogen. However, XPS analyses conducted at the interface showed that the titanium sponge nitrogen getter only lowered the nitrogen partial pressure in the gas phase to a limited extent since the amount of nitrogen identified at the interface was approximately 30% of the initial value corresponding to the condition of no nitrogen control.

It is also apparent that the Ti-O coadsorption at the metal/gas phase interface demonstrates that the presence of small concentrations of titanium and oxygen in copper can completely modify the nominal copper/gas phase interfacial region. Thus, the segregation at the metal/gas interface due to the Ti-O coadsorption, which has typically been neglected in the

literature, should now be incorporated in the determination of the Work of Adhesion (W_{ad}) from Cu-Ti/sapphire sessile drop experiments.

The ppm-level hydrogen addition to the argon gas-phase which was intended to shift the water vapor/hydrogen/oxygen equilibria proved to be a very effective strategy in the control of extremely low oxygen partial pressure ranges ($< 10^{-20}$ atm).

2. The Metal/Sapphire Interfacial Region

The Cu-O-Ti/sapphire interfacial region was subjected to extensive SEM and XPS analysis. Ultimately, it is this interface that is responsible for bonding between the Cu-Ti alloy and the sapphire.

a. XPS Analyses of the Metal/Sapphire Interfacial Region

XPS analysis of the metal/sapphire interfacial region was conducted on the metal side interfacial region of the weakly bonded Cu-Ti/sapphire interface displayed in Figure 6. In other samples that featured much stronger metal-sapphire interaction, fracture was observed to occur within the near-surface region of the sapphire but not at the metal/sapphire interface itself. This sample was processed without the nitrogen gettering system. The formation of TiN on the metal side of the metal/gas interface, as discussed in the previous section, was responsible for encapsulating the "sessile drop" and maintaining it in the original pancake shape. The observed weak metal-sapphire interaction was attributed to the presence of nitrogen in the gas phase combined with an oxygen partial pressure below 10^{-27} atm. The overall photoemission spectra for this interface is shown in Figure 11 for the as-received and sputtered condition. The presence of nitrogen at the metal/sapphire interface is confirmed in the spectra shown in Figure 11a corresponding to the as-received condition. However, no nitrogen were detected in the sputtered interface (after 1 min.) as shown in Figure 11b. As expected, the nitrogen concentration at the metal/sapphire interface is much less than at the metal/gas interface which is in direct contact with the gas phase. Nevertheless, it is important to note that even a

relatively small concentration of nitrogen at the interfacial region could hinder the interaction between the metal and sapphire.

The overall photoemission-spectra in Figure 11 also indicated that titanium and oxygen represent the predominant elements on the metal side of the Cu-O-Ti/sapphire interfacial-region, with no copper present. The expanded titanium photoemission spectra displayed in Figure 12 show the same features as presented by the previously analyzed metal/gas interface, with TiO_2 being identified at the surface in the as-received condition. Again, the electron binding energies shifted to lower levels toward TiO as the first layers of the surface were removed. The intensities of oxygen, on the other hand, did not present any significant changes for both surface conditions as can be observed in Figure 3.

The weak metal-sapphire interaction can be further characterized by the very small aluminum peak detected in the interfacial-region (only for the sputtered condition) observed in Figure 11b. The important implication of this result is that the oxygen present at the interface is not due to the sapphire decomposition, since the small aluminum concentration identified at the surface is not commensurate with the large oxygen concentration at this location on the basis of the sapphire stoichiometry. The oxygen at the metal/sapphire interfacial-region is not transferred from the gas phase either, since this interface is not directly exposed to the gas phase. Thus, the titanium and oxygen concentrations on the metal side of the metal/sapphire interface are due to Ti-O coadsorption from the bulk of the Cu-O-Ti alloy in accordance with the model developed in Section 3. In fact, this conclusion is definitive in identifying that the titanium enrichment in the metal at the sapphire interface is due to the simultaneous oxygen enrichment from the bulk as proposed in Section 3 and 3. The reaction that is responsible for bonding between the sessile drop and sapphire is in fact the interaction of this Ti-O adsorption layer with the sapphire, and not of the solute titanium with sapphire.

With regards to the specific results of this experiment, the presence of the nitrogen hindered more extensive metal-sapphire interaction. In the absence of nitrogen, the unimpeded interaction at the interface will depend on the titanium-to-oxygen surface ratio as determined

by the Ti-O coadsorption in the Cu-O-Ti system. To maximize the reactivity between the Ti-O adsorbed layer and the sapphire, a high titanium-to-oxygen ratio is necessary.

b.   SEM Analysis of the Metal/Sapphire Interfacial Region

The predictions for Ti-O coadsorption in the Cu-O-Ti ternary system presented above show that the interphase titanium and oxygen concentrations are highly dependent on the bulk compositions as well as the processing temperature. The model, however, does not provide details about the growth of the adsorption interphase as a function of these same variables.

In addition to the XPS analyses described previously, SEM analyses of cross-sections of the interfacial region were conducted so that the behavior of the interphase thickness could be quantified as a function of the bulk oxygen concentration, temperature and time. The X-ray dot maps for titanium, copper and aluminum for three selected at 1110°C and 15 min. holding time are shown in Figures 13, 14 and 15, corresponding to the bulk oxygen concentrations of 100, 860 and 2,400 ppm, respectively. The X-ray dot maps were generated separately for each element within the entire interfacial region. These maps indicate that the width of the Ti-O adsorption region (shown on the left of the top photograph and repeated on the right of the bottom photograph) increased significantly - from approximately 1 to 5 μm - with an increase in the bulk oxygen content in the Cu-Ti alloy, from 100 ppm (Figure 13) to 2,400 ppm (Figure 15). This result provide additional verification that the observed titanium enrichment (and simultaneous oxygen enrichment) in the coadsorption interphase is determined by the bulk oxygen concentration present in the system.

At lower bulk oxygen concentrations (e.g., 100 and 860 ppm), the boundaries between the Ti-O coadsoprtion layer and the bulk filler metal are extremely sharp and well defined, as indicated in the X-ray maps for copper, titanium and aluminum shown in Figures 13 and 14. Similarly, the boundaries between the Ti-O coadsorption layer and the sapphire are also sharp and well defined. The higher bulk oxygen concentration specimen (2,400 ppm), however, exhibited a different behavior. Only the Ti-O/sapphire interface boundary remained sharp,

composed predominantly of titanium and oxygen. The Cu-Ti/Ti-O interface boundary became wide and diffuse, with a higher concentration of copper. The duplex character of this interfacial region is revealed more clearly in the X-ray dot maps shown in Figure 16.

The occurrence of this duplex Ti-O coadsorption layer has also been reported in the investigations of Bang and Kritsalis et al.[20,21]. For the alloy compositions they reported, it was demonstrated in Section 2 that a mixture of copper, TiO and the ternary compound Ti_3Cu_3O should be the equilibrium phases to solidify. Although the oxygen bulk concentration in the Cu-Ti alloy was not reported in either investigations, it is believed the copper used by Bang [21] to produce Cu-Ti filler metals contained between 4,000 to 5,000 ppm of oxygen, which would confirm that the formation of the duplex phase Ti-O coadsorption layer is associated with a high bulk oxygen concentration in the Cu-Ti alloy.

The results of the measurements of the adsorption layer thickness, corresponding to the processing temperature of 1110°C, are summarized by the plots in Figure 17. The significant increase in the Ti-O coadsorption interphase with increased bulk oxygen concentration in the Cu-Ti alloy is clearly evident. The asymptotic behavior of the adsorption interphase thickness beyond a holding time of five minutes should also be noted, whereas the portion of the curve below five minutes is indeterminate. It was discussed in Section 2 that the Ti-O coadsorption at the interface occurs in a time that is of much smaller-scale, of the order of fractions of a second, before any intimate contact between the sessile drop and the sapphire can occur. In addition, development of what can now be identified as the Ti-O coadsorption layer has been claimed by some investigators [11,21] to be a diffusion-controlled reaction involving the titanium in the alloy and oxygen from the stoichiometric decomposition of the sapphire.

C   CONCLUSIONS

The following conclusions are listed to summarize the accomplishments achieved in this research program:

- The currently accepted modeling of the bonding in the Cu-Ti/sapphire brazing system based on direct reaction between titanium and sapphire to produce $TiO_{(s)}$ as the interfacial product should be expanded to also consider titanium and oxygen cosegregation.

- The Cu-O-Ti ternary phase diagram indicate that $TiO_{(s)}$ is not an equilibrium phase that would occur naturally in the ternary system.

- Thermodynamic calculations using regular solution model determined that titanium is not surface active in molten copper.

- Titanium segregation to the Cu-O-Ti alloy/sapphire interface was shown to occur due to a coadsorption mechanism with oxygen.

- The predictions from the model for the Ti-O coadsorption in the Cu-O-Ti indicated that the titanium-to-oxygen equilibrium interfacial ratio is determined by both the bulk oxygen and titanium concentrations as well as the system temperature.

- A model for the static equilibrium for a Cu-O-Ti sessile drop in contact with sapphire was proposed. It incorporates the Ti-O coadsorption and the pertinent O_2 and $TiO_{(g)}$ species. The reaction responsible for the bonding between the sessile drop and the sapphire was demonstrated to be a solution reaction between the Ti-O coadsorbed layer and the Al_2O_3.

- The interfacial Ti-O coadsorption layer has been shown to increase monotonically with increases in the bulk oxygen concentration. In addition, the duplex phase Ti-O coadsorption layer has been shown to be linked to high oxygen bulk concentrations in the Cu-O-Ti alloy, in excess of 2,400 ppm.
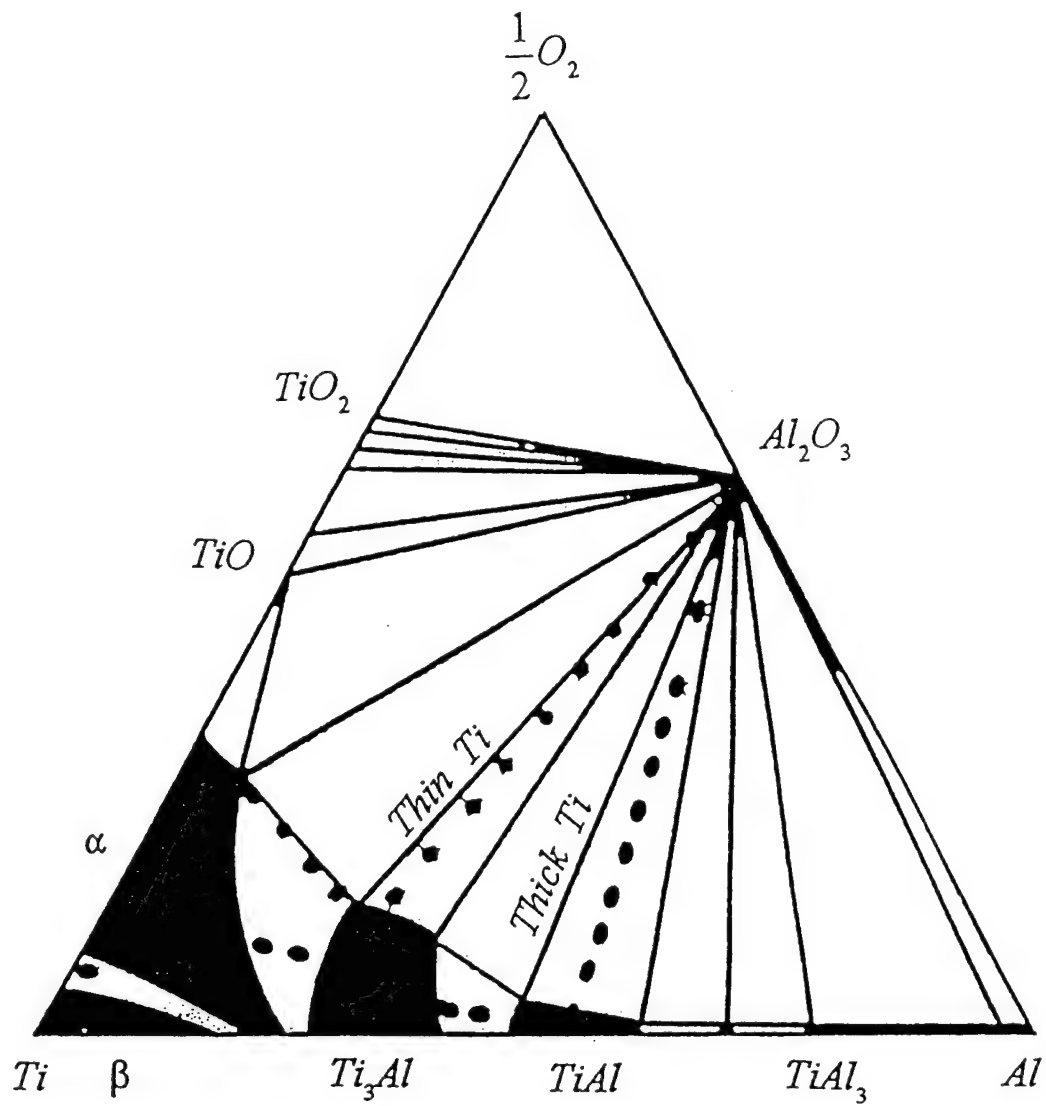
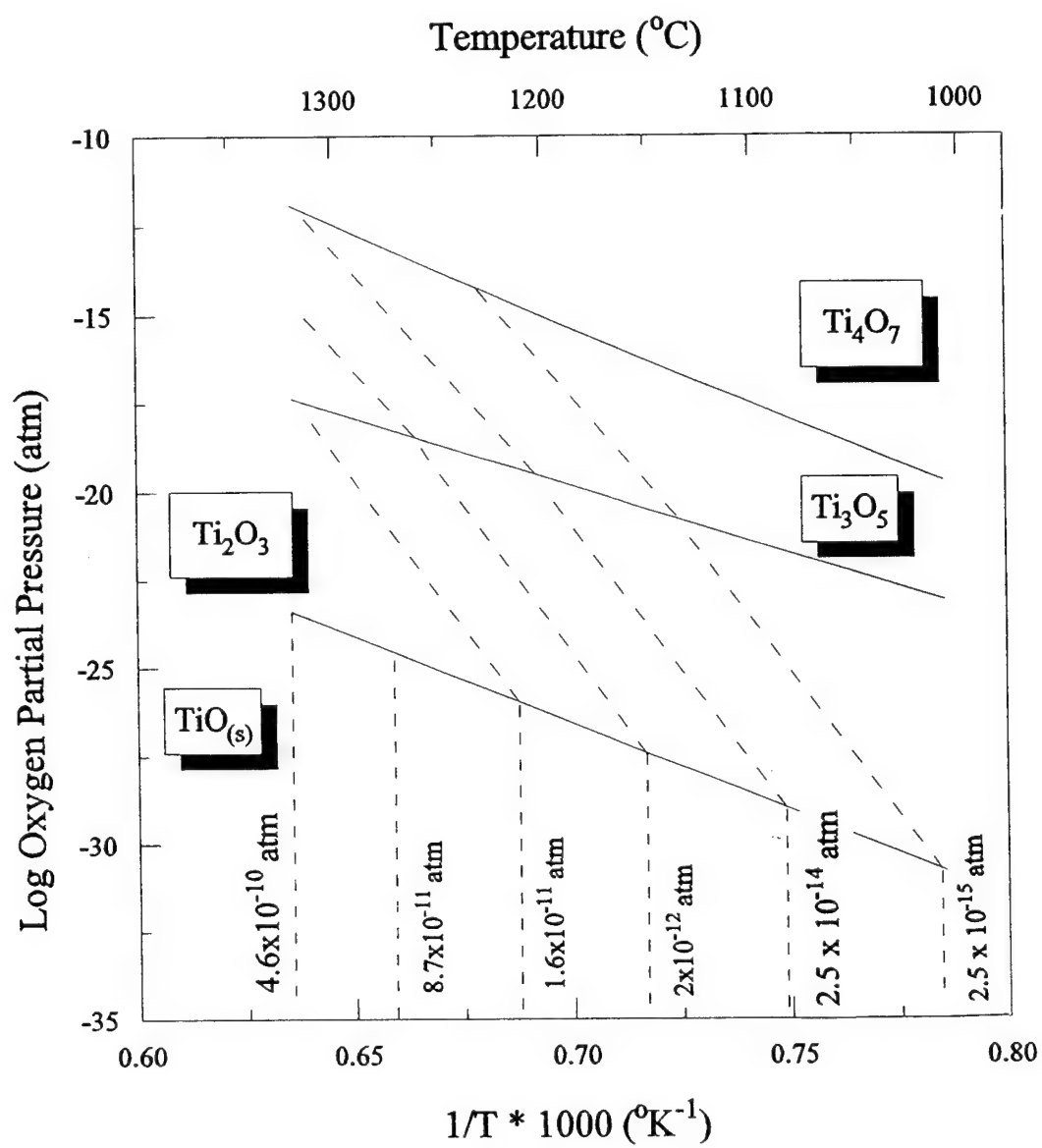Figure 1: Isothermal section of the Al-O-Ti ternary phase idagram at 1100°C [26].

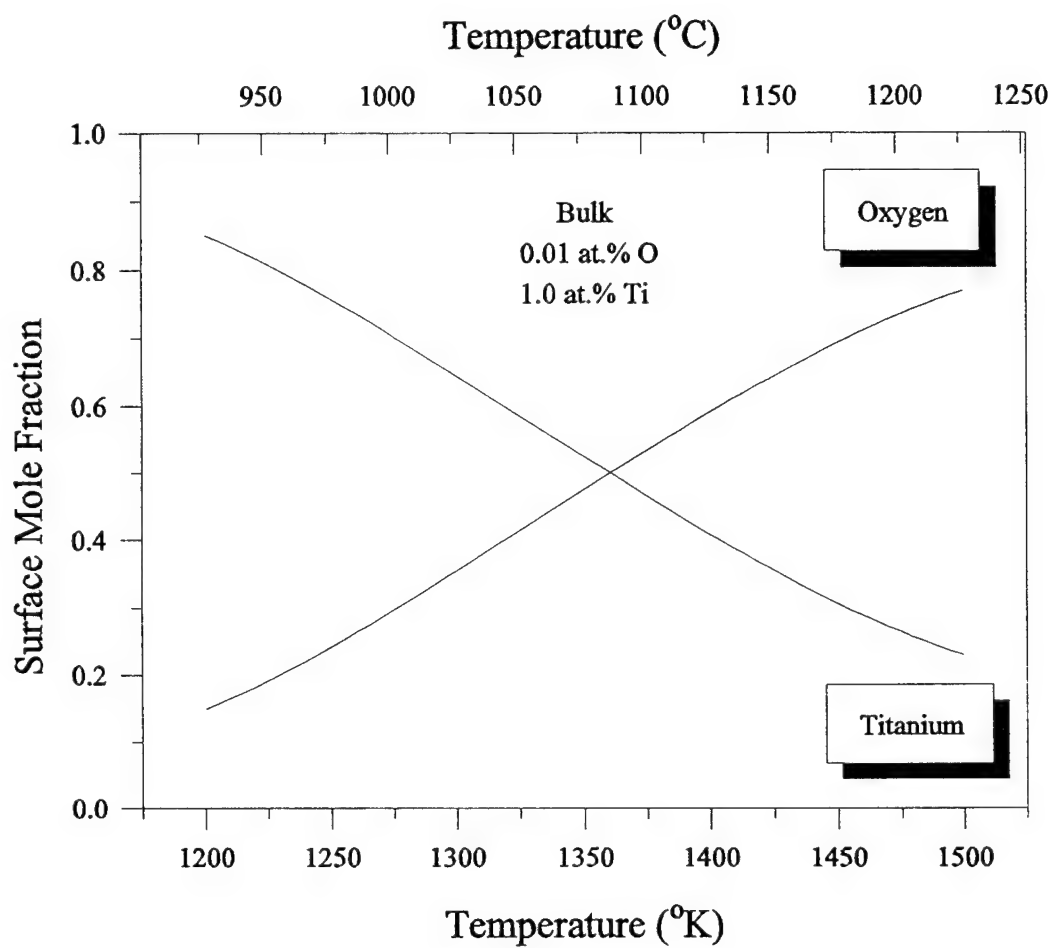Figure 2: Ti-O stability diagram including the $TiO_{(g)}$ isobars.

Figure 3: Equilibrium oxygen and titanium surface mole fraction as a function of the temperature (Bulk concentrations: 0.01 at. % O; 1.0 at. % Ti).
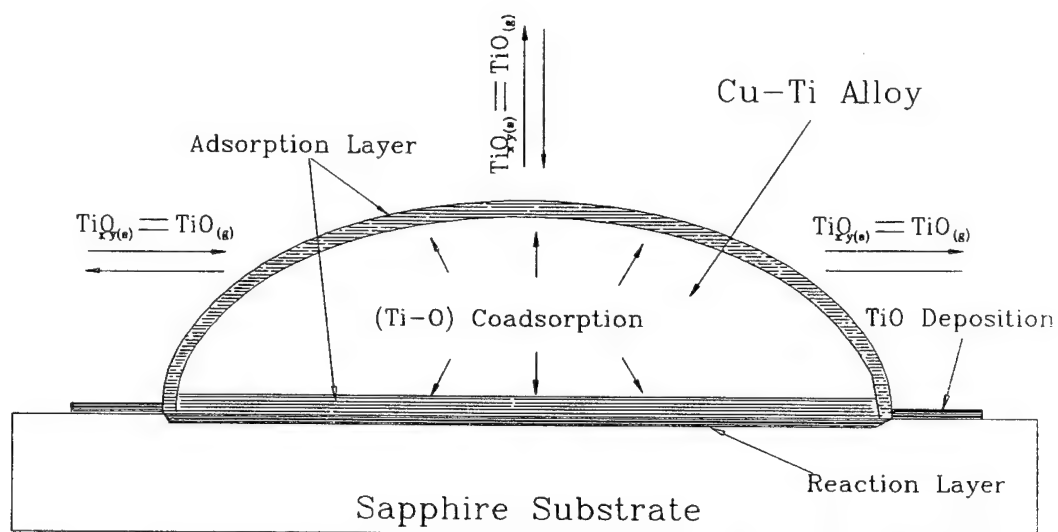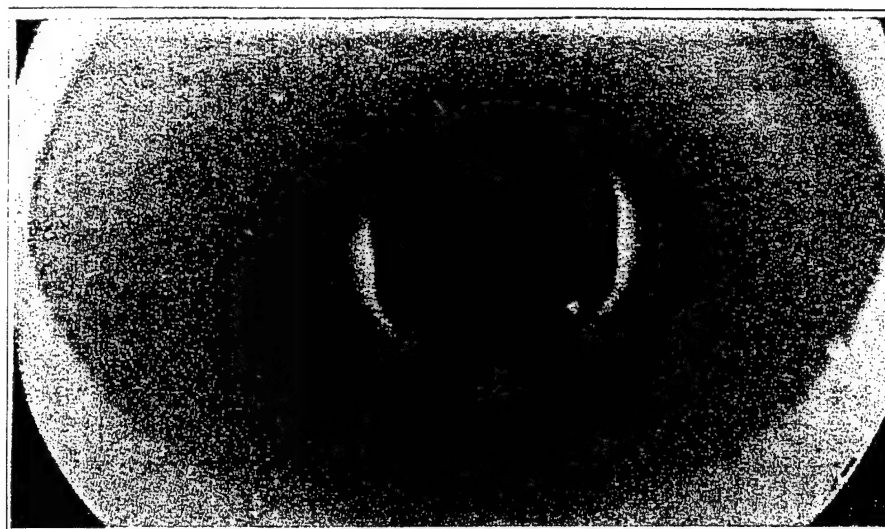
Figure 4: Modelling of the equilibrium situation for a Cu-O-Ti sessile drop experiment on sapphire incorporating the concepts of Ti-O coadsorption and the $TiO_{(g)}$ species.

(a)

(b)

2 mm

Figure 5: Sessile drops on sapphire illustrating the features of vapor deposition of $TiO_{(g)}$ on the sapphire substrate. Processing conditions: Cu-Ti 1at. %, 1110°C, 30 min., oxygen bulk concentration = 500 ppm; (a) view from the top of the sessile drop; (b) view from the bottom through the sapphire.

(Sessile Drop Free Surface)   (Cu-Ti/Sapphire Interface)

2 mm
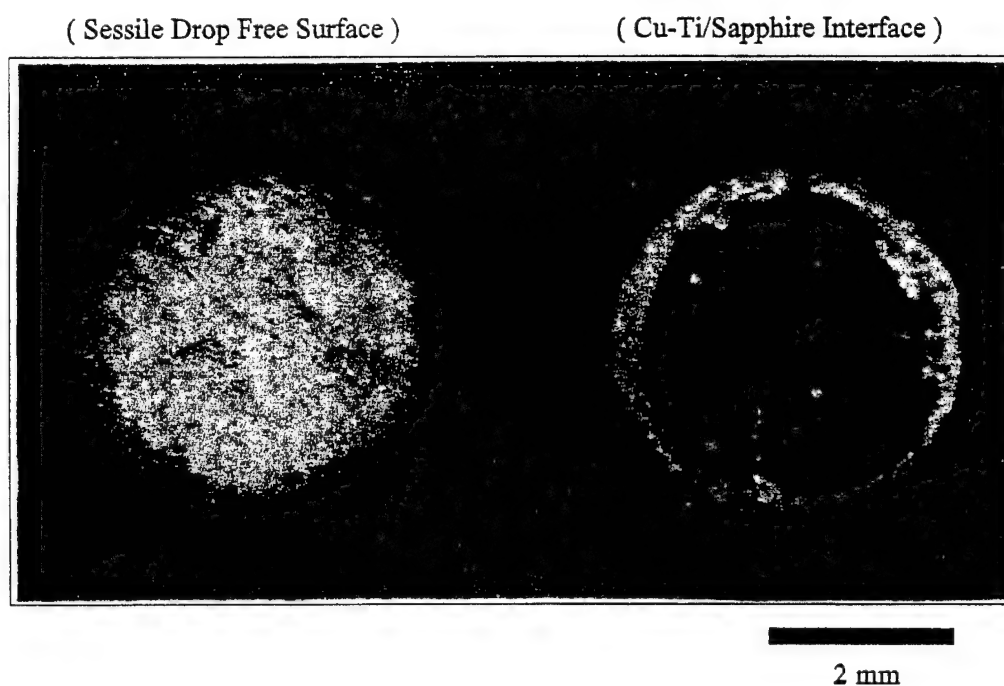
Figure 6: TiN formation on Cu-Ti alloy sessile drop. TiN is present at both the gas-metal and "weakly bonded" Cu-Ti/sapphire interfaces. Processing conditions: Cu-Ti 4 at %, no nitrogen control, 1150°C, 15 min., oxygen bulk concentrations = 860 ppm, oxygen partial = 10^{-27} atm.
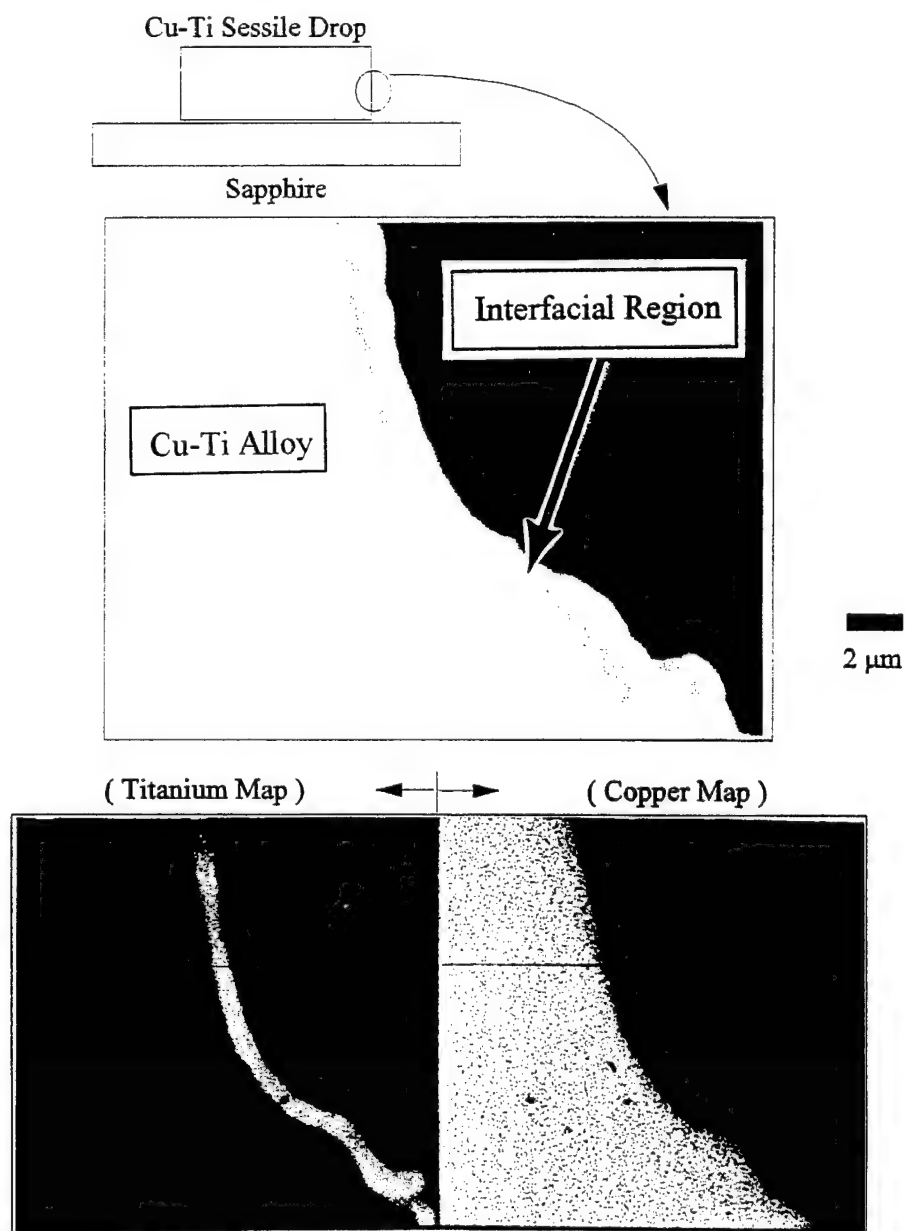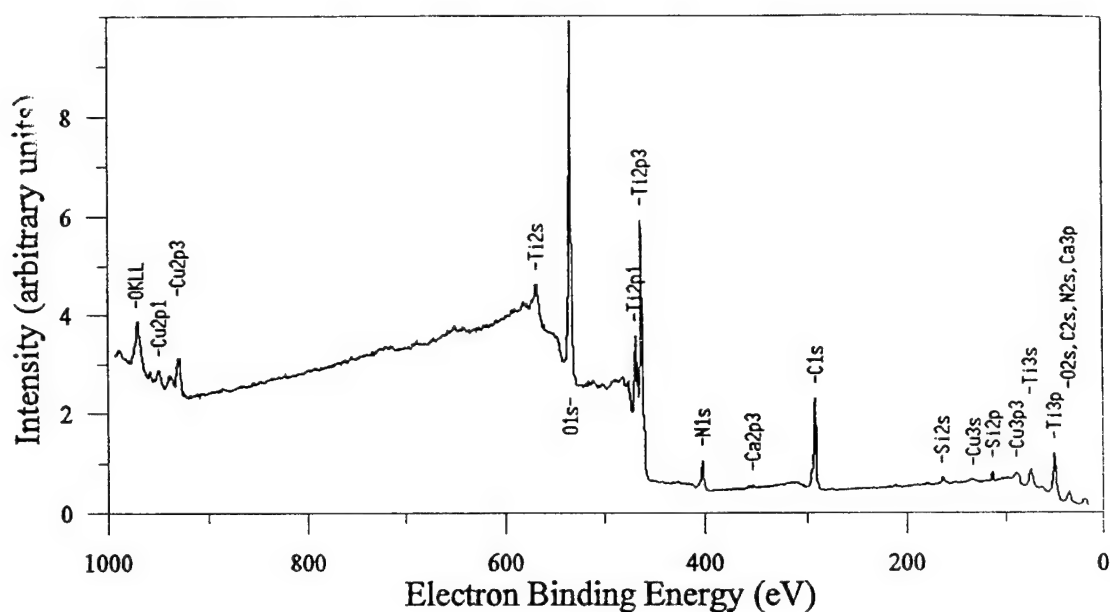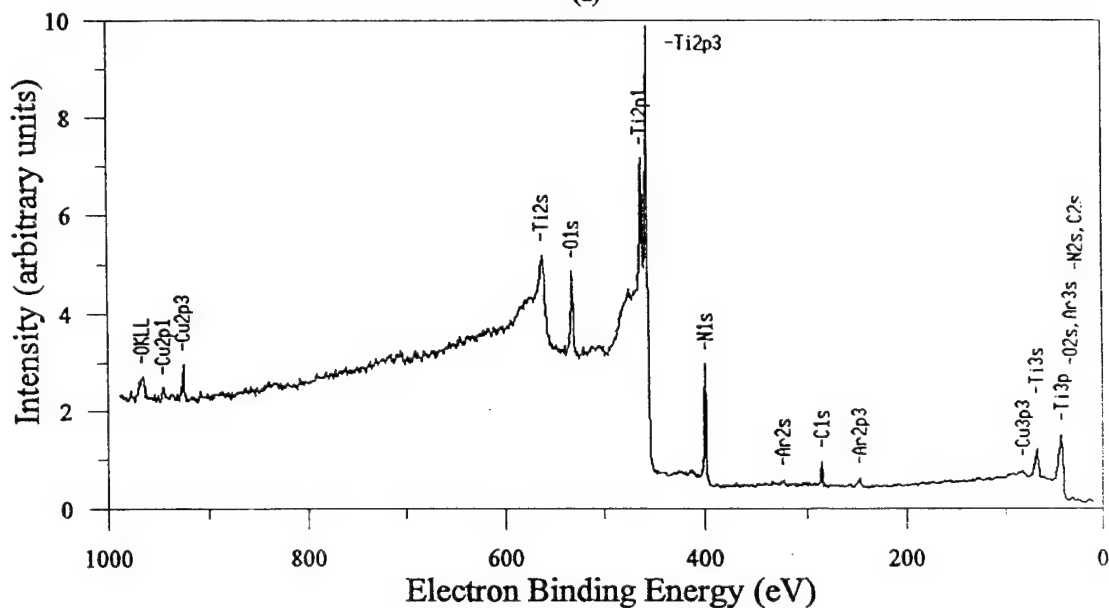
Figure 7: X-ray dot maps of Ti and Cu for the metal side interfacial region of the Cu-Ti
alloy/gas interface. Processing conditions: Cu-Ti 4 at. %, no nitrogen control,
oxygen partial pressure = 10^{-27} atm., 1150°C; 15 min., oxygen bulk
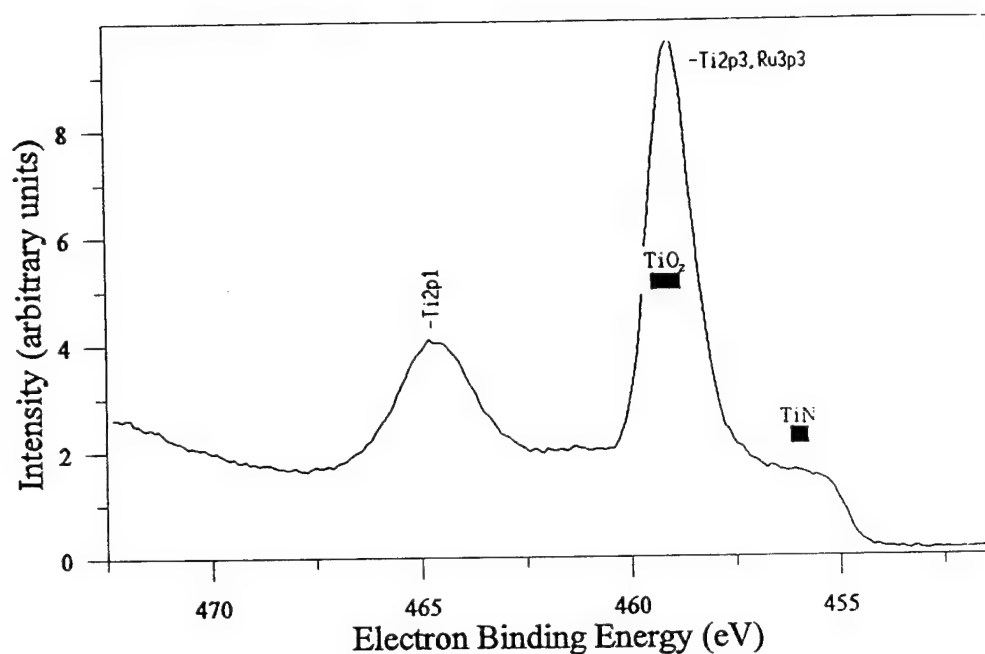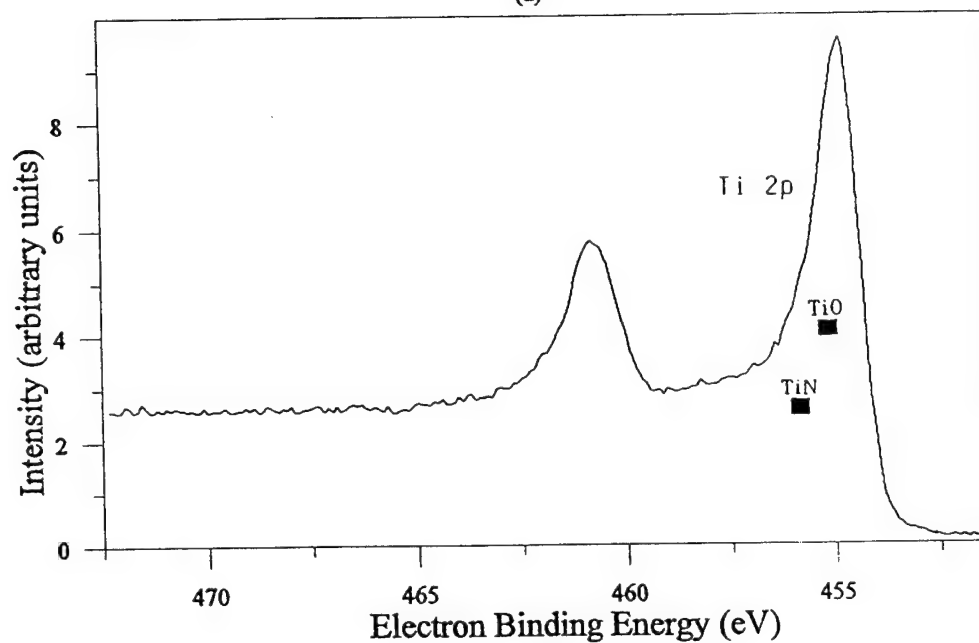concentration = 860 ppm.

(a)

(b)

Figure 8: Overall photoemission spectra, corresponding to the metal side interfacial region of the Cu-Ti alloy/gas interface displayed in Figure 7. Processing conditions: Cu-Ti 4 at. %, no nitrogen control, oxygen partial pressure = 10^{-27} atm., 1150°C; 15 min., oxygen bulk concentration = 860 ppm; (a) as received, (b) after 3 min. sputtering.

Figure 9: Titanium 2p3 photoemission spectra, corresponding to the overall spectra displayed in figure 8. Processing conditions: Cu-Ti 4 at. %, no nitrogen control, oxygen partial pressure = 10^{-27} atm., 1150°C; 15 min., oxygen bulk concentration = 860 ppm; (a) as received, (b) after 3 min. sputtering.
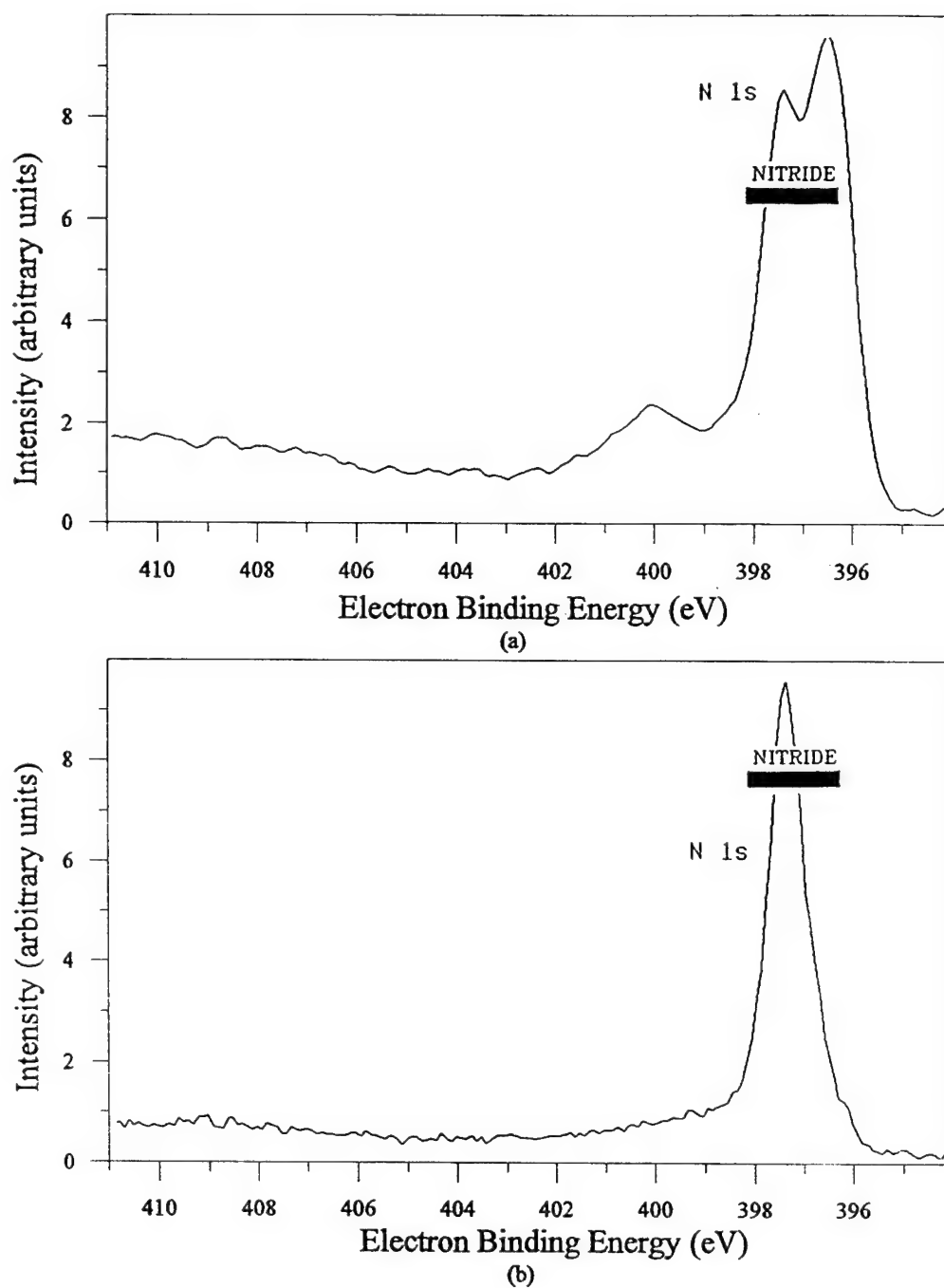
Figure 10: Nitrogen 1s photoemission spectra, corresponding to the overall spectra displayed in figure 8. Processing conditions: Cu-Ti 4 at. %, no nitrogen control, oxygen partial pressure = 10^{-27} atm., 1150°C; 15 min., oxygen bulk concentration = 860 ppm; (a) as received, (b) after 3 min. sputtering.

Figure 11: Overall photoemission spectra, corresponding to the metal side interfacial region of the "weakly bonded" Cu-Ti alloy/sapphire interface displayed in Figure 6. Processing conditions: Cu-Ti 4 at. %, no nitrogen control, oxygen partial pressure = 10^{-27} atm., 1150°C; 15 min., oxygen bulk concentration = 860 ppm; (a) as received, (b) after 1 min. sputtering.
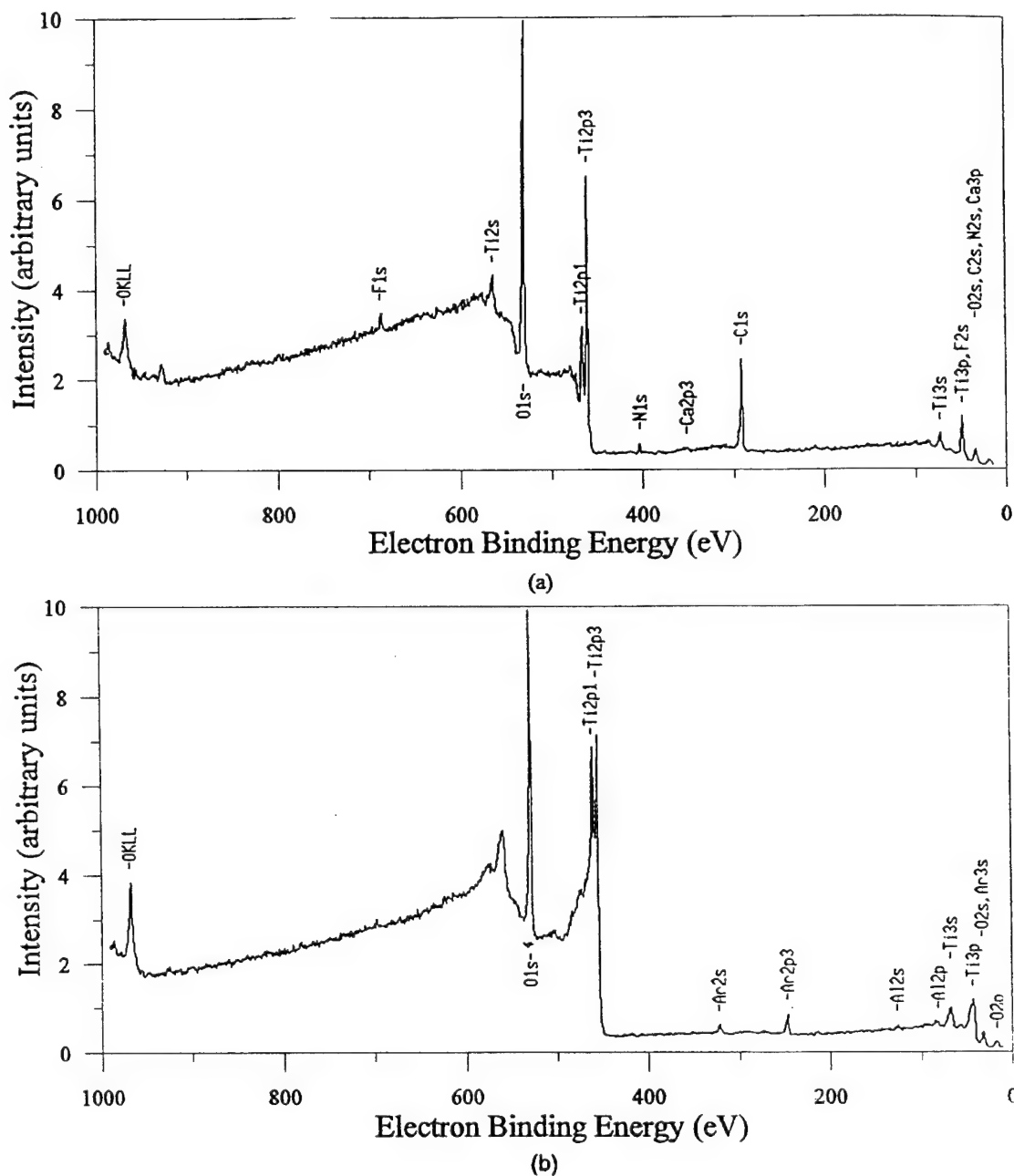
Figure 12: Titanium 2p3 photoemission spectra corresponding to the overall spectra displayed in Figure 11. Processing conditions: Cu-Ti 4 at. %, no nitrogen control, oxygen partial pressure = 10^{-27} atm., 1150°C; 15 min., oxygen bulk concentration = 860 ppm; (a) as received, (b) after 1 min. sputtering.
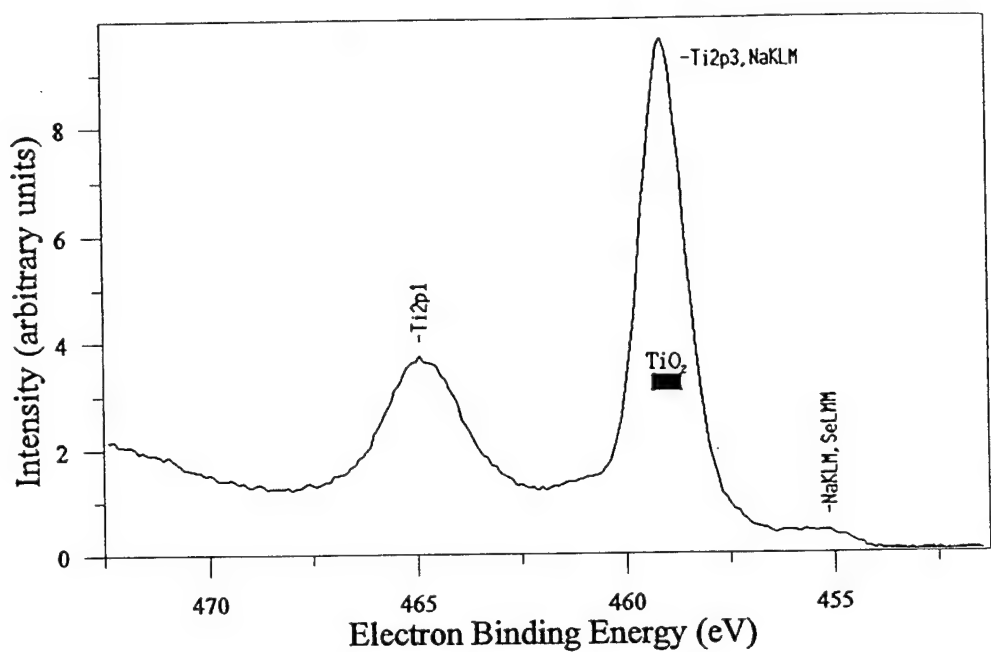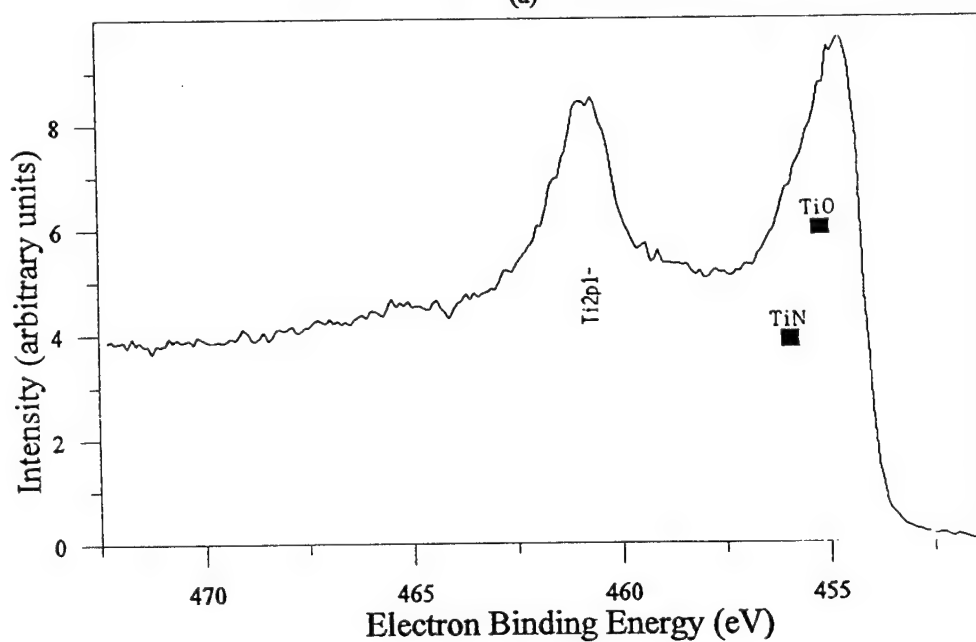
Figure 13: X-ray dot maps of Ti, Al, and Cu at the Cu-Ti/sapphire interface. Processing conditions: Cu-Ti 4 at. %, 1110°C, 15 min., titanium sponge nitrogen getter, oxygen partial pressure $= 10^{-21}$ atm., oxygen bulk concentration = 100 ppm.

Figure 14: X-ray dot maps of Ti, Al, and Cu at the Cu-Ti/sapphire interface. Processing conditions: Cu-Ti 4 at. %, 1110°C, 15 min., titanium sponge nitrogen getter, oxygen partial pressure $= 10^{-21}$ atm., oxygen bulk concentration = 860 ppm.
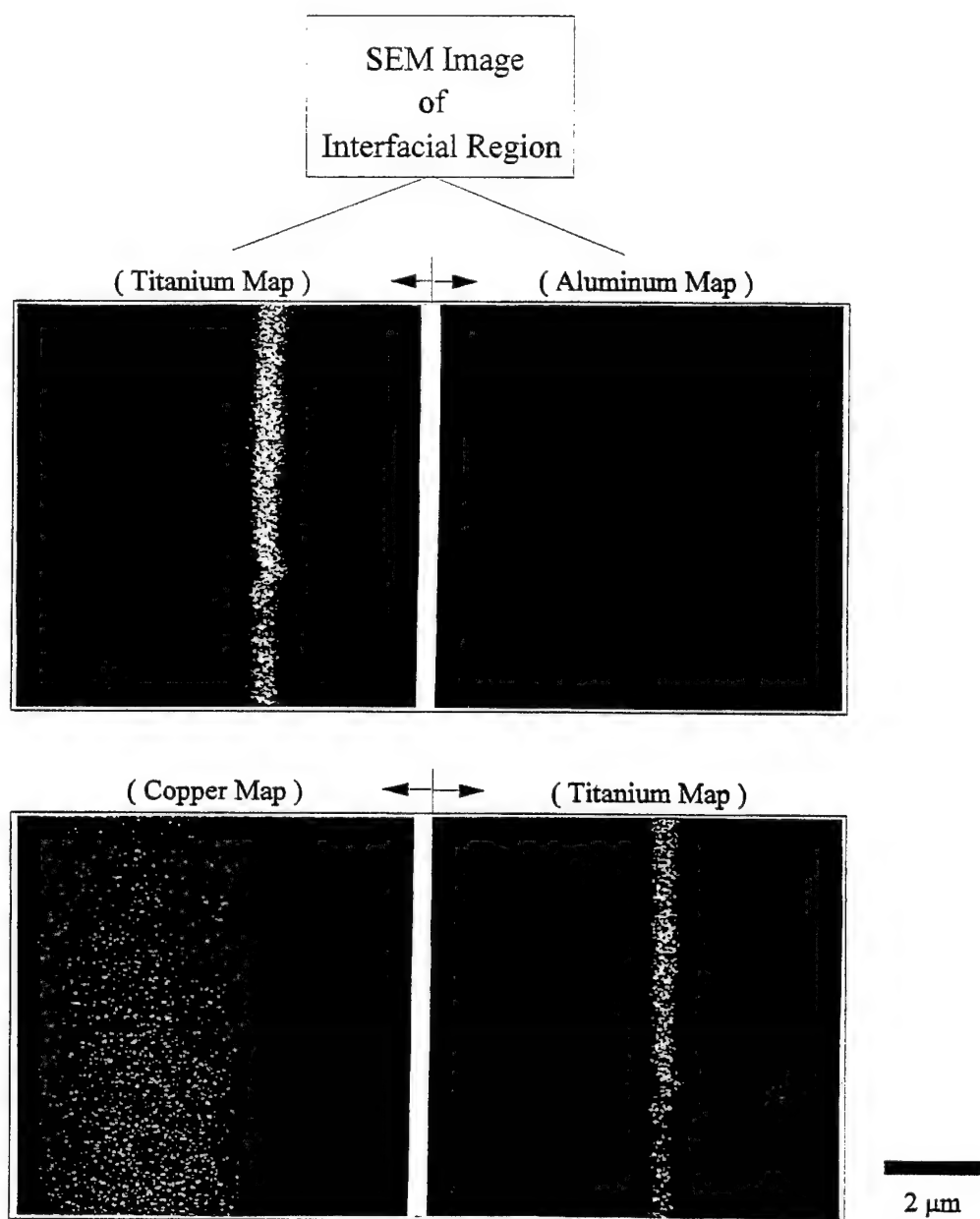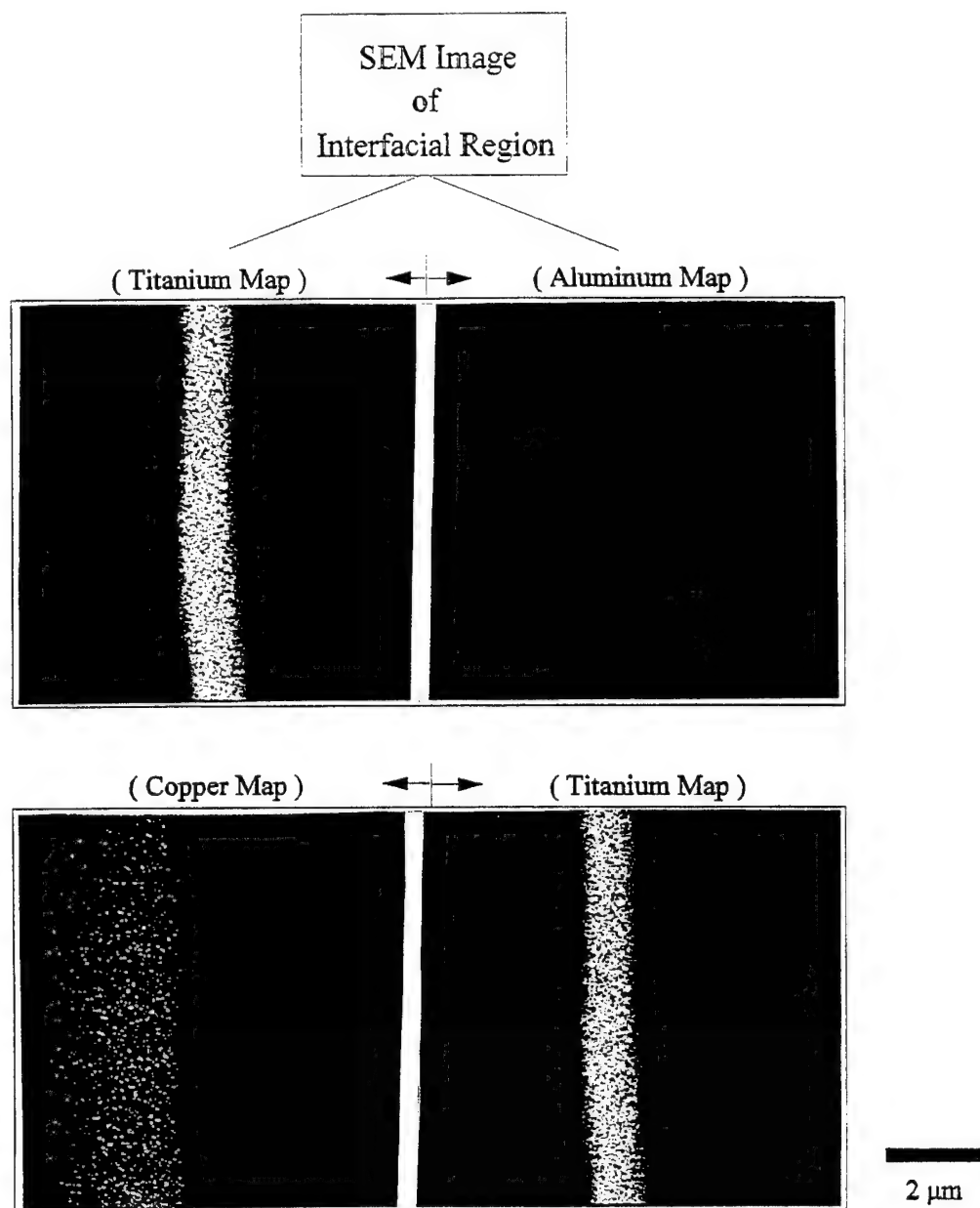
Figure 15: X-ray dot maps of Ti, Al, and Cu at the Cu-Ti/sapphire interface. Processing conditions: Cu-Ti 4 at. %, 1110°C, 15 min., titanium sponge nitrogen getter, oxygen partial pressure $= 10^{-21}$ atm., oxygen bulk concentration = 2,400 ppm.

Figure 16: X-ray dot maps of Ti, Al, and Cu at the Cu-Ti/sapphire interface illustrating the formation of a duplex phase Ti-O coadsorption layer. Processing conditions: Cu-Ti 4 at. %, 1190°C, 5 min., titanium sponge nitrogen getter, oxygen partial pressure $= 10^{-21}$ atm., oxygen bulk concentration = 860 ppm.
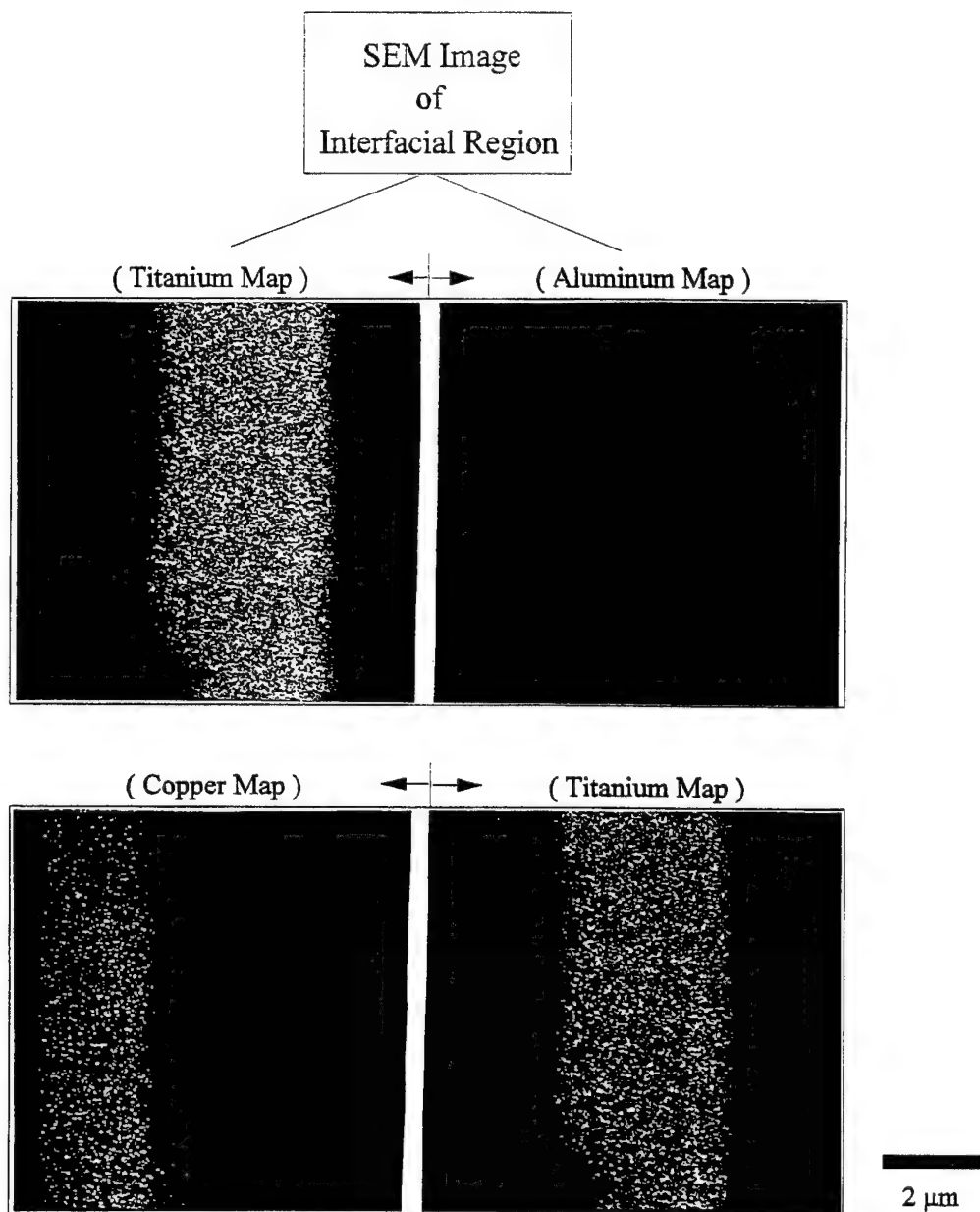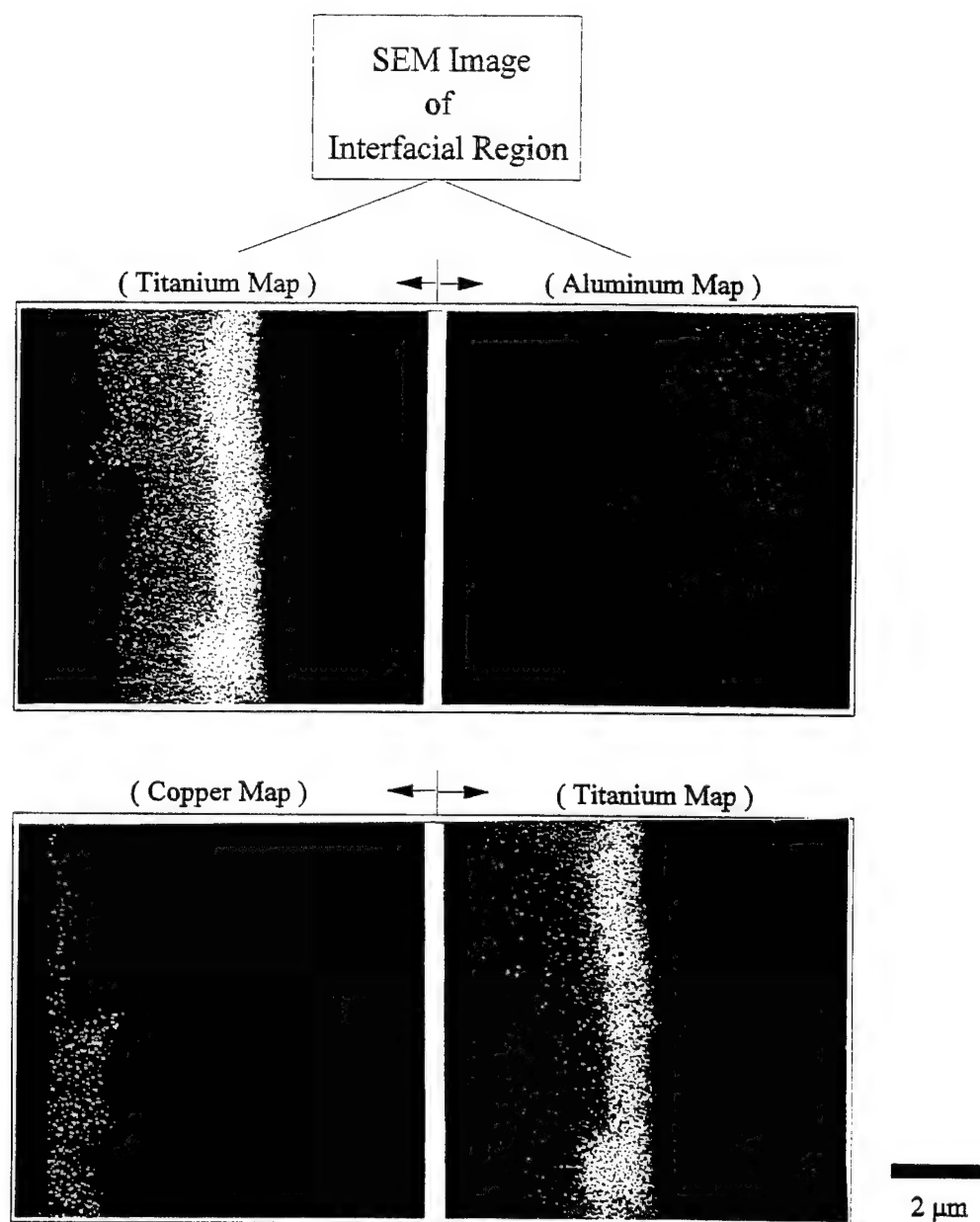
D. REFERENCES

1   Humenik, M.; Kingery, W.D. (1954), "Metal-Ceramic Interactions: III, Surface Tension and Wettability of Metal-Ceramic Systems", J. Am. Ceram. Soc. V.37 pp. 18-23.

2   McDonald, J.E.; Eberhart, J.G. (1965), "Adhesion in Al Oxide-Metal Systems", Transactions of Metallurgical Society of AIME V.233 pp. 512-517.

3   Johnson, K.H.; Pepper, S.V. (1982), "Molecular-Orbital Model for Metal-Sapphire interfacial Strength", J. Appl. Phys. V.53(10) pp. 6634-6637.

4   Ohuchi, F.S. (1991), "Electronic Structure and Chemical Reactions at Metal-Al_2O and Metal-Al Nitride Interfaces", J. Am. Ceram. Soc. V.74(6) pp. 1163-1187.

5   BlackBurn, A.R.; Shevlin, T.S.; Lowers, H.R. (1949), "Fundamental Study; and Equipment for Sintering and Testing of Cermet Bodies, I-III", J. Am. Cer. Soc., V.32(3) pp. 81-98.

6   Ohuchi, F.S.; French, R.H.; Kasowski, R.V. (1987), "Cu Deposition on Al_2O_3 and AlN Surfaces: Electronic Structure and Bonding", J. Appl. Phys. V.62(6) pp. 2286-2289.

7   Ohuchi, F.S. (1989), "A Surface Science Investigation of Metal-Ceramic Interfacial Reactions", Proc. of Japan International SAMPE Symposium, pp. 1404-1411 Nov.28-Dec.1.

8   Ohuchi, F.S.; Zhong, Q. (1990), "Electronic Structure of Metal-Ceramic Interfaces", ISIJ International V.30(12) pp. 1059-1065.

9   BlackBurn, A.R.; Shevlin, T.S.; Lowers, H.R. (1949), "Fundamental Study; and Equipment for Sintering and Testing of Cermet Bodies, I-III", J. Am. Cer. Soc. V.32(3) pp. 81-98.

10 Suganuma, K. (1990), "Recent Advances in Joining Tecnology of Ceramic to Metals", ISIJ International, V. 30(12) pp. 1046-1058.

11 Chidambaram, P.R (1993), "Thermodynamic and Kinetic Aspects of Reactive Metal Liquids in Contact with Oxide Ceramics", Ph.D. Thesis, Colorado School of Mines.

12   Plessis, J. du; van Wyk, G.N. (1989a), "A Model for Surface Segregation in Multicomponent Alloys - Part III: The Kinetics of Surface Segregation in a Binary Alloy", J. Phys. Chem. Solids, V.50(3) pp. 237-245.

13   Gallois, B.; Lupis, C.H.P. (1981), "Effect of O on the Surface Tension of Liquid Cu", Metallurgical Transactions B V.12B pp. 549-557.

14   O'Brien, T.E.; Chaklader, A.C.D. (1974), "Effect of O on the Reaction Between Cu and Sapphire", J. of Am. Ceram. Soc. V.57(8) pp. 329-332.

15   Naidich, J.V. (1981), "The Wettability of Solids by Liquid Metals", in Progress in Surface and Membrane Science, V.14 pp. 353-485.

16   Mukherjee, S. (1987), "Surface Segregation in Transition-Metal Alloys and in Bimetallic Alloy Clusters", Surface Science 189/190 pp. 1135-42.

17   Pajunen, M.; Kivilahti, J. (1992), "Thermodynamic Analysis of the Titanium - Oxygen System", Z. Metallkd, V. 83(1) pp. 17-20.

18   Klomp, J.T. (1987a), "Interface Chemistry and Structure of Metal-Ceramic Interfaces", in Fundamentals of Diffusion Bonding, Tokyo, Elsevier Science Publishers, pp. 3-24 .

19   Nicholas, M.G. (1988), "Interactions at Oxide-Metal Interfaces", Materials Science Forum V.29 pp. 127-150.

20   Kritsalis, P.; Coudurier, L.; Eustathopoulos, N. (1991), "Contribution to the Study of Reactive Wetting in the $Cu-Ti/Al_2O_3$ System", J. of Mat. Sci. V.26 pp. 34003408.

21   Bang, K. (1991), "Kinetics of Interfacial Reactions in Reactive Metal Brazing", Ph.D. Thesis, Colorado School of Mines, Golden Colorado.

22   Naidich, Y.V.; Zhuravlev, V.S. (1973), "Adhesion, Wetting, and Formation of Intermediate Phases in Systems Composed of a Ti-Containing Melt and an Oxide", Poroshkovaya Metallurgiya V.11(131) pp. 40-46.

23   Nicholas, M.G.; Crispin, R.M. (1989), "Brazing Ceramics with Alloys
      ContainingTi", Ceram. Eng. Sci. Proc. V.10(11-12) pp. 1602-1612.

24   Nicholas, M.G. (1991), "Reactive Metal Brazing of Ceramics", Scandinavian Journal
      of Metallurgy V.20 pp. 157-164.

25   Li, X.L.; Hillel, R.; Teyssandier, F.; Choi, S.K.; Van Loo, F.J.J. (1992), "Reactions
      and Phase Relations in the Ti-Al-O System", Acta Metallurgica and Materialia,
      V.40(11) pp. 3149-3157.

26   Choi, S.K; Froyen, L.; Brabers, M.J. (1987), in High Tech Ceramics, Elsevier
      Science Pub, Amsterdam, p. 407.

27   Zhang, M.X; Hsieh, K.C., DeKock, J.; Chang, Y.A. (1992), "Phase Diagram of Ti-
      Al-O at 1100 °C", Scripta Metallurgica et Materialia, V.27 pp. 1361-1366.

28   Chaug, Y.S.; Chou, N.J.; Kim, Y.H. (1987), "Interaction of Ti with Fused Silica and
      Sapphire During Metallization", J. Vac. Sci. Technol. A, V.5(4) pp. 1288-1291.

29   Wahlbeck, P.G.; Gilles, P.W. (1966), "Dissociation Energy of $TiO_{(g)}$ and the High
      Temperature Vaporization and Thermodynamics of the Titanium Oxides. II.
      Trititanium Pentoxide", The Journal of Chemical Physics, V.46(7) pp. 2465-2473.

30   de Camargo, Paulo R., Role of Oxygen in the Cu-O-Ti/Sapphire Interfacial-Region
      Formation, Thesis (Ph. D.), Colorado School of Mines 1995

31   Pankratz, L.B. (1984a), Thermodynamic Properties of Elements and Oxides, United
      States Department of Interior, Bureau of . Mines, V. 672 pp. 427-437.

32   Gilles, P.W.; Carlson, K.D., Franzen, H.F.; Wahlbeck (1967), "High Temperature
      Vaporization Characteristics of the Crystalline Phases", The Journal of Chemical
      Physics, V.46(7) pp. 2461-2465.

33   Ownby, P.D.; Liu, J. (1988), "Surface Energy of Liquid Cu and Single-Crystal
      Sapphire and the Wetting Behavior of Cu on Sapphire", J. Adhesion Sci. Technol.
      V.2(4) pp. 255-269.

34   Kritsalis, P.; Li, J.G.; Eustathopoulos, N. (1990), "Role of Clusters on the Wettability and Work of Adhesion of the Cu-Cr/Al_2O_3 System", J. of Mat. Sci Letters V.9 pp. 1332-1335.

35   Kritsalis, P.; Merlin, V.; Eustathopoulos, N. (1992), "Effect of Cr on Interfacial Interaction and Wetting Mechanism in Ni Alloy/Al_2O_3 systems", Acta Metall. Mater. V.40(6) pp. 1167-1175.

36   Guttmann, M. (1975), "Equilibrium Segregation in a Ternary Solution: A Model for Temper Embrittlement", Surface Science, V.53 pp. 213-227.

37   Plessis, J. du; van Wyk, G.N. (1988a), "A Model for Surface Segregation in Multicomponent Alloys - Part I: Equilibrium Segregation", J. Phys. Chem. Solids, V.49(12) pp. 1441-1450.

38   McMahon, Jr. C.J.; Marchut, L. (1978), "Solute Segregation in Iron-Based Alloys", J. Vac. Sci. Technol., V.15(2) pp. 450-466.

39   Schmid, R. (1983), "A Thermodynamic Analysis of the Cu-O System with an Associated Solution Model", Metallurgical Transactions B V.14B pp. 473-481.

40   Hoshino, H.; Shimada. T.; Yamamoto, M.; Iwase, M. (1992), "Activities of Titanium in Molten Copper at Dilute Concentrations Measured by Solid-State Electrochemical Cells at 1373 K", Metallurgical Transactions B, V. 23B pp. 169-173.

41   Pajunen, M.; Kivilahti, J. (1992), "Thermodynamic Analysis of the Titanium - Oxygen System", Z. Metallkd, V. 83(1) pp. 17-20.

42   Miedema, A.R. (1978), "Surface Segregation in Alloys of Transition Metals", Z. Metallkunde, V.69(7) pp. 455-461.

43   Gerasimov, V.V. (1990), "Estimation of the Energies of Adsorption of Oxygen on Metals", Russian Journal of Physical Chemistry, V. 64(12) pp. 1822-1823.

44   Toyoshima, I.; Somorjai, G.A. (1979), "Heats of Chemisorption of O_2, H_2, CO, CO_2, and N_2 on Polycrystalline and Single Crystal Transition Metal Surfaces", Catalysis Review - Science Engeneering, V.19(1) pp. 105-159.

45   Pankratz, L.B.; Stuve, J.M.; Gokcem, N.A. (1984c), Thermodynamic Data for
      Mineral Technology, United States Department of Interior, Bureau of . Mines, V.
      677 pp. 258.

46   Loehman, R.E., (1989), "Interfacial Reactions in Metal-Ceramic Systems", Ceramic
      Bulletin, V.68(4) pp. 891-896.

47   Chastian, J. (1992), Handbook of X-ray Photoelectron Spectroscopy, Perkin-Elmer
      Corporation.

III. DIFFUSION BONDING CERAMIC TO METAL USING DUCTILE, MULTILAYER REACTIVE METAL COATINGS:

The main objectives of this study are to investigate and model the behavior of ductile, multilayer reactive metal coatings as filler metal for bonding ceramics to metals. Activities for the past year were directed towards characterization of the bond layer, understanding the interface formation, variation of the initial ductile and reactive metal deposition conditions and their relation to process parameters. Detailed chemical analysis of the bond layer cross section was also necessary for the development of a multilayer interdiffusion model. Multilayer Ni/Ti coatings of 1 and 25μ total thickness, with variations in the total number of layers, were produced for joining specimens. They undergo heat treatment where time at temperature, temperature and bonding pressure are the process variables. The composition and structure of the multilayer coatings and bonded cross section were analyzed using x-ray diffraction, SEM/EDS. TEM work is also planned for the bond region characterization. Using literature data for comparison, the measured composition profiles are being modeled to understand the interdiffusion in the Ni-Ti multilayers.

A. EXPERIMENTAL PROCEDURE

As previously reported, characterization of the sputtering deposition rates were done by depositing Ti and Ni onto glass slides at 0.25, 0.5 and 1.0 kw, for 1, 5 and 10 minutes in an argon atmosphere at 1 mtorr. The film thickness were measured with surface tracing profilometer. The thickness measurements were used to derive an empirical model for use in controlling individual metal layers. Once the empirical model was derived, layers having a total thickness of approximately 10,000Å were deposited on glass and Coors ADS 995 ceramic substrates. The number of layers were varied in an odd numbered sequence from 3 to 15 layers ($i = 1$ to 7). The Ti thickness was varied between $309x10^{-9}$m and $77x10^{-9}$m, the Ni thickness was varied between $382x10^{-9}$m and $55x10^{-9}$m. Sputtering power for the multilayer films was 0.5kw for the Ni and 0.3kw for the Ti. Sputtering pressure was constant at 1mtorr.

To determine the interdiffusion characteristics of Ti-Ni and Al_2O_3, thick (25μm total) multilayer films were deposited on alumina substrates. Two thick film layering arrangements, composed of Ti/Ni/Ti (3 layers) and Ti/Ni/Ti/Ni/Ti (5 layers) were used as diffusion couples. Titanium layers were 61.92% of the total thickness, nickel layers made up the balance. The layer thickness were designed to produce equiatomic reaction product, NiTi. These were then heat treated in vacuum (10^{-6}Torr, flushed with 99.999 Ar) at 500°C for 10 and 20 hours. Specimens were examined by SEM/EDS, x-ray diffraction and some limited TEM prior to and following heat treatment.

B.   Results and Discussion

Prior to heat treatment, x-ray diffraction measurements of both the $1\mu m$ and the $25\mu m$ films showed only the structures of Ni, Ti and alumina. As previously reported [1], when heating the $1\mu m$ films at 500°C for 5 hours, both NiTi and Ni_3Ti could be seen to form and was shown in the x-ray diffraction spectra. In the thicker, $25\mu m$ films, only NiTi was observed after heating for 10 or 20 hours at 500°C in both the 3 layer and 5 layer specimens. This was in contrast to the $1\mu m$ films where Ni_3Ti was observed to form at 500°C in five hours, but was consistent with the previous observation [1] that coarser (thicker) metal layering diminished the Ni_3Ti formation. As was the case with the $1\mu m$ films where heat treatment at low temperatures (200-300°C) showed incomplete reaction in the form of primary Ni and Ti diffraction peaks, the $25\mu m$ films heat treated for 10 hours also showed there was some unreacted Ni and Ti. this was due to the diffusion distance required at the given temperatures. Thinner specimens ($1\mu m$) heat treated at lower temperatures (200-300°C) for short times (2-10 hours) show some of the same reaction product formation characteristics as the thicker ($25\mu m$) specimens heat treated at higher temperature (500°C) for longer times (10-20 hours). Assuming a thin film solution to the diffusion distance, and applying some of the Ni-Ti interdiffusion data from the literature [2,3,4] the observations seemed reasonable.

The composition profiles of the 25μm, 3 layer specimens are shown in figure 1. Areas approximately 1μm apart were examined and the compositions plotted against the distance from the alumina/metal interface. With a diffusion distance relationship such as:

$$x = 2\sqrt{Dt}$$

where x is the diffusion distance (cm), D is the diffusion coefficient (cm^2/s) and t is time (seconds). Using the appropriate D's the diffusion distance for the 500°C-10 hours specimen, diffusion distances of around 6μm would have been expected, similarly, at the same temperature for 20 hours, a distance of around 8μm coincides with the observed distance (fig. 1). Not enough data has been taken to determine the diffusion coefficient for Ni and Ti across the alumina interface and the effect of metal loss into the alumina would have implications for the thin film assumption. Still, as preliminary observations, the system seems fairly well behaved.

The limited amount of TEM observations have been consistent with the x-ray diffraction and EDS work so far. The initial Ni/Ti layering on alumina has been observed, and the NiTi intermetallic could also bee seen. There appears to be, and the analysis was not yet complete, a small amount of undefined material at the alumina/metal interface. This would be expected to be some form of nickel aluminide, titanium aluminide spinel or one of the other Ti-Ni intermetallics. The methodology for good cross section preparation has not been completed so careful characterization remains a priority.

C.   Conclusions

The behavior of the thin (1μm) multilayer films can be compared to the thick

(25μm) multilayer films with regards to NiTi formation for given time and temperature

heat treatments. With consideration of the Ni-Ti interdiffusion coefficients the system

responds in a predictable manner. The effects of metal solute loss into the ceramic

substrate during long time exposure to high temperatures (in excess of 500°C) remains to

be determined. Additional work on the interfacial product formation and identification is

planned to coincide with determination of the metal-ceramic interdiffusion behavior. Thus

far, the number and thickness of metal layering and the formation of the desired NiTi

intermetallic as well as the formation of other Ni-Ti intermetallics have been determined

for a range of temperatures (200-800°C) and times (2-20 hours).

The primary significance of the work was in the determination that a desired

intermetallic compound could be formed through the use of sputter deposited multilayer

metal films. The relation to the diffusion bonding process shows that it is possible to

increase or control the maximum service temperature of the bonded joint through the use

of this layering to produce a particular intermetallic product. With additional chemical

analysis of the bonded cross section, development of a multilayer inter diffusion model and

further evaluation of bonding pressure as related to mechanical properties several things

are possible. A fundamental understanding of the process kinetics would have application

not only to this system but to other alloy systems as well. That fundamental model

correlated with process variables and product properties would then allow for greatly

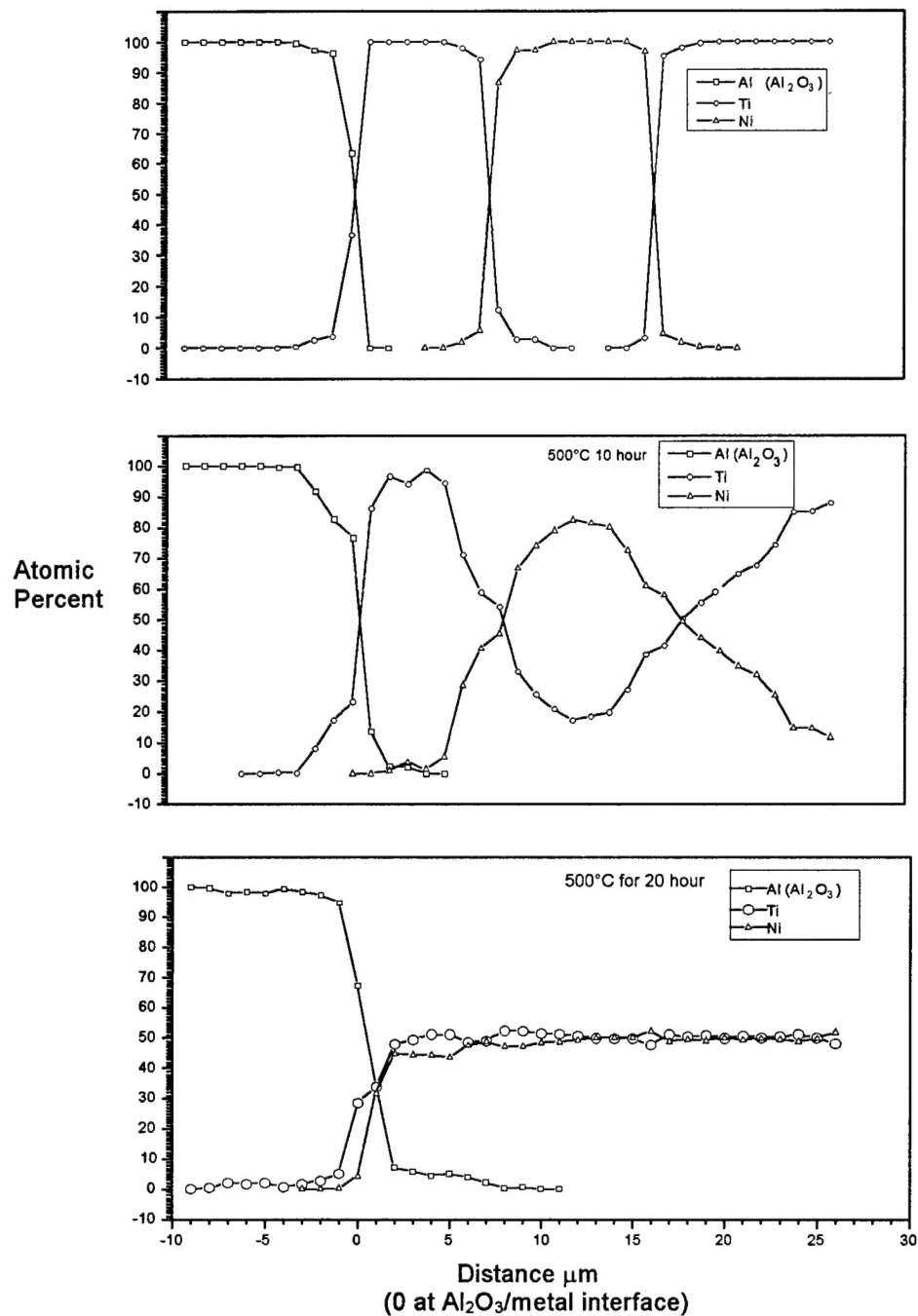improved process development and materials selection.

Figure 1: EDS composition profile of 25μm thick 3 layer (Ti/Ni/Ti) film deposited on alumina. Top profile is as-deposited; middle profile, heat treated for 10 hours at 500°C; bottom profile, heat treated for 20 hours at 500°C.

D.   REFERENCES

1   Edwards, G. R., Liu, S.: "Fundamental Aspects of Metal-to-Ceramic Brazing", MT-CWJR-94-037, (Oct. 1994), pp.94-100.

2.   Burminskaya, L. N.: "Diffusion Processes in a Ti-Ni Composite", Metalloved. Proch. Mater, n.3 (1971), pp.251-5.

3   Marinkovic, Z.: "Comparative Analysis of Interdiffusion in Some Thin Film Metal Couples at Room Temperature", Thin Solid Films, v. 127, n. 1/2, (Sept. 1992), p.26.

4   Maza, M., Sella, C., Ambroise, J. P., "Determination of Diffusion Coefficient, D, and Activation Energy, Q_a, of Nickel into Titanium I Ni-Ti- Multilayers by Grazing-Angle Neutron Reflectometry", Journal of Applied Crystallography, v. 25, n. 3, (Jun. 1993), p.334.

IV. PERSONNEL

Dr. Glen R. Edwards, PI

Dr. Stephen Liu, Co-PI

Dr. Alan Meyer, Concluded Ph.D. degree

Dr. Paulo Camargo, Concluded Ph.D. degree (stipend paid from other source)

Mr. Donald Bucholz, Ph.D. candidate

V. PUBLICATIONS AND PRESENTATIONS

1. A. Meier, P.R. Chidambaram and G.R. Edwards. "Generation of Isothermal Spreading Data and Interfacial Energy Data for Liquid Reactive metal on Ceramic Substrates: The Copper-Titanium/Alumina System", accepted for publication in the Journal of Materials Science, V. 30, pp. 3791-3798 (1995).

2. A. Meier, V. Gabriel, P.R. Chidambaram, and G.R. Edwards. "The Wettability of Copper-Manganese Alloys on Alumina and Their Potential as Direct Brazing Filler Metals", Materials and Manufacturing Processes, V. 10, No. 4, pp. 625-641 (1995).

3. A. Meier, M.D. Baldwin, P.R. Chidambaram, and G.R. Edwards. "The Effect of Large oxygen Addition to Copper on the Wettability and Work of Adhesion on Polycrystalline Alumina", Materials Science and Engineering, V. A196, pp. 111-117 (1995).

4. M.D. Baldwin, P.R. Chidambaram and G.R. Edwards. "Spreading and Interlayer Formation at the Copper-Copper Oxide/Alumina Interface", Met. Trans. A, V. 25, pp. 2497-2506 (1994).

5. A. Meier, P.R. Chidambaram, G.R. Edwards, and S. Liu. A Model for the Spreading of Copper-Titanium Brazing Alloys on Alumina", presented at the American Welding Society Annual Convention, Cleveland, Ohio (1995).

6. P.R. Camargo, S. Liu, G.R. Edwards, and G.P. Martins. "Role of Oxygen on the Interface Formation in the Cu-Ti-O/Sapphire System", presented at the American Welding Society Annual Convention, Cleveland, Ohio (1995).

7. Bucholz, S. Liu and G.R. Edwards. "Sputter Deposited nickel/Titanium for Diffusion Bonding Ceramic to Metal", presented at the American Welding Society Annual Convention, Cleveland, Ohio (1995).